KAIRON MÁRCIO DE OLIVEIRA

Synthesis, Characterization, and Application of Polyaniline Supramolecular Structures

Thesis submitted to the Physics Graduate Program of the Universidade Federal de Viçosa in partial fulfillment of the requirements for the degree of Doctor Scientiae.

Adviser: Alvaro Vianna Novaes de Carvalho Teixeira

Co-advisers: Eduardo Nery Duarte de Araújo

Márcio Santos Rocha

VIÇOSA
2024

Ficha catalográfica elaborada pela Biblioteca Central da Universidade Federal de Viçosa - Campus Viçosa

T
O48s
2024

Oliveira, Kairon Márcio de, 1997-
Synthesis, characterization, and application of polyaniline supramolecular structures / Kairon Márcio de Oliveira. – Viçosa, MG, 2024.
1 tese eletrônica, 159 f.: il. (algumas color.).

Orientador: Álvaro Vianna Novaes de Carvalho Teixeira.
Tese (doutorado) - Universidade Federal de Viçosa, Departamento de Física, 2024.
Referências bibliográficas: f. 153-158.
DOI: https://doi.org/10.47328/ufvbbt.2024.126
Modo de acesso: World Wide Web.

1. Polímeros. 2. Polímeros condutores. 3. Polianilina - Síntese. 4. Sensores. I. Teixeira, Álvaro Vianna Novaes de Carvalho, 1973-. II. Universidade Federal de Viçosa. Departamento de Física. Programa de Pós-graduação em Física. III. Título.

CDD 22. ed. 620.192

Bibliotecário(a) responsável: Advania Elza da Silva CRB-6/3263

KAIRON MÁRCIO DE OLIVEIRA

Synthesis, Characterization, and Application of Polyaniline Supramolecular Structures

Thesis submitted to the Physics Graduate Program of the Universidade Federal de Viçosa in partial fulfillment of the requirements for the degree of Doctor Scientiae.

APPROVED: March 08, 2024.

Assent:

Kairon Márcio de Oliveira
Author

Alvaro Vianna Novaes de Carvalho Teixeira
Adviser

ACKNOWLEDGEMENTS

Agradeço primeiramente a Deus por tudo e todas as oportunidades, bem com por ter colocado em minha vida pessoas muito especiais e imporatntes. Sem elas não seria possível esta defendendo está tese de doutorado, pois não é possível conquistar nada sem a ajuda e o amparo de outras pessoas.

Agradeço a toda minha família. Em especial meu Pai, Márcio, e minha Mãe, Marilene, por toda a ajuda, amparo, ensinamentos, carinho e amor em toda minha vida sempre apoiando nos meus sonhos e guiando para escolher os melhores caminhos. Sem eles com toda certeza eu não estaria aqui. A minha Irmã, Kamirian, por todo o amparo, carinho e amor durantes todos anos me ajudando desde da infância nas minhas conquistas. Por fim, a minha Namorada, Gabriela, que está comigo desde do início da graduação me amparando e ajudando em todos momentos com muito amor e carinho. Sem eles tenho certeza que eu não conseguiria estar complentando mais esta etapa na minha vida.

A todos meus colegas de laboratório e da salinha de pós graduação por todos os bons momentos e risadas fazendo com que os momentos difíceis se tornassem mais leves. Em especial agradecer o Pedro, Lucas Goes, Tiago Moura, Juliano, Andriele, Rayane, Milton, Hamilton, Janaísa, Tiago Azevedo, Arthur Schulenburg, Lair, Iago, Kelly, Gabs, Eloi, Sidnei, Lara, Diogo, Milena, Arthur, Konstantine, Dobner e Rúbia.

A toda comissão orientadora por todo auxílio, aprendizado e atenção dada durante o doutorado. O Prof. Dr. Eduardo Nery por toda a colaboração e entusiasmo com o projeto. Dra. Patrycja Bober pelo amparo e ensinamentos passados durante o meu período sanduíche no Institute of Macromolecular Chemistry em Praga – República Tcheca que foram essenciais para a finalização do projeto. Em especial agradecer ao meu orientador e amigo, Prof. Dr. Alvaro Vianna, por todo o amparo, ensinamentos e apoio durante a graduação e o doutorado me ajudando a me torna o pesquisador que sou hoje.

E por fim, agradeço as agências de fomento Coordenação de Aperfeiçoamento de Pessoal de Nível Superior (CAPES), Conselho Nacional de Desenvolvimento Científico e Tecnológico (CNPq), Fundação de Amparo à Pesquisa do Estado de Minas Gerais (FAPEMIG) e a Universidade Federal de Viçosa pela oportunidade da realização da meu curso de gradução e doutorado.

Por fim, agradeço à CAPES pelo provimento da minha bolsa de doutorado. O presente trabalho foi realizado com apoio da Coordenação de Aperfeiçoamento de Pessoal de Nível Superior - Brasil (CAPES) - Código de Financiamento 001.

“Isso também passa”.

(Chico Xavier)

RESUMO

OLIVEIRA, Kairon Márcio de, D.Sc., Universidade Federal de Viçosa, Março de 2024. **Síntese, Caracterização e Aplicação de Estruturas Supramoleculares de Polianilina**. Orientador: Alvaro Vianna Novaes de Carvalho Teixeira. Coorientadores: Eduardo Nery de Araújo, Patrycja Magdalena Bober e Márcio Santos Rocha.

Polianilina (PANI) é um conhecido polímero semicondutor que pode alterar suas características condutoras através de processo de dopagem e desdopagem por soluções ácidas e básica, respectivamente. Estas características permitem que estes polímeros sejam aplicados em equipamentos eletrônicos, óticos e sensores eletroquímico. Contudo, uma alternativa para melhorar a aplicabilidade e eficiência da PANI polímero é através da produção de estruturas supramoleculares como: partículas, tubos, bastões, placas e core-shell. A produção destas estruturas ocorre mediante a adição de moléculas anfifílicas (estabilizadores) como surfactantes e polímeros durante a polimerização da anilina, gerando como produto final diferentes morfologias. Neste trabalho, nosso objetivo foi produzir partículas de PANI utilizando como estabilizador o polímero Poli(vinil pirrolidona) (PVP) e analisar as características destas partículas em medidas de pinça ótica comparando com partículas semicondutoras inorgânicas. Utilizando técnica de Espalhamento Dinâmico de Luz (DLS) foi possível notar que o raio hidrodinâmico das partículas varia com o pH, mostrando que quando o polímero está carregado a tendência é que as partículas tenham um tamanho menor. A técnica de microscopia eletrônica de varredura permitiu avaliar que as partículas produzidas são esféricas e pouco amorfas. A presença de PANI e PVP nas partículas foi constatada pelos resultados de espectroscopia Raman. Por fim, a caracterização utilizando pinça ótica mostrou que a absorção nas partículas de PANI muda com a potência do laser. Também foi possível notar que por mais que as partículas não obedeçam a ótica linear para tamanhos pequenos o comportamento dos resultados foi parecido com o do modelo teórico. Também tivemos como objetivo produzir estruturas supramoleculares de PANI e o estabilizador Dodecil Sulfato de Sódio (SDS) com o formato de tubos, bastões e placas e avaliar a influência do agente oxidante (persulfato de amônio (APS)) e da temperatura de síntese na morfologia das estruturas. Foi verificado que para a razão entre [APS]/[Ani] igual a 1 ocorre a formação de placas, e com a diminuição desta razão há o favorecimento da formação de bastões. Estruturas como bastões possui uma razão de 1:1 de moléculas de anilina e SDS, sendo que para altas concentrações de APS esta razão é igual a 4:1, mostrando que o número de moléculas de anilina e SDS na célula unitária que forma

as estruturas cristalinas desempenha um papel fundamental. Resultados de espectroscopia Raman e espectroscopia no infravermelho por Transformada de Fourier (FTIR) mostram que para pequenas concentrações de APS não há a formação de polímeros e, somente a presença de oligômeros, fazendo com que as amostras sejam pouco condutoras. Já para a razão de [APS]/[Ani] igual a 1, ocorre a formação de polímeros condutores e também a presença de oligômeros. A técnica de Difração de Raios-X evidencia que a presença do SDS torna as amostras mais cristalinas que a PANI pura. Eletroquímica analises foram realizadas com o objetivo de caracterizar as estruturas para a aplicação em sensores de ácido ascórbico. Os resultados de Voltametria Cíclica foram possíveis observar para todas amostras as presenças dos picos de oxidação (redução) da PANI, mostrando a qualidade das amostras. Foram realizadas medidas de Cronoamperiometria em 15 diferentes concentrações de ácido ascórbico revelando que as amostras com SDS possuem uma corrente resposta duas vezes maior do que a PANI pura, aumentando a sensibilidade do sensor. Testes com suco de laranja comercial mostraram que os sensores são seletivos, reutilizáveis e precisos com a variação do valor esperado em menos de 10%. Por fim, a influência da adição de um copolímero p-fenilenodiamina (PDA) na síntese da anilina com e sem SDS foi avaliada para tentar melhorar os sensores produzidos anteriormente. Também foi avaliado a substituição do ácido clorídrico como dopante pelo ácido sulfúrico e ácido canforsulfônico. Raman e FTIR mostraram que ocorre a formação de estruturas hibridas de anilina com PDA comprovando a formação de copolímeros. Pode-se notar que a adição do ácido sulfúrico e canforsulfônico aumentou a cristalinidade das estruturas sem o SDS. Quando ocorre a adição de SDS a cristalinidade das estruturas não altera. Medidas de condutivimetria cíclica mostraram que as amostras sintetizadas utilizando o ácido sulfúrico possuem os maiores valores de capacitância, tornando-as escolhidas para as aplicações em sensores de ácido ascórbico. Foram realizadas medidas de Cronoamperiometria em 15 diferentes concentrações de ácido ascórbico revelando que as amostras com SDS possuem uma corrente resposta um pouco maior do que a PDA e anilina copolímero, aumentando a sensibilidade do sensor. Testes com suco de laranja comercial mostraram que os sensores são seletivos, reutilizáveis e precisos com a variação do valor esperado em menos de 17%.

Palavras-chave: Polianilina; Polímeros condutores; Sensores; Polímeros-surfactantes compósitos.

ABSTRACT

OLIVEIRA, Kairon Márcio de, D.Sc., Universidade Federal de Viçosa, March, 2024. **Synthesis, Characterization, and Application of Polyaniline Supramolecular Structures**. Adviser: Alvaro Vianna Novaes de Carvalho Teixeira. Co-advisers: Eduardo Nery de Araújo, Patrycja Magdalena Bober, and Márcio Santos Rocha.

Polyaniline (PANI) is a well-known semiconductor polymer that can change its conductive characteristics by doping and dedoping processes using acidic and basic solutions, respectively. These characteristics allow these polymers to be applied in electronic, optical, and electrochemical sensor equipment. An alternative to improving the PANI polymer's applicability and efficiency is the production of supramolecular structures such as particles, tubes, rods, plates, and core shells. The production of these structures occurs by adding amphiphilic molecules (stabilizers) such as surfactants and polymers during the aniline polymerization, generating different morphologies as the final product. In this work, our objective was to produce PANI particles using the polymer Poly(vinyl pyrrolidone) (PVP) as a stabilizer and analyze the characteristics of these particles in optical tweezer measurements compared to inorganic semiconductor particles. Using the Dynamic Light Scattering (DLS) technique, it was possible to note that the hydrodynamic radius of the particles varies with pH, showing that when the polymer has a charge, the tendency is for the particles to have a smaller size. The scanning electron microscopy technique allowed us to evaluate whether the particles produced are spherical and not amorphous. The results of Raman spectroscopy confirmed the presence of PANI and PVP in the particles. Finally, characterization using optical tweezers showed that the absorption in PANI particles changes with laser power. It is possible to note that the particles do not follow the linear optics for small sizes; however, the behavior of the results was similar to that of the theoretical model. We also aimed to produce supramolecular structures of PANI and the stabilizer Sodium Dodecyl Sulfate (SDS) in the shape of tubes, rods, and plates and evaluate the influence of the oxidizing agent (ammonium persulfate (APS)) and the synthesis temperature on the morphology of the structures. It was found that for the ratio of [APS]/[Ani] equal to 1, the formation of plates occurs, and with a decrease in this ratio, the formation of rods is favored. Structures such as rods have a 1:1 ratio of aniline and SDS molecules. For high concentrations of APS, this ratio is equal to 4:1, showing that the number of aniline and SDS molecules in the unit cell that form the structures plays a fundamental role. Results from Raman spectroscopy and Fourier transform infrared spectroscopy (FTIR) show

that for small concentrations of APS, there is no formation of polymers and only the presence of oligomers, making the samples poorly conductive, for the ratio of [APS]/[Ani] equal to 1, the formation of conductive polymers and the presence of oligomers occurs. The X-ray Diffraction technique shows that SDS makes the samples more crystalline than pure PANI. Electrochemical analyses were carried out to characterize the structures for application in ascorbic acid sensors. The Cyclic Voltammetry results made it possible to observe the presence of PANI oxidation (reduction) peaks for all samples, showing the quality of the samples. Chronoamperometry measurements were carried out in 15 different ascorbic acid concentrations, revealing that samples with SDS have a current response twice as high as pure PANI, increasing the sensor's sensitivity. Tests with commercial orange juice showed that the sensors are selective, reusable, and accurate, with an expected value variation of less than 10%. Finally, the influence of adding a p-phenylenediamine (PDA) copolymer on the synthesis of aniline with and without SDS was evaluated to improve previously produced sensors. The replacement of hydrochloric acid as a dopant with sulfuric acid and camphor sulfonic acid was also evaluated. Raman and FTIR showed that the formation of hybrid structures between aniline and PDA occurs, proving the formation of copolymers. It can be noted that the addition of sulfuric and camphor sulfonic acid increased the crystallinity of the structures without SDS. When SDS is added, the crystallinity of the structures does not change. Cyclic voltammetry measurements showed that samples synthesized using sulfuric acid have the highest capacitance values, making them chosen for applications in ascorbic acid sensors. Chronoamperometry measurements were carried out in 15 different concentrations of ascorbic acid, revealing that samples with SDS have a current response slightly higher than PDA and aniline copolymer, increasing the sensitivity of the sensor. Tests with commercial orange juice showed that the sensors are selective, reusable, and accurate, with an expected value variation of less than 17%.

Keywords: Polyaniline; Conductive Polymers; Sensors; Polymer-surfactant composites.

LIST OF ILLUSTRATIONS

LIST OF TABLES

SUMMARY

1 INTRODUCTION

Polymers are large molecules with a molecular mass in the order of magnitude of tenths or thousands of grams per mol or larger. They are formed by the reaction of small molecules known as monomers. The word polymer comes from Greek, where ‘polus’ means ‘many’ and ‘meros’ means ‘parts’. These macromolecules are present in every part of our lives, from clothes to electronic devices. There are three main categories of polymers: natural, bio, and synthetic. The first category includes cotton, starch, amber, latex rubber (Amazonia rubber tree), cellulose, silk, and wool. These polymers were the first that humans have used throughout history to advance in the textile and food industries (SPERLING, 2005). Biopolymers are polymers occurring in living organisms, such as proteins and DNA/RNA. They are essential to life due to their importance to organism protection (antibodies), oxygen transport (hemoglobin), cellular communication, chemical transport through the cellular wall, chemical catalysis, and the genetic code (YAASHIKAA; KUMAR; KARISHMA, 2022). Synthetic polymers started to be produced in the middle of the 19th century by Friedrich Ludersdorf and Nathaniel Hayward; they produced polyisoprene (independently) by adding sulfur to natural rubber. Posteriorly, Charles Goodyear synthesized a new flexible and waterproof material by adding sulfur to natural rubber and then vulcanized the sample to improve these characteristics. However, just at the beginning of the 20th century, these macromolecules started to be studied to understand their chemical structures and formation. In 1922, Hermann Staudinger proposed that polymers were formed by an extended chain of atoms bonded by covalent interaction. This work gave him a Nobel Prize in 1953 (FELDMAN, 2008). After that, another six Nobel Prizes were given for studies dedicated to understanding or synthesizing new polymers until today.

Polymers are a giant class of materials with different characteristics such as crystallinity, permeability, resistance, color, refraction index, absorption coefficient, heat capacity, conductivity, resilience, high strength, transparency, and permeability (BRINSON *et al.*, 2015). These qualities, allied to a low cost of production, make them attractive to apply in different industry sectors, for example, polyethylene (plastic and pipes), polypropylene (vehicle pieces and synthetic fibers), polystyrene (plastic containers), polyvinyl chloride (electrical isolators and textile industry), nylon (textile industry), Teflon (wire isolator and metal protection), and polybutadiene (tire industry).

Alan J. Heeger, Alan G. MacDiarmid, and Hideki Shirakawa discovered in 1977 a new class of high-conductivity polymers known as conductive polymers. They studied a polyacetylene partially oxidized doped by bromine, and this research gave them a Nobel Prize in Chemistry in 2000 for the discovery and development of conductive polymers (INZELT, 2012). These macromolecules can transfer electric current as a metallic material and change the conductive characteristics like a semiconductor, making them of great interest for improving electronic devices or substituting inorganic semiconductors. Conductive and optic characteristics appear in conductive polymers due to the presence of alternative single and double bonds in the backbone chain (conjugated chain), where the polarization and high delocalized of the electrons (after the doping process) in the π-bonds make possible the conductivity in these polymers (HAZELTON; YE; CHEN, 2023; NASAJPOUR-ESFAHANI *et al.*, 2023). Some well-known conductive polymers are polyaniline (PANI), polypyrrole (PPy), poly(3,4-ethylene dioxythiophene) (PEDOT), poly(p-phenylene sulfide) (PPS), polythiophene (PTH), polyacetylene (PAC), poly(vinyl alcohol) (PVA), poly(vinyl pyrrolidone) (PVP), and poly(phenylenevinylene) (PPV).

Polyaniline is a semiconductor polymer obtained through radical aniline (monomer) polymerization. As a semiconductor, PANI can change the conductivity characteristics through a doping (or undoping) process, which occurs using acid (or basic) solutions. So, the PANI chain incorporates protons in low pH and becomes a conductor polymer. Moreover, the incorporation of protons, known as the doping process, changes the optic properties of the polymer, which becomes evident with the change in the sample color with the pH. Due to these properties allied with the low cost of production, PANI is a polymer extremely attractive to apply in electronic and optics devices, electrochemical sensors, energy storage systems (as supercapacitors and batteries), displays, protection of metals, and biological treatment (DING *et al.*, 2021; SHI; BAI; LI, 2018; WU *et al.*, 2021).

Although the PANI has excellent optics and conductivity properties, the films formed only with polymer are easily degraded for electrical current and temperature. This problem could be solved by adding stabilizer molecules to form a supramolecular structure of PANI. A supramolecular structure is a material of more than one molecule and normally uses some polymer and/or surfactant as stabilizers. The stabilizer protected the PANI, giving more stability and changing the sample morphology to increase the superficial area without losing the properties of the PANI. The stabilizers are amphiphilic molecules that can interact with hydrophobic and hydrophilic materials, enabling the formation of structures with spherical particles (RIEDE *et al.*, 1998; STEJSKAL; KRATOCHVÍL; HELMSTEDT, 1996), rods

(ZHOU; HAN; GUO, 2009), tubes (STEJSKAL *et al.*, 2022; ZHOU; HAN; GUO, 2008), plates, or sheet morphology.

Surfactants contain one part hydrophilic (head) and another hydrophobic (tail), which characterizes their amphiphilicity. In an aqueous solution, these molecules can interact with a hydrophobic molecule and the water while simultaneously reducing the superficial tension and the free energy and increasing the entropy of the solution. Some surfactants used to synthesize supramolecular structures of PANI are sodium dodecyl sulfate (SDS) and sodium dodecyl benzene sulfate (SDBS). Polymers also can exhibit amphiphilicity, such as poly (vinyl alcohol) (PVA) (RIEDE *et al.*, 1998) and poly (vinyl pyrrolidone) (PVP) (KIM *et al.*, 2001; STEJSKAL; KRATOCHVÍL; HELMSTEDT, 1996), which contain blocks or chemical groups that are hydrophilic and other hydrophobic.

This work studied supramolecular structures obtained by the interaction between PANI and surfactants or polymers. First, we evaluate the interaction of PANI and PVP, resulting in spherical particles. Second, the interaction between PANI and SDS resulted in the formation of rods, plates, tubes, and gels. In the first case, the particles were characterized using Raman spectroscopy, Dynamic Light Scattering (DLS), Scanning Electron Microscopy (SEM), Transmission Electron Microscopy (TEM), Optical Tweezers, and applying optical tweezers. The second samples were characterized using Raman spectroscopy, X-ray diffraction (XRD), Elemental Analysis, Maldi-TOF, Fourier Transform Infrared Spectroscopy (FTIR), Electrochemical Analysis, Thermogravimetric Analysis (TGA), Scanning Electron Microscopy (SEM), and Transmission Electron Microscopy (TEM), where the samples were successfully applied in electrochemical sensors of ascorbic acid.

1.1 Objectives

This work synthesized supramolecular structures using the conductive polymer polyaniline and surfactants. Two stabilizers were used: sodium dodecyl sulfate (SDS) and poly(vinylpyrrolidone) (PVP). An interesting and vast types of structures were prepared and they were characterized to understand the chemical composition and the formation process of these materials. The secondary goal was to use the rod and plate structures obtained by the association PANI and SDS in electrochemical sensors and/or supercapacitors and the particles

obtained by the association of PANI and PVP in optical tweezers measurements for biological measurements.

2 LITERATURE REVIEW

2.1 Polyaniline

Polyaniline is a well-known conductive polymer obtained through the polymerization of its monomer aniline. The synthesis could be done in an acid (WU *et al.*, 2021) or basic (ZHOU *et al.*, 2008) solution using chemical oxidants or electrochemical deposition (DING *et al.*, 2021). The synthesis of aniline comes from the nitration of benzene by adding nitric acid and sulfuric acid at a temperature around 60 °C. This process results in the nitrobenzene that passes for the protonation process at 600 °C (Figure 2-1).

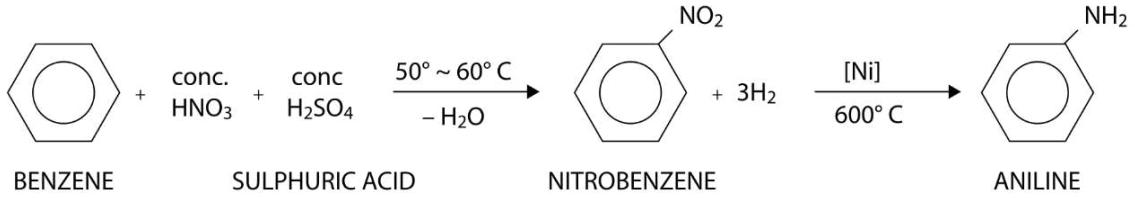

Figure 2-1. Process to produce the monomer Aniline. Adapted from the reference (LIU; SLECK; JONES, 2023).

The standard method of synthesizing polyaniline involves adding the monomer to an acid solution, for instance, hydrochloric acid, and adding ammonium persulfate (APS) as a chemical oxidant to initiate polymerization. This route of production of the polymers is used in this work. In this process, the monomers in an acid solution are protonated. After the addition of APS, the ion persulfate ($S_2O_8^{2-}$) interacts with the monomers, taking one of the paired electrons (e^-) pair of the nitrogen atom, oxidating the aniline and creating a free radical, Figure *2-2*. The unpaired electron could stay in the nitrogen or change the other three resonant positions in the aromatic ring (ortho, meta, and para), as shown in Figure *2-3* (BEYGISANGCHIN *et al.*, 2021). Typically, the radical stays in the nitrogen atom or the para position of the aromatic ring, so the polymer form is head-to-tail or tail-to-tail coupling through the covalent bond between the two free radicals, as shown in Figure *2-2*, forming the dimer (two monomers) (KHALID; HONORATO; VARELA, 2018). The propagation of the polymerization reaction continues by the repetition of the oxidation to the formation of trimers and so on until it reaches hundreds or

thousands of monomeric units bounded forming the polymer (STEJSKAL; SAPURINA; TRCHOVÁ, 2010).

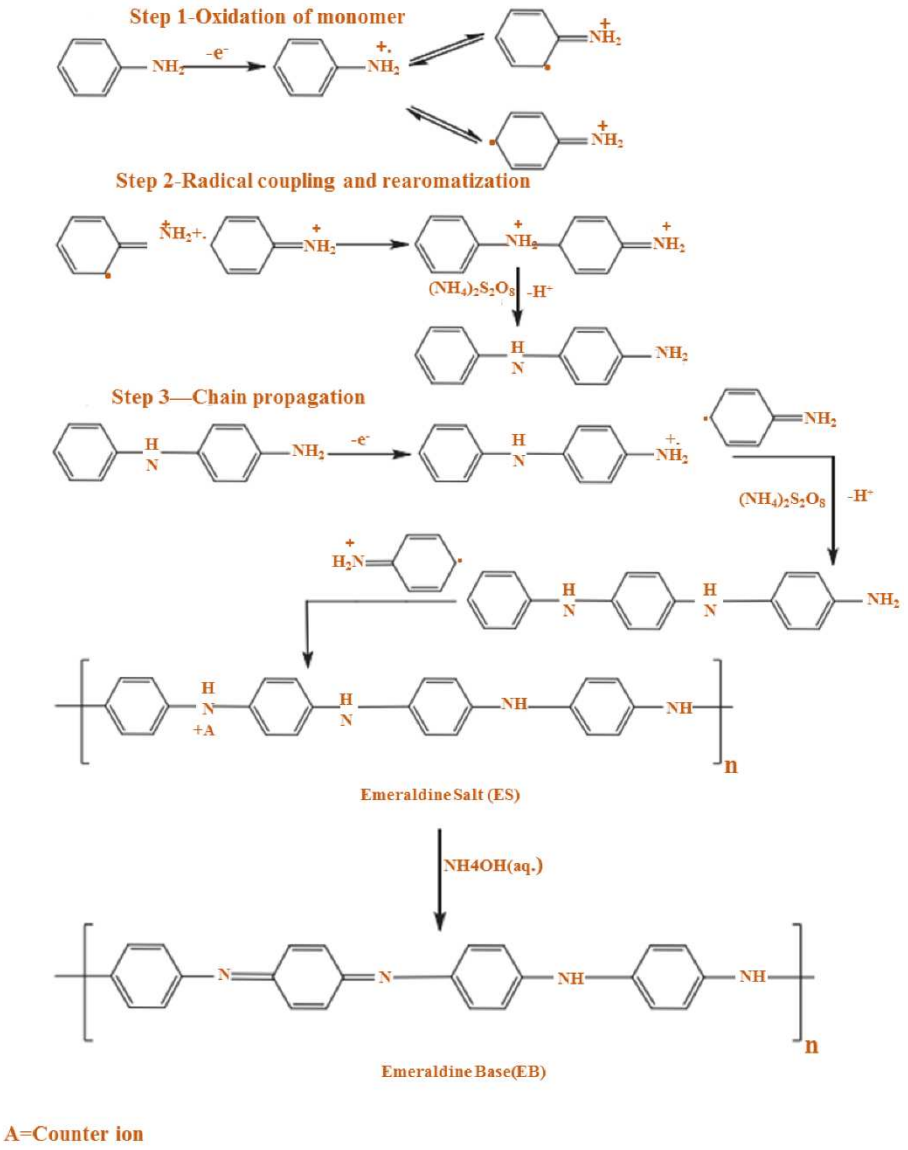

Figure 2-2. The polymerization process of aniline in acid solution. Adapted from the reference [*(BEYGISANGCHIN et al., 2021)*].

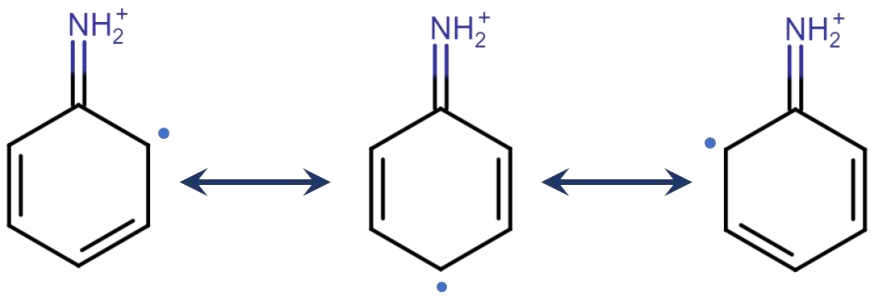

Figure 2-3. Resonant positions for the free radical in the aniline molecule.

The PANI obtained by the polymerization of aniline is a conductive polymer in a stable form of the Salt Emeraldine (half oxidized). Other stable bases of PANI are the Blue Emeraldine base (half oxidized), Colorless Leucoemeraldine (fully reduced), Violet Pernigraniline (fully oxidized), and Violet Pernigraniline Salt (fully oxidized), shown in Figure *2-4* (BOEVA; SERGEYEV, 2014). In the Emeraldine Salt form, the polymer is a conductor, and the other, the PANI, is an insulator. All these forms of polyaniline can be modified in the others through doping (dedoping), meaning the addition or removal of a proton and/or oxidation (reduction) processes. Some doping techniques can be achieved by the exposure of the PANI to acid (gas or solution), electrochemical, or induced radioactive (KHALID; HONORATO; VARELA, 2018). Changing the PANI Emeraldine Salt (green) to Emeraldine base (blue) is made by the dedoping process that uses an alkaline solution. The conversion of these two bases is reversible simply by the addition of an acid/alkaline solution. For the conversion from Emeraldine base to Pernigraniline base or Colorless Leucoemeraldine, an oxidation(reduction) process is required, which can be achieved by electrochemical or induced radioactive methods.

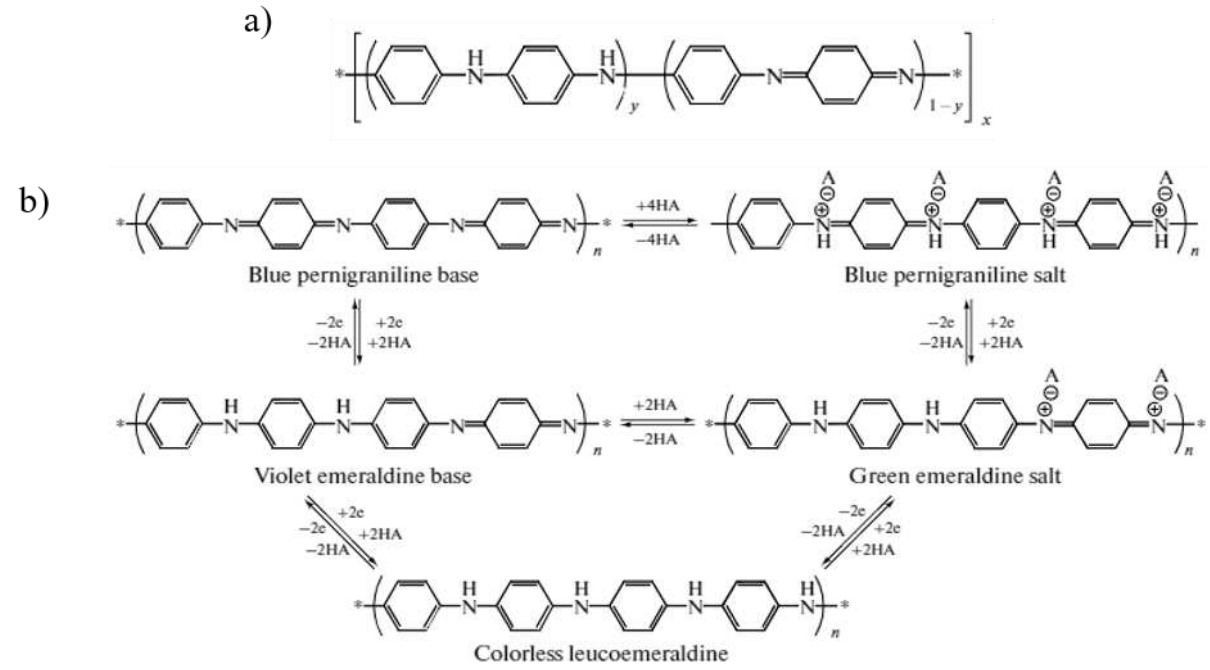

Figure 2-4. a) Polyaniline amina (fully reduced) and imina (fully oxidized) structures. b) Polyaniline bases in different oxidation and doping states. Adapted from the reference [(BOEVA; SERGEYEV, 2014)].

Conduction only occurs in conjugated polymers where carbon atoms alternate between double and single bonds. Some examples of conductive polymers and their electrical

conductivity are shown in Figure *2-5*. To have this configuration, the carbon atoms undergo sp^2 hybridization, whereupon the $2s^2$ and $2p^6$ orbitals combine into three *sp* and one *p* orbitals, Figure 6. This permits the atom to do three covalent *σ (sp)* bonds and one covalent *π (p)* bond. The *σ* bonds are formed by the overlap of sp orbitals of two atoms in the head-to-head position, and *π* bonds are formed by the overlap of *p* orbitals side-to-side of two atoms in the lateral position (LOWER, 1999), causing them *σ* be stronger than *π* bonds shown in Figure *2-6* (LOWER, 1999). Because of the low energy and delocalization of the electrons in *π* bonds, the conduction in polymers happens in the *π* orbitals in the backbone bond (*π*-electron) (SINGH; RIAZ, 2022).

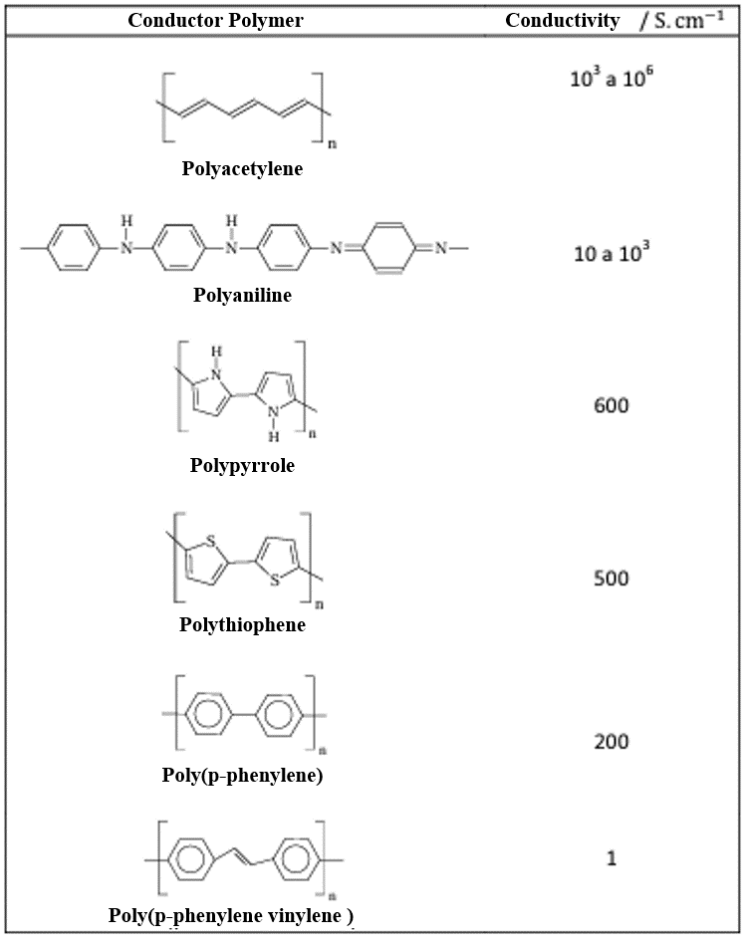

Figure 2-5. Some of the more important conductive polymers. Adapted from the reference (CEREGATTI, 2018).

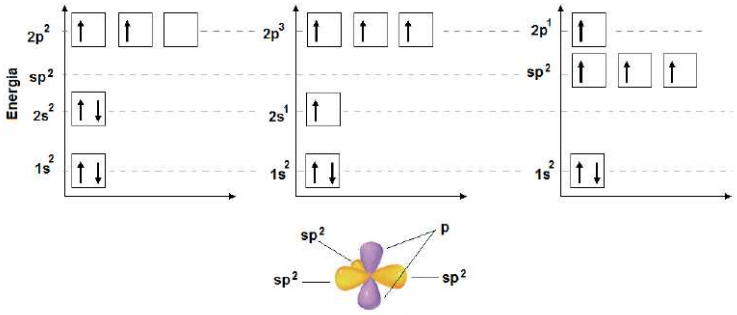

Figure 2-6. Carbon molecule sp^2 hybridization. Adapted from the reference: (LOWER, 1999).

Metals, semiconductors, and insulators are different in conductive because of the gap between the valence and conducting band; the same happens in polymers. To describe the properties of conductivity, it is usual to use the term Highest Occupied Molecular Orbitals (or HOMO) to the highest energy value in the valence band and the term Lowest Unoccupied Molecular Orbitals (or LUMO) is associated with the lowest energy value of the conducting band (MIRSAKIYEVA, 2017; NARAYANANKUTTY, [*s. d.*]). It is known that the size of polymer chains affects the energy gap between HOMO and LUMO orbitals, resulting in PANI oligomers being less conductive than PANI polymers.

Conduction in polymers occurs in π orbitals. The HUMO is the bonding π orbital, and the LUMO is the π^* unbonding orbital (Figure *2-7*). It is necessary to undergo a doping process in conductive polymers to create defects in the backbone chain. This produces extrinsic charge carriers such as polarons, bipolarons, solitons, and excitons, which create bands in the middle of the gap and reduce the energy necessary to go from π to π^* (NARAYANANKUTTY, [*s. d.*]; SINGH; RIAZ, 2022). The PANI can obtain the charge carried in a p-doping process using an acid solution, where the imina nitrogens interact with the H^+ release by the acid, gain two positive charges, and form a bipolaron as shown in Figure *2-8*. The double bond between nitrogens and carbons could be broken, separating the bipolaron into two polarons, resulting in a PANI Emeraldine Salt forming a polaronic lattice. The undoping process could be done in PANI and occurs with the addition of an alkaline solution. Polarons (radical ions) are pseudo-particles formed by the interaction between electrons or holes with defects in the chain. They have a charge equal to e^- (electron) or e^+ (hole) and spin 1/2. At PANI, polarons are related to holes. Bipolarons (dications) are the association of two polarons and, because of this, have a charge equal to 2e and a spin of 0.

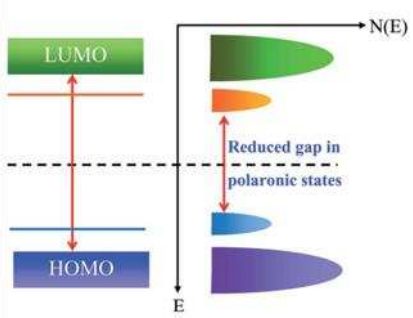

Figure 2-7. HOMO and LUMO orbitals in conductive polymers. Adapted from the reference (DEB; BERA; SAHA, 2016).

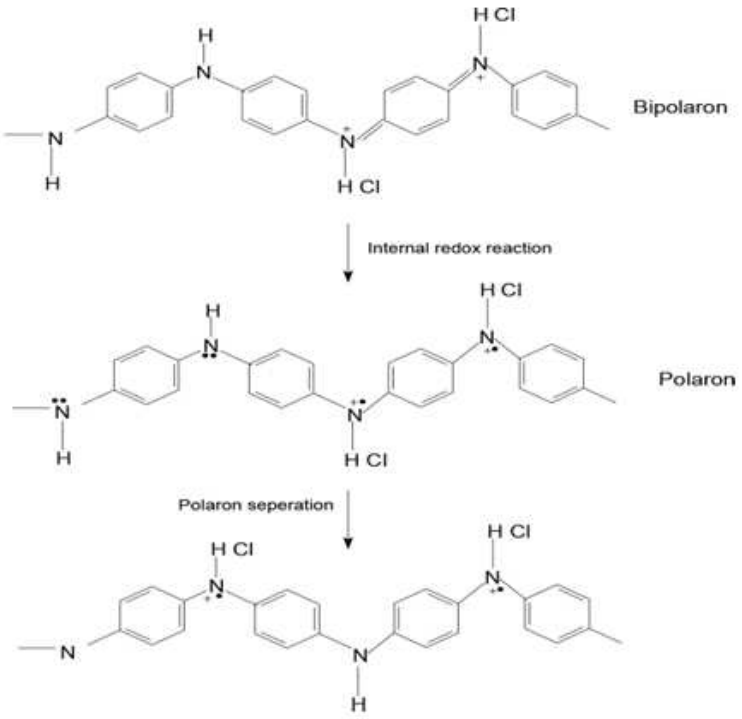

Figure 2-8. Bipolarons disassociate in to two polarons. Adapted from the reference [(KHALID; HONORATO; VARELA, 2018)].

These characteristics of conductivity that depend on the formation of charged groups and free radicals make the conductivity of polymers like PANI sensitive to the surrounding chemical environment. So, applying these materials in electrochemical and biological sensors is very interesting because the electrical conductivity could be tuned by chemical or biological compounds added to the solution. Also, since the color of the solutions can be changed by electric and chemical responses, this same material can be used in optics devices. Finally, there is the potential to apply this material in electric storage devices because of the possibility of oxidation/redox with electric response. Therefore, these properties allied with the low price and

facility to synthesize the polymer and to dope (undope), occasion the high interest in applying these macromolecules in electronic and optics devices, electric storage equipment (batteries and supercapacitors), biological systems, electrochemical sensors, purification of water, and protection of metals for corrosion (HEEGER, 2001).

2.2 Stabilizers

Surfactants (abbreviation for surface active agents) are molecules that have both hydrophobic (tail) and hydrophilic (head) parts, which allow them to favorable interact with both types of solvents regarding its polar or apolar behavior. In mixtures of insoluble solvents, the surfactant molecules usually concentrate in the interface, reducing the surface tension. The head part (usually a chemical group with an ionic bond) has an affinity with polar solvents (water) due to van der Waals or ionic forces. The tail (usually a hydrocarbon chain) has an affinity with apolar solvents (oil) or molecules (polymers) due to the hydrophobic interaction. The surfactants are classified as nonionic, anionic, cationic, and amphoteric, depending on the head's charge in the solution, as shown in Figure *2-9*.

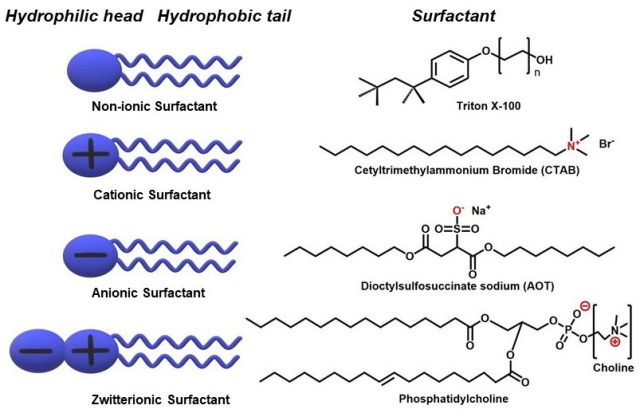

Figure 2-9. Examples of Surfactants. Adapted from the reference [(SOLEIMANI ZOHR SHIRI; HENDERSON; MUCALO, 2019)].

Because of these characteristics, surfactants can form self-organized aggregated structures depending on the concentration of this molecule. One of these structures is called micelles, and the concentration of surfactant required to create them is known as the Critical Micelle Concentration (CMC). Micelles are spherical-shaped surfactant aggregates with the

hydrophobic, or apolar, part of the molecules directed to the interior of the micelles and the hydrophilic, or polar groups facing the exterior. This happens in water solutions, but it is possible to have the opposite conformation (polar parts in the interior and the apolar outside the micelles) if organic solvents are used. These are the so-called inverse micelles. Due to this local phase separation (apolar interior and polar shell), micelles enable other apolar molecules to be enveloped in a polar solution, increasing their solubility. This property makes micelles widely used in the pharmaceutical and cosmetical industry. Increasing the surfactant's concentration makes it possible to change micelles' morphology for rod-like, hexagonal, cubic, or lamellar (DAVE; JOSHI, 2017). In this work, the surfactant used is the anionic sodium dodecyl sulfate (SDS), which is one of the most studied surfactants. This molecule has 12 carbons in the backbone chain, and the polar part is composed of ion SO_4^- (Figure *2-10*) and the CMC equal 8.2 mM at 25 °C. Poly(vinyl pyrrolidone) (PVP) is a polymeric surfactant often used as a stabilizer and it was also used in this work (SONG *et al.*, 2021) and its structure is shown in Figure *2-10*. The polymer has a hydrophilic part (the quinoid ring) and a hydrophobic part (the carbon chain). PVP can cover hydrophobic molecules in a solution, increasing their solubility.

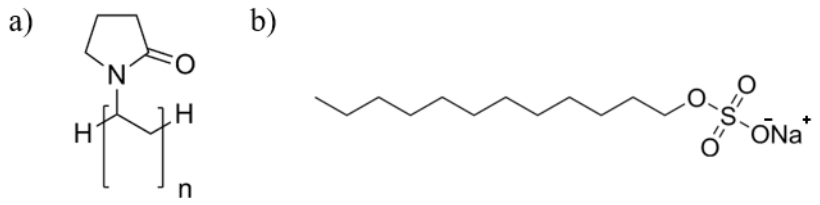

Figure 2-10. Chemical structure of a) PVP (on the left) and b) SDS (on the right) molecules.

2.3 Supramolecular structures of PANI

One of the supramolecular structures of PANI is obtained by adding stabilizers before the synthesis reaction starts with the objective of changing the morphology and properties of the PANI samples. Usually, surfactants or polymers surfactants as stabilizers because these macromolecules have amphiphilic properties, allowing interactions of van der Waals, ionic, and hydrophobic forces with the monomers (before the synthesis) and the polymers (after the synthesis). The common supramolecular structures formed using PANI and stabilizers are Rods, tubes, plates, and particles.

2.3.1 Rods and tubes

PANI rod and tube structures are commonly produced using SDS and SDBS as stabilizers. These surfactants are preferred because their negatively charged head attracts the positively charged PANI when doped in an acid solution, resulting in an ionic interaction. The difference between the two molecules is the presence of an aromatic ring in the head of the SDBS surfactant, as shown in Figure *2-11*.

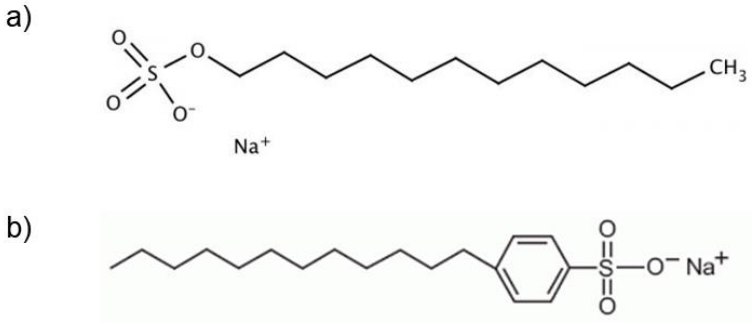

Figure 2-11. Molecular structure of a) SDS and b) SDBS.

(ZHOU; HAN; GUO, 2008) and (ZHOU; HAN; GUO, 2009) studied the supramolecular structures of PANI and SDS. They synthesized these structures using radical polymerization, with aniline as the monomer, SDS as the stabilizer, HCl as the acid dopant, and APS as the oxidant. By altering the concentrations of the stabilizers, acid dopants, and oxidants, they created different morphologies, such as tubes and rods.

To achieve the desired morphology of the samples, the concentration of SDS in the solution plays a crucial role, as illustrated in Figure *2-12*. The influence of SDS concentration was studied to maintain the [APS]/[aniline] ratio equal to 1 and 0.38 mM of HCl concentration. Increasing the concentration of SDS causes a transition of the morphology of the structures from tubes to rods. At an SDS concentration of 0.20 mM, tubes with square transversal sections are formed, measuring a few micrometers in length and a few hundred nanometers in diameter (Figure *2-12* a)). When the concentration is increased to 0.53 mM, the tubes continue to have a square transversal section, but their length and diameter increase and nanorods are formed (Figure *2-12* b)). When the SDS concentration is increased to 0.88 mM, significant changes can be noted in the surface of the rods and an increase in the number of nanorods (Figure *2-12* c)).

Finally, at a concentration of 1.27 mM of SDS (Figure *2-12* d)), the tubes turn into rods/plates, and the nanorods and granular structures on the surface of the rods disappear.

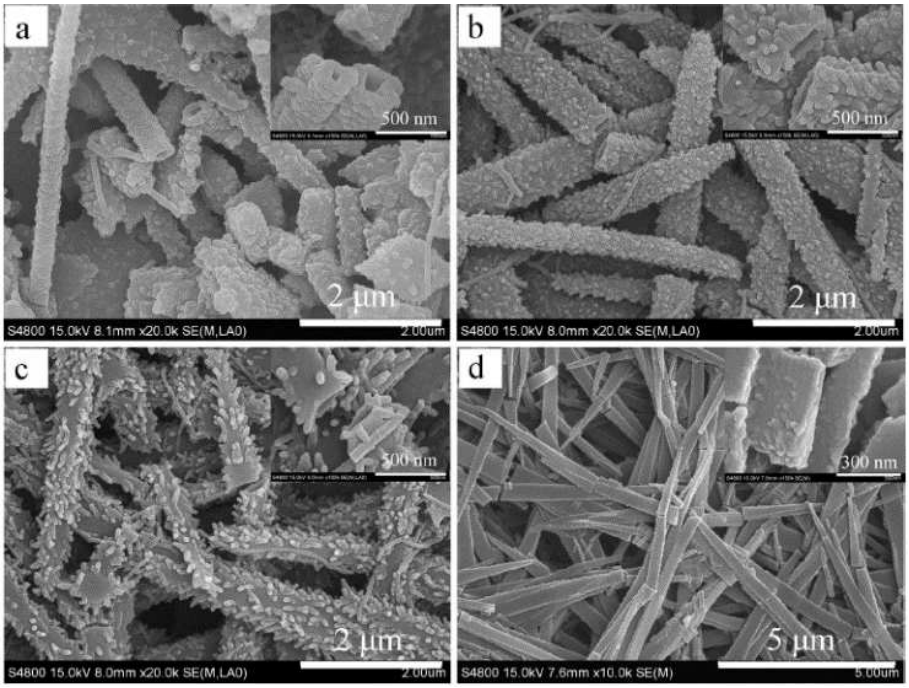

Figure 2-12. Zhou et al. studied the influence of SDS on the morphology of supramolecular structures of PANI-SDS. The SDS concentrations are a) 0.20 mM, b) 0.53 mM, c) 0.88 mM, and d) 1.27 mM. Adapted from the reference (ZHOU; HAN; GUO, 2009).

In the same study, the authors investigated the effect of varying the ratio of [APS]/[aniline] (0.4, 0.6, and 0.8) on the morphology of the samples. The concentration of SDS was kept constant at 0.87 mM and 0.38 mM HCl. The results showed that a lower ratio of [APS]/[aniline] promoted the formation of rods, while a higher ratio of [APS]/[aniline] (greater than 0.6/1) promoted the formation of tubes. Moreover, a higher ratio led to an increase in the granular structures on the surface of the tubes.

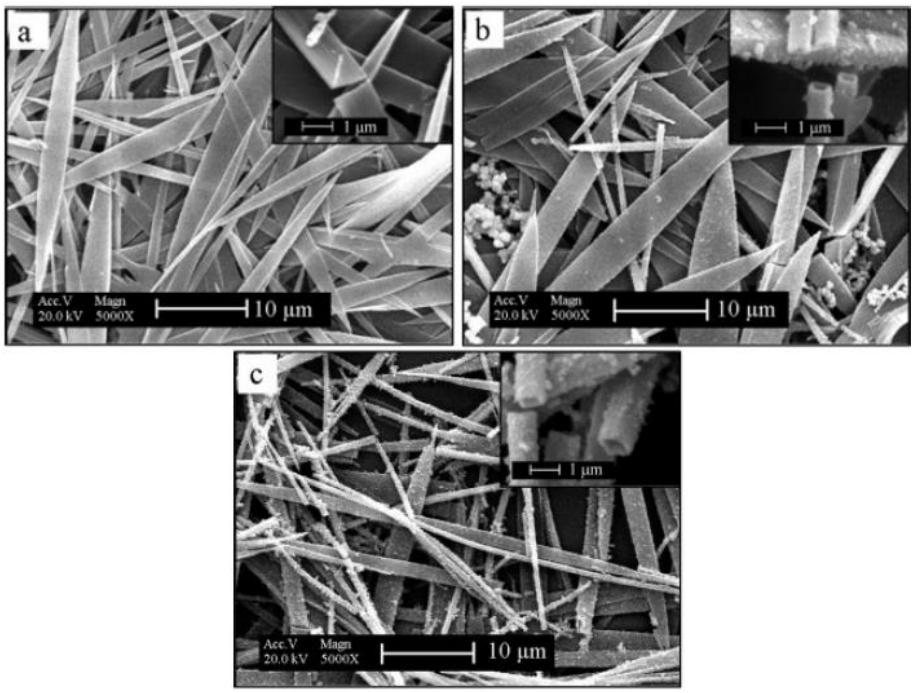

Figure 2-13. Influence of APS concentration in the morphology. [APS]/[aniline]: a) 0.4/1, b) 0.6/1, and 0.8/1. Adapted from the reference (ZHOU; HAN; GUO, 2008).

Zhou et al. studied the effect of varying HCl concentrations on the formation of nanorods on the tube surface at [SDS] of 0.53 mM and [APS]/[aniline] of 1. The HCl concentrations analyzed were 0.075 mM, 1.15 mM, 2.5 mM, and 5.25 mM. The results showed that an increase in HCl concentration leds to a rise in the number of nanorods formed, as shown in Figure *2-14*. Therefore, supramolecular structures with rod and tube morphology can be achieved by altering the SDS, APS, or HCl concentration.

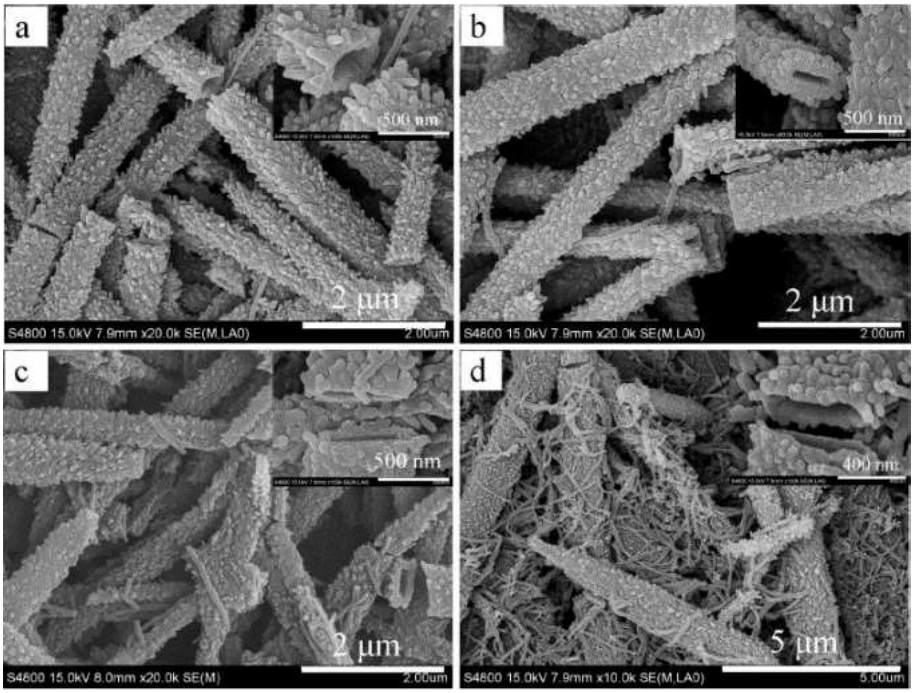

Figure 2-14. The influence of HCl concentration in the rods is a) 0.075 mM, b) 1.15 mM, c) 2.5 mM, and d) 5.25 mM. Adapted from the reference (ZHOU; HAN; GUO, 2009).

2.3.2 Particles

The most commonly observed morphology of polyaniline samples in the literature is particle-like structures. These particles can be produced through the use of surfactant polymers like poly(vinyl alcohol) (PVA) (RIEDE *et al.*, 1998; STEJSKAL; KRATOCHVÍL; HELMSTEDT, 1996), poly(vinyl pyrrolidone) (PVP) (RIEDE *et al.*, 1998; STEJSKAL; KRATOCHVÍL; HELMSTEDT, 1996), hydroxypropyl cellulose (HPC) (RIEDE *et al.*, 1998; STEJSKAL *et al.*, 1999), and colloidal silica (CS) (RIEDE *et al.*, 1998; STEJSKAL *et al.*, 1996), as well as surfactants such as SDS and dodecyl trimethyl ammonium chloride (DTAC) (PRASANNAN *et al.*, 2011).

Stejskal et al. published several works using PANI for diverse applications. Here, the focus is on his study to produce PANI particles using the PVA, PVP, HPC, and CS and investigate the influence of temperature, polymerization time, and aniline concentration in the morphology of the particles. Particles of PANI and HPC, shown in Figure *2-15*, were synthesized in the following conditions: [aniline]/[APS] = 1; [aniline] = 0.2 M; and 2 wt% of

hydroxypropyl cellulose. It could be noted that the particles have a hydrodynamic radius (R_h) of around 300 nm and low size dispersity.

Temperature influence during the polymerization was also studied using three values: 0°C, 20°C, and 40°C, as shown in Figure *2-16*. It is possible to note that particles are obtained at 0°C temperature. High temperatures potentialize the aggregation of the particles and the formation of connecting rods or coral-like structures.

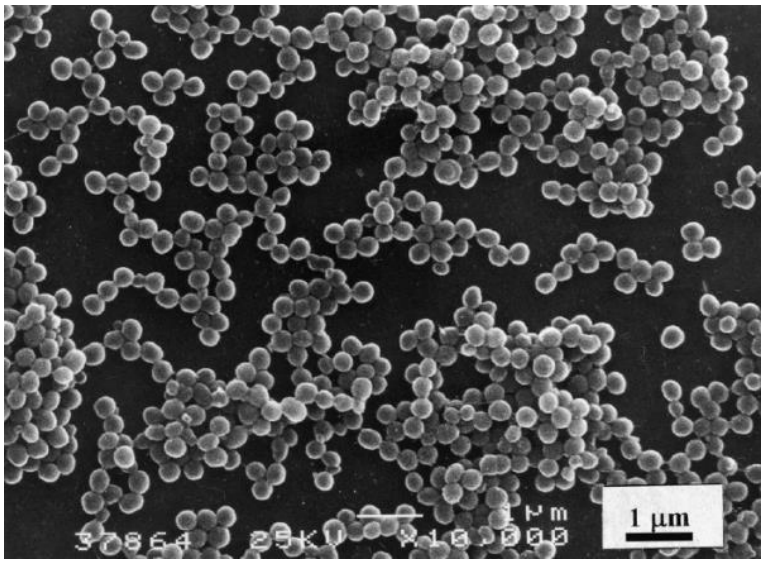

Figure 2-15. PANI particle stabilizers using HPC. Adapted from the reference (STEJSKAL *et al.*, 1999).

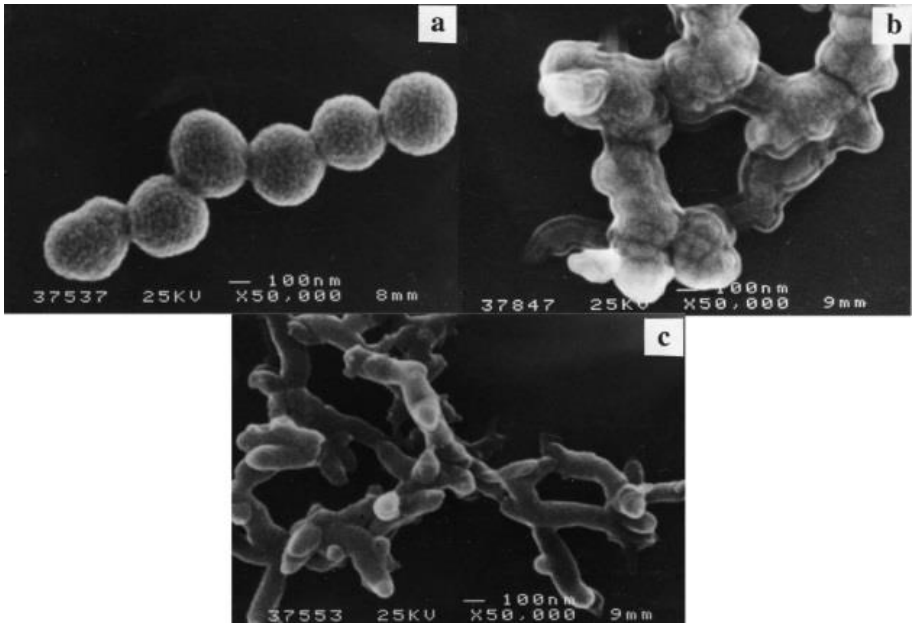

Figure 2-16. Temperature influences the formation of PANI and HPC particles from a) 0°C, b) 20°C, and c) 40°C. Adapted from the reference (STEJSKAL *et al.*, 1999).

Hydrodynamic radius (R_h) dependence with the time of polymerization was studied and it is shown in Figure *2-17*. The morphology change can be noted by the increase of R_h with temperature because the R_h of the coral-like structures will be bigger than that of the particles. Also, the temperature influences the time interval to stabilize the particles or the end of polymerization. For high temperatures, the time for the end of polymerization is lower.

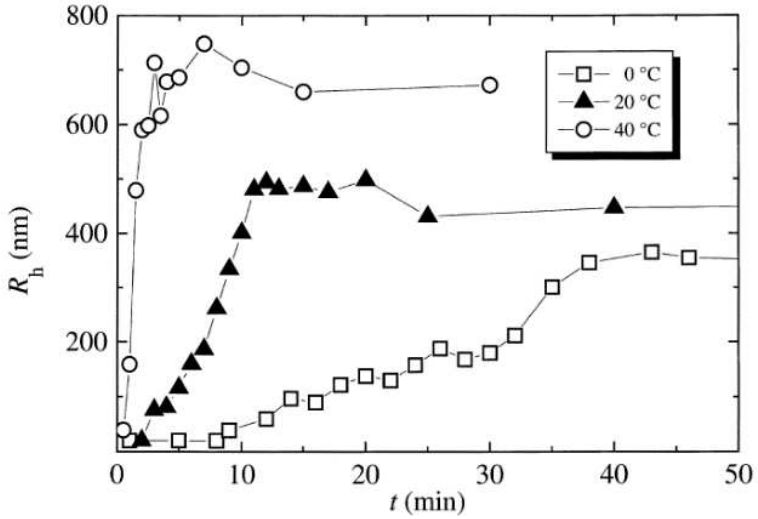

Figure 2-17. The hydrodynamic radius of PANI and HPC colloids depends on temperature (0°C, 20°C, and 40°C). Adapted from the reference (STEJSKAL *et al.*, 1999).

PANI particles synthesized with PVA as stabilizers were made using polymer surfactant concentration equal to 20 g/L, [aniline]/[peroxydisulfate] = 2, and temperature 0 °C are shown in Figure *2-18*. It is possible to note that particles are less regular and more polydisperse than using HPC as stabilizer.

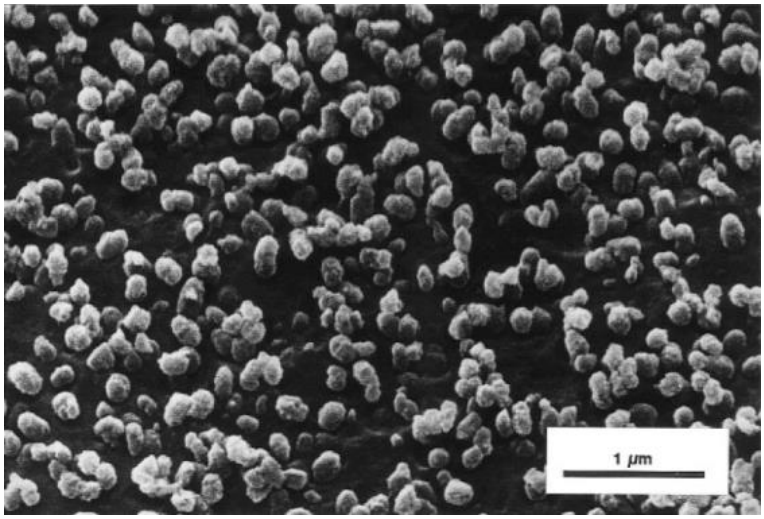

Figure 2-18. SEM images of PANI particle stabilizers using PVA. Adapted from the reference (STEJSKAL *et al.*, 1996).

Stejskal analyzed the influence of aniline concentration in the particles' hydrodynamic diameter (D_h) using dynamic light scattering (DLS) and the effect of stirring the samples during the polymerization time. Figure *2-19* shows that the stirred process change has a slight reduction in the D_h and an improvement in the uniformity of the particles (reduction from 0.28 to 0.22 the statistical variance of the size of particles). Also, the size of the particles increases with the concentration of aniline, probably because the aggregation of particles occurs in high concentrations.

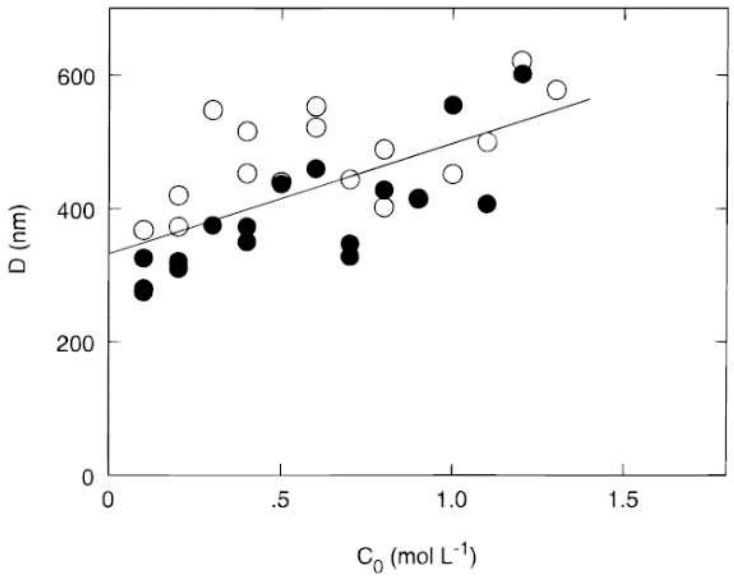

Figure 2-19. Hydrodynamic diameter in dependence of aniline concentration for PANI and PVA particles. The empty circles are without, and the full circles are with the stirred process during the polymerization. Adapted from the reference (STEJSKAL *et al.*, 1996).

PVP particles was also studied by Stejskal using 20 g/L of polymer surfactant, [aniline]/[peroxydisulfate] = 2, and temperature 0 °C. His analysis also showed the influence of aniline concentration in the D_h and the stirred in the polymerization period of the particles shown in Figure *2-20*. It could be noted that the hydrodynamic diameter changes slightly with the concentration of aniline and the stirred. There was no improvement in the uniformity of particles and the statistical variance of the size of particles from 0.29 to 0.27.

Varying the temperature of synthesis of PANI and PVP particles, Figure *2-21* shows that the increase in temperature reduces the time to stabilize the particle size (end of polymerization). It is possible to see that particles produced at 0°C have a radius bigger than those produced at 10°C, 20°C, and 30°C. However, the R_h increases for temperatures bigger than 10°C.

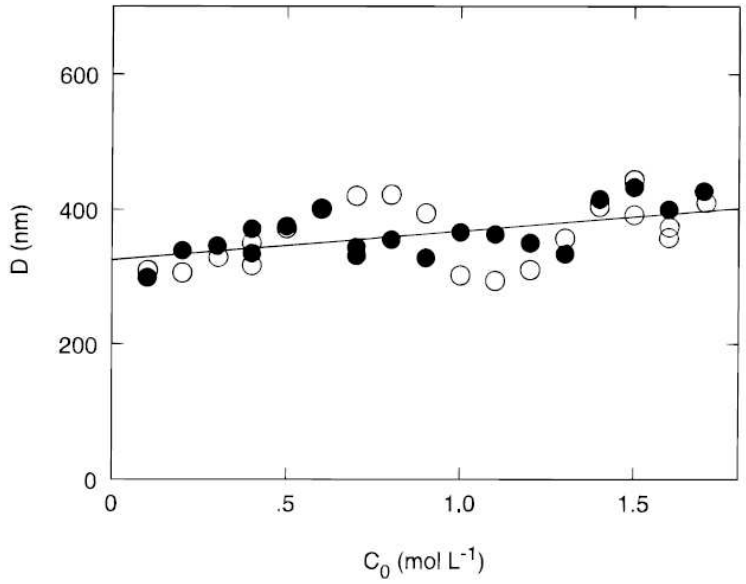

Figure 2-20. Hydrodynamic diameter in dependence of aniline concentration for PANI and PVP particles. The empty circles are without, and the full circles are with the stirred process during the polymerization. Adapted from the reference (STEJSKAL *et al.*, 1996).

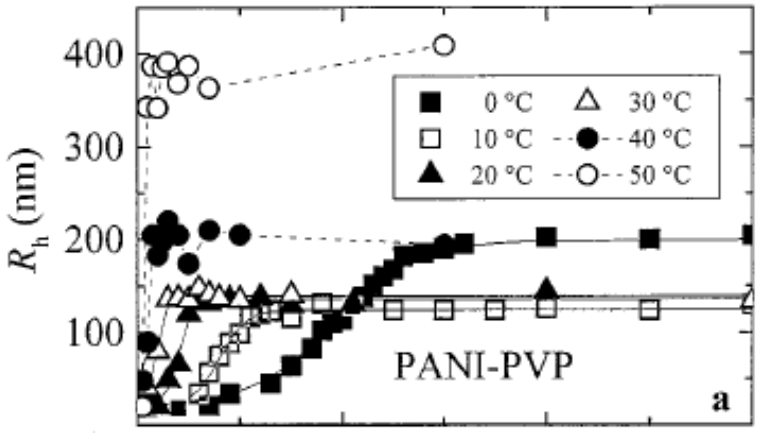

Figure 2-21. Temperature influences the polymerization of PANI and PVP particles. Adapted from the reference (RIEDE *et al.*, 1998).

3 MATERIALS AND METHODS

This section outlines the process of producing and treating PANI samples and the methods used to characterize and apply the materials.

3.1 MATERIALS

3.1.1 Synthesis of PANI

Polyaniline was obtained using a radical synthesis with an oxidant agent as an initiator of the polymerization. The chemical products used in the synthesis were aniline (132934 99%) and ammonium persulfate (A3678), both of which were purchased from Sigma Aldrich, and hydrochloride acid 37% (0607400) was purchased from Vetec. The procedures for producing the polymers are shown in Figure *3-1* and detailed as follows: 10 mL of water (milli-Q) was added to the flask, and aniline and HCl was added so the final concentration was [aniline] = 115 mM and [HCl] = 100 mM. The flask was wrapped in aluminum paper to protect the samples from light degradation and kept at around 0° C. Then 1.25 mL of APS (1 M) solutions was slowly added at a rate of 20 μL/min to the 10 mL of aniline and HCl solution for around of 1 hour using a syringe pump or by drops using the decantation funnel for better control of the volume injection, the final concentration of APS in solution is 115 mM. Along the titration of the APS solution and in the next hour a gradative change in the solution color could be observed from transparent to dark green. After the 1 hour of the APS addition, the samples were kept stirred for more 4 hours. Past 5 hours from the beginning of the synthesis (1 hour of injection and kept stirred for more 4 hours), the sample was taken out to the ice bath and let to rest protected from light for 24 hours.

PANI polymers synthesized using radical synthesis required cleaning to remove non-reactive substances such as monomers, oligomers, salts, and APS. The process involves filtering samples through a paper filter and a vacuum pump. Simultaneously, the samples are washed with a 0.2 M HCl solution and acetone until the solution passing through the filter

becomes colorless. The samples were dried in a dissector, and a dark green powder was obtained as a final product.

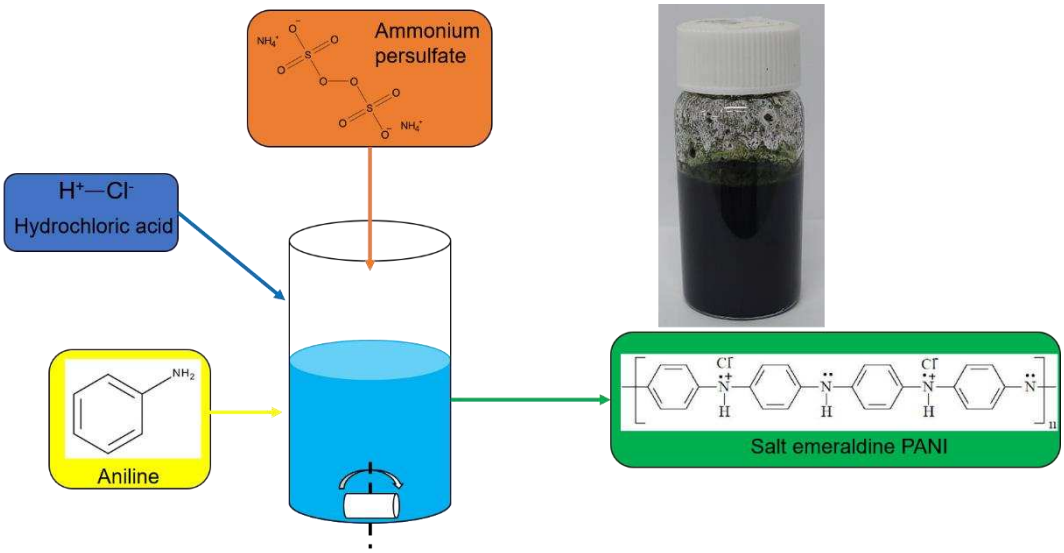

Figure 3-1. Illustration of PANI synthesis process

3.1.2 Synthesis of particles of PANI and PVP

Particles of PANI and PVP were synthesized using the same components described in the previous section with the addition of poly(vinyl pyrrolidone) (81440) purchased from Sigma Aldrich. The difference between producing PANI polymers and PANI particles is the addition of the stabilizer in a water solution and waiting until the samples become homogeneous. After this happens, aniline is added, and the procedure is continued, as described before shown in Figure *3-2*. The PVP concentration used for producing the particles was 2.5% m/m (0.0056 mM), and the ratio of [aniline]/[APS] was equal to 1 as before.

PANI and PVP particles were cleaned in the same filtering process. The difference is that in the particles, the samples were dedoping using a high concentrate sodium hydroxide (NaOH) solution (1 M), causing the aggregation of particles and facilitating the filtering. For washing, the same NaOH solution and acetone were used until the solution from the filter became colorless.

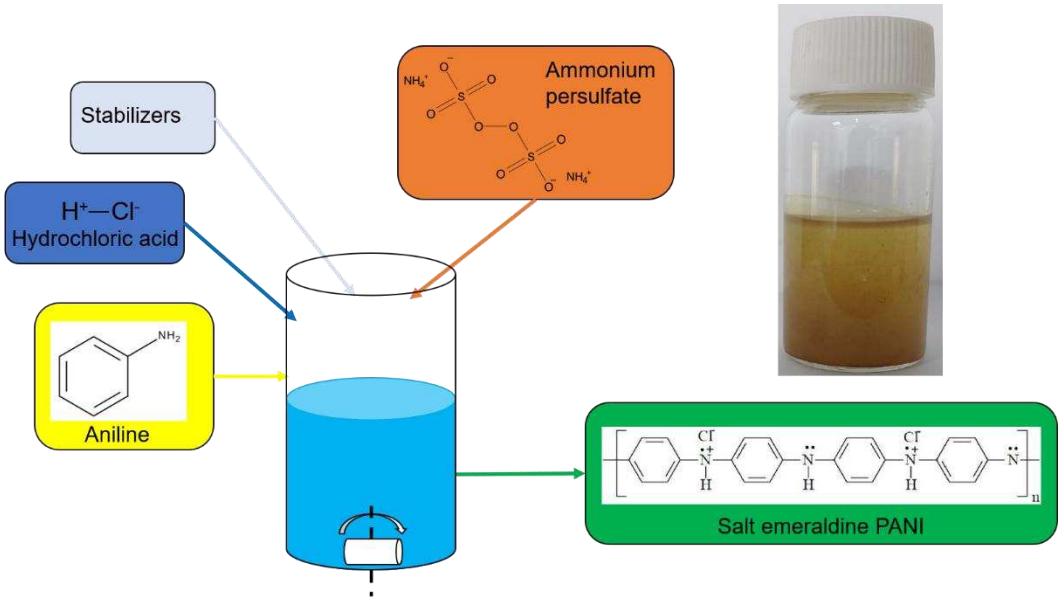

Figure 3-2. Illustration of PANI supramolecular structures.

3.1.3 Synthesis rods/plates of PANI-SDS

PANI-SDS composites were produced following the same procedure as described in the previous section (PANI and PVP) but using SDS instead of PVP, Figure *3-2*. The SDS concentration used was 17.5 mM for all the experiments, this concentration was higher than the CMC of this surfactant in water (8.2 mM). For PANI-SDS samples were studied the influence of temperature and [aniline]/[APS] ratio in the chemical structures and the morphology of the sample change these components during the synthesis. Two different temperatures were studied during the synthesis: 0°C and room temperature (~20°C). The influence of the APS concentration was tested by change the concentration of the injected solution from 5, 20, 50, 100, 200, 500, and 1000 mM remain 1.25 mL of solution injected. This represents values for [aniline]/[APS] ratio of 0.005, 0.02, 0.05, 0.1, 0.2, 0.5, and 1, respectively. In all samples the titration of the APS solution was still maintained for 1 hour for all the samples.

The cleaner process for these samples was filtration using a paper filter and vacuum pump. The solution of PANI-SDS samples was firstly diluted in an HCl (0.2 M) and ethanol solution in a 1:5 proportion; after this, the samples were passed through the paper filter, and the powder results were dried in a dissector.

3.1.4 Synthesis rods/plates of copolymers and SDS

Copolymer synthesis consists of samples using two monomers; in these cases, the monomers used are aniline and p-phenylenediamine (PDA). They differ by the number of amina (NH_2) groups: aniline has one amina group, and PDA has two amina groups, with the second in the para position, Figure *3-3* a). The synthesis follows the illustration shown in Figure *3-2*, with the difference being that the two monomers were added simultaneously. The influence of three types of dopant agents was studied using the different acid solutions: HCl acid, sulfuric acid (H_2SO_4), and camphor-10-sulfonic acid (CSA - Figure *3-3* b)), all with 0.2 M concentration. The concentrations of the monomers used were 0.05 M of aniline and 0.05 M of PDA, causing the ratio of aniline/PDA to be equal to 1, and the APS concentration was 0.1 M, maintaining the ratio of monomers and initiator equal to 1. Samples were made with and without SDS using the same concentration as before (17.5 mM). All the synthesis were performed at room temperature.

To clean the samples, a paper filter and filtration by gravity were made. After the solution passed through the filter, the precipitate was washed using 30 mL of HCl solution (0.2 M) and 20 mL of ethanol. Then, the samples were dried in a dissector, and the final product was obtained.

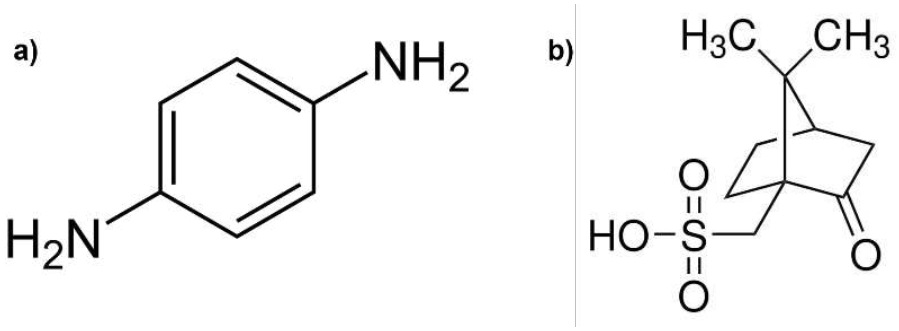

Figure 3-3. Chemical structures of a) PDA and b) CSA.

3.2 EXPERIMENTAL TECHNIQUES

3.2.1 Conductometry

Conductometry is an experimental technique that measures the electrolyte conductivity and it is used to understand the chemical reactions and interactions in the solution. It is an interesting technique for following, for instance, a polymerization reaction in situ. The equipment is formed by a probe electrode which is immersed in the sample. To measure the electrolyte conductivity, this probe has two platinum electrodes covered by platinum oxide organized like two parallel plates between them. An electrical potential difference is applied between them to produce an electric field. As solutions have ions dissolved, this electric field will accelerate them between the electrodes, forming an electrophoretic current. The potential difference applied and the electric current response measured by the equipment give us the sample resistance (R) necessary for calculating the specific conductance or electrolytic conductance (κ). It is possible to write the sample resistance in the function of the distance between the electrodes (d), the surface area of the electrodes (A), and the specific resistivity (ρ) as shown in Eq. (1).

$$R = \rho \frac{d}{A}. \tag{1}$$

As the conductance (L) is the inverse of the resistance, it is possible to write the conductance as a function of the electrode properties, Eq. (2).

$$L = \frac{1}{R} = \frac{A}{\rho d}. \tag{2}$$

The electrolytic conductance (κ) can be related to the conductance by Eq. (3). Showing that κ is the inverse of the specific resistivity (ρ).

$$\kappa = L\frac{d}{A} = \frac{1}{\rho}. \tag{3}$$

In this work, the equipment used was the Digimed DM-32, shown in Figure *3-4*, with a range of electrolytic conductance between 0 to 20 mS/cm. The equipment is available in the Laboratório de Microfluídica e Fluidos Complexos in the Department of Physics at Universidade Federal de Viçosa (UFV).

Figure 3-4. Equipment Digimed DM-32. Adapted from the reference: Digimed website acess by https://www.digimed.ind.br/br/.

3.2.2 Dynamic Light Scattering

Dynamic Light Scattering (DLS) is a technique that characterizes the dynamic properties of colloidal solutions by the interaction of the molecules with a coherent and colimate light source, usually a laser beam. This technique permits obtaining information about the diffusivity of the samples like the diffusion coefficient, the hydrodynamic radius and even the length and thickness for rod-like structures. Also, it is possible to obtain the molar mass, the second virial coefficient, and the gyration radius (for Static Light Scattering (SLS) using the same equipment). The principle of the technique consists of the fact that the laser beam is an electromagnetic wave source. So, when a laser beam reaches a colloidal solution, the electric charges present in the sample will be accelerated by the oscillatory electric and magnetic field. Charges accelerated emit radiation in all directions with different wavelengths (DE CARVALHO TEIXEIRA, 1998), Figure *3-5*. This emitted radiation is the so called scattered light.

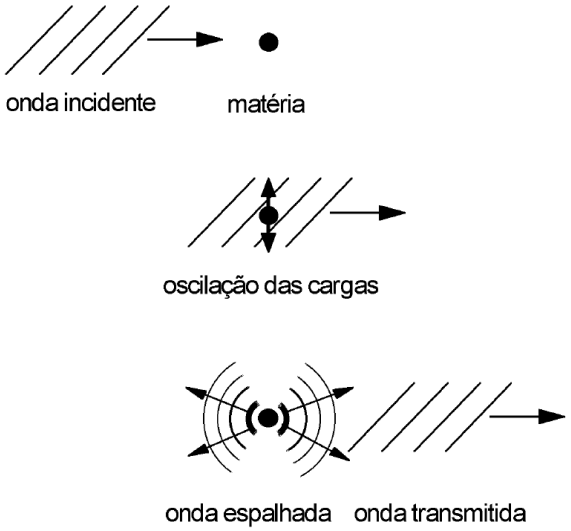

Figure 3-5. Illustration of a light scattering of a charged spherical particle. The first line before the light interacts with the particle. The second line is the particle oscillation caused by the electromagnetic wave. The third line is the light scattering of particles in all directions. Adapted from the reference (DE CARVALHO TEIXEIRA, 1998).

There are two kinds of scattering: elastic (Rayleigh) or inelastic. If the light scattering has the same wavelength as the light source, it is called elastic scattering; otherwise, it is called inelastic scattering. In the DLS technique, we are interest is in the elastic scattering because this kind of light gives information about the motion of particles. To select the wavelength, the equipment owns a filter for the detector. It is well-known that in temperatures over 0 K, the particles present in a material have enough energy to move and interact with each other. At room temperature, the particles in a solution are moved freely in a Brownian motion (aleatory). This movement will influence the light scattering of the samples and make them float around at an average intensity; analyzing these fluctuations using an autocorrelation function can give us information about the diffusion of these particles. The autocorrelation function $\left(g^{(2)}(\tau)\right)$ correlates the intensity of light scattering at different times, normalized by the square of the average intensity normalizes it:

$$g^{(2)}(\tau) = 1 + \frac{\langle I(t)I(t+\tau)\rangle}{\langle I\rangle^2}. \quad (4)$$

A typical curve obtained for an autocorrelation function is shown in Figure *3-6*. For monodisperse particles in dilute regime These curves have an exponential behavior, where β is the amplitude, and Γ the decay, as seen in Eq. (5).

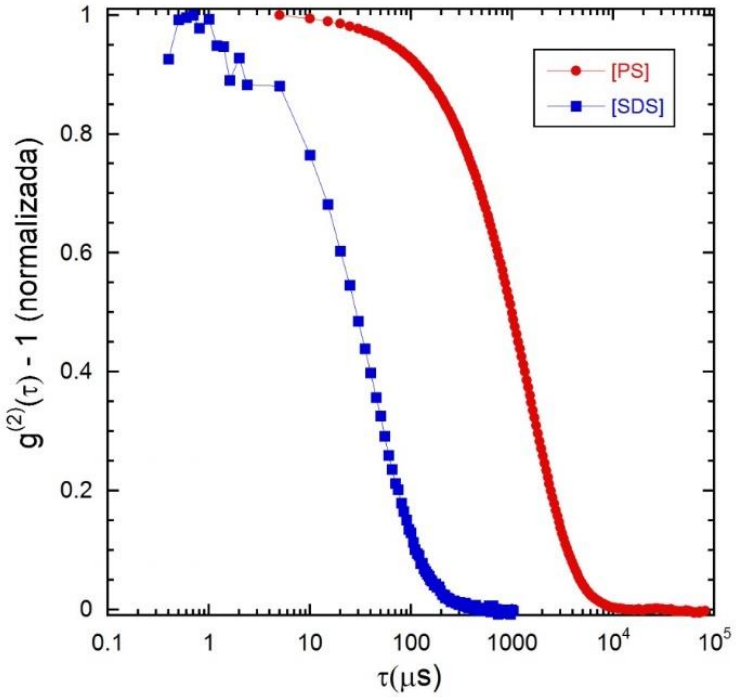

Figure 3-6. Autocorrelation function for different-sized particles, where the red circles represent polystyrene particles and the blue square represents an SDS micelle.

$$g^{(2)}(\tau) = 1 + \beta \exp(-2\Gamma\tau). \tag{5}$$

Eq. (5) is valid only for diluted systems where the particles are free and have the same size. The coefficient Γ can be related to the diffusion coefficient (D) and the scattering vector (q) by Eq. (6).

$$\Gamma = Dq^2. \tag{6}$$

The module of the scattering vector (q) depends on the solvent index of refraction (n), scattering angle (θ), and the laser wavelength (λ), by:

$$q = \frac{4n\pi}{\lambda} \operatorname{sen} \frac{\theta}{2}. \tag{7}$$

The diffusion coefficient for spherical particles inside a liquid with a low Reynolds number can be calculated by the Stokes-Einstein equation, where the diffusion coefficient is related to the solution viscosity (η), Boltzmann constant (k_B), temperature (T), and the hydrodynamic radius (R_h), shown in Eq. (8).

$$D = \frac{k_B T}{6\pi\eta R_h}. \tag{8}$$

The DLS measurements were made using Brookhaven Co. equipment for multiangular dynamic and static light scattering (goniometer BI9000 and correlator TurboCorr) and a He-Ne laser with a wavelength of 632.8 nm. The equipment is shown in Figure *3-7* and is available in the Laboratório de Microfluídica e Fluidos Complexos (LMFFC) in the Department of Physics of UFV.

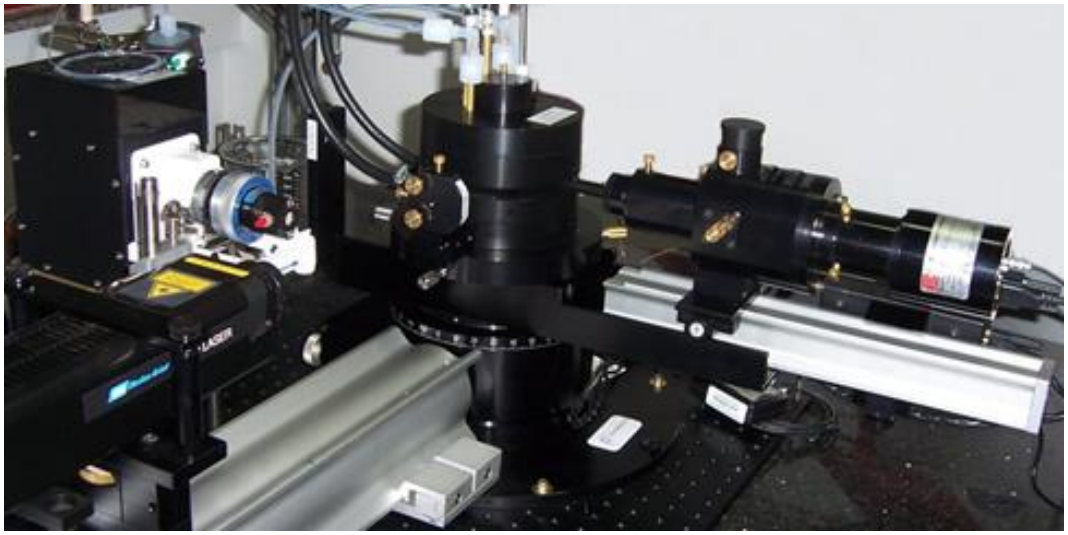

Figure 3-7. Light scattering equipment Brookhaven Co. Adapted from: Website of Laboratorio de Microfluidica e Fluidos Complexos access by http://www.lmffc.ufv.br/.

3.2.3 Raman spectroscopy

Raman spectroscopy is also an experimental technique that uses an electromagnetic wave to interact with the sample and take the properties from the scattering light. Raman is a vibrational spectroscopy used to characterize the chemical structures and orientation of the

sample. The equipment uses a laser with a fixed wavelength and analyzes the inelastic scattering light from the samples. The inelastic scattering light comes from a photon that interacts with a molecular vibrational and changes its energy, giving information about the molecular vibrational energy levels. If the photon excites the molecule from the ground state to a virtual state and then the molecule decays directly to a ground state, the photon emitted will have the same energy, giving the Rayleigh scattering. However, if the photon excites the molecules from the ground state to a virtual state and after the molecule drops down to a higher vibrational level, then the ground state will have a Stokes-Raman scattering, Figure 3-8. It is possible that the molecule starts at a higher vibrational level and is excited to a virtual level; when it returns, it goes to a ground state level and the so-called Anti-Stokes Raman scattering happens. Rayleigh scattering is more intense than Stokes-Raman scattering (around 10^7 times more), making it necessary for the equipment to use filters to obtain just the Stokes-Raman scattering light.

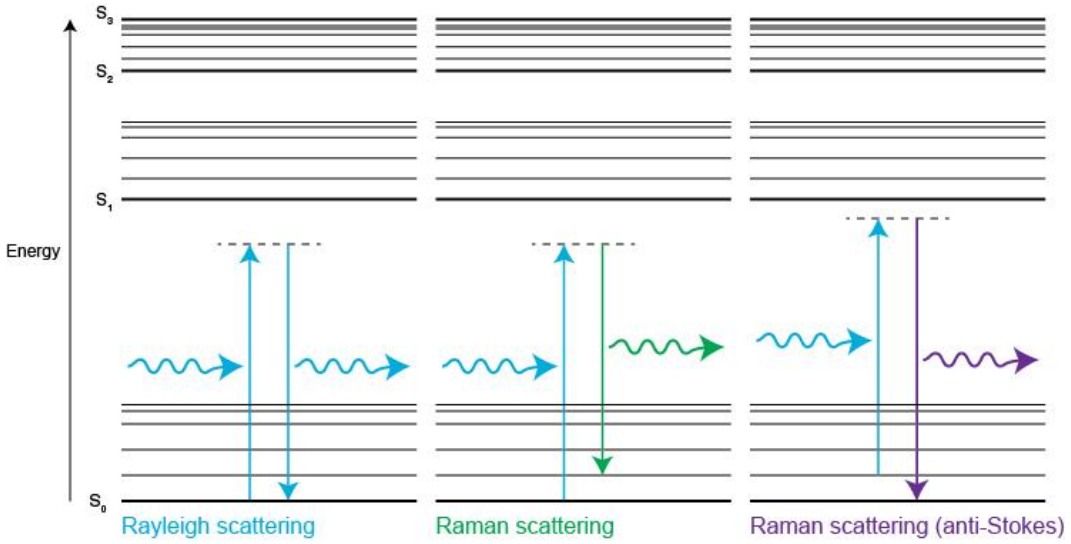

Figure 3-8. Different scattering happens when a molecule with a light. Adapted from: *https://www.renishaw.com/en/what-is-raman-scattering--25805.*

Raman spectroscopy is related to molecular polarizability, so the Raman selective rules are shown in Figure *3-9* (DONOSO, 2012), where it can be seen that Raman is active just if the molecular vibration and rotations change the molecule polarizability (α) in relation to the normal coordinate at the equilibrium configuration (Q). Figure *3-9* is an example of the vibration modes of diatomic molecules with two equal atoms (N_2) in the second column and two different atoms (CO) in the third column. The three last column is for a triatomic molecule as (CO_2). The first line shows the molecules in the equilibrium configuration, and the second line shows some vibration modes of these molecules. The third line has an illustration of the

polarizability variation in relation to *Q*. The forth line show the derivate of the polarizability in the position Q and when the derivate is different from zero the vibrations is active in Raman (fifth line).

molecule	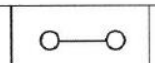	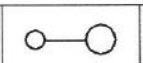	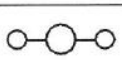		
vibration	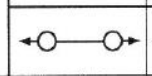	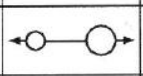	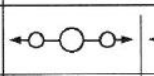	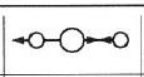	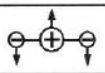
change of α with Q	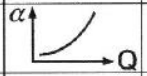	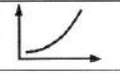	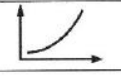	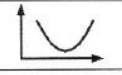	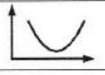
$\frac{d\alpha}{dQ}$	≠0	≠0	≠0	=0	=0
Raman active	yes	yes	yes	no	no
change of $\vec{P}_D$ with Q	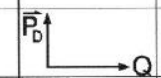	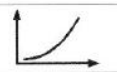		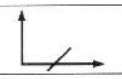	
$\frac{d\vec{P}_D}{dQ}$	=0	≠0	=0	≠0	≠0
infrared active	no	yes	no	yes	yes

Figure 3-9. Raman and FTIR selective rules for diatomic and triatomic molecules. Adapted from the reference (DONOSO, 2012).

Figure 3-10. Equipment MicroRaman - Renishaw Invia is available at Laboratorio de Espectroscopia Raman in the Physics Department (UFV). Adapted from the Website from Physics Department at UFV access by the link http://www.posfisica.ufv.br/?page_id=81#ER.

Raman spectroscopy analysis can identify the materials present in the sample using the spectral fingerprint, amount of material, molecular orientation, stress/strain tensions, and uniformity of the crystallinity. This work will use the equipment to identify the materials and

molecular orientation. The equipment used is the MicroRaman Renishaw Invia, laser excitation 514 nm, 633 nm, and 785 nm, as shown in Figure 3-10. It is available in the Laboratorio de Espectroscopia Raman in the Physics Department of Physics from of UFV. Also, the equipment Renishaw inVia Raman micro spectrometer (633 nm laser line; Leica DM LM microscope; holographic grating with 1800 lines mm^{-1}) and a Renishaw inVia Qontor Raman micro spectrometer (488 and 830 nm laser lines; Leica DM LM microscope; holographic gratings with 1800- and 1200-lines mm^{-1}) available in the Institute of Macromolecular Chemistry (Czech Academic of Science) in Prague, Czech Republic.

3.2.4 Fourier-Transform Infrared spectroscopy (FTIR)

Fourier-transform infrared spectroscopy is a technique that identifies the chemical structure in organic and inorganic materials like Raman spectroscopy. The measurements consist of the sample (powder) reached for infrared radiation varying the wavelength from around 100 to 10000 cm^{-1}, and this radiation can be absorbed or transmitted by the sample. The absorbed light will be converted into vibrational and rotational energy for the molecules in the samples, giving information about the chemical structures present in the material, such as fingerprints of the molecules. Figure *3-9* shows the FTIR selective rules, showing that FTIR is a technique that requires changes in the molecule's dipole moment when excited by the electromagnetic wave to be active. Because of this, FTIR and Raman spectroscopies are complementary, powerful techniques to understand the chemical structures of samples.

FTIR spectra were obtained using a Bruker VERTEX 70 instrument, using the Attenuated Total Reflectance method in the 400-4000 cm^{-1} range, available in the Department of Chemistry at UFV. Also, the Thermo Nicolet NEXUS 870 FTIR spectrometer with DTGS detector in transmission mode in KBr pellets in the range 400-4000 cm^{-1} with resolution 2 cm^{-1}. The spectra were corrected for the carbon dioxide and humidity in the optical path, available in the Institute of Macromolecular Chemistry (Czech Academic of Science) in Prague, Czech Republic.

3.2.5 Optical Tweezers

Optical tweezers are ais the name given to the technique that possibly holds and moves manipulates individual colloidal structures with sizes ranging from tenths of nanometers to micrometers. For this, the equipment consists of a laser beam that passes from an optical path to be intensely focused by some optical components, such as an objective lens. The highly focused electromagnetic wave can interact with the samples by attractive or repulsive forces with the typical range of femtoNewtons to hundreds of picoNewtons. Depending on the intensity of these forces, the samples can be held or scattered. Suppose the samples are formed by spherical particles with a size bigger than the wavelength of the light. In that case, the attractive and repulsive forces can be explained using ray or geometric optics by the refraction and scattering of the light by interaction with the particle. The light could be reflected and refracted when the laser beam passes through the particle (see Figure 3-11 a)). The light refracted and reflected by the particle changes the total linear momentum ($\vec{p}$) because its components change the directions. By Newton's second law, Eq. 9, and the conservation of the linear momentum, the change of the light momentum will create a force in the particle with the direction of the focus of the beam. However, the light reflected by the particle will create a force in the opposite direction of the refracted force. If $\vec{F}_{\text{reflected}}$ is bigger than the $\vec{F}_{\text{refracted}}$ the particle will be expelled by the laser. However, if the $\vec{F}_{\text{refracted}}$ is bigger than the $\vec{F}_{\text{reflected}}$, the particle will be trapped in the focus of the laser where the position of stability occurs when the forces are equal.

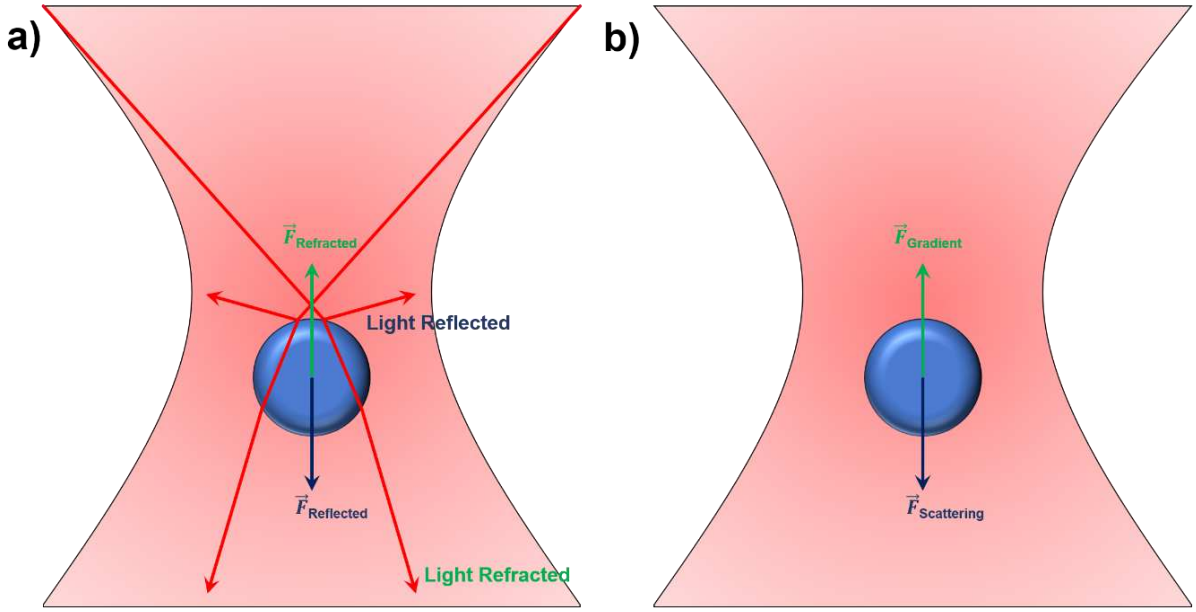

Figure 3-11. Illustration of the optical forces acting in the particle: a) geometric optics ($D_{particle} >> \lambda_{laser}$) and b) Rayleigh regime ($D_{particle} << \lambda_{laser}$).

$$\vec{F} = \frac{d\vec{p}}{dt} \tag{9}$$

The scattering (reflected) and gradient (refracted) forces can be obtained using Newton's second law (ASHKIN, 1992; ROCHA, 2009):

$$F_s = \frac{nP}{c}\left\{1 + R\cos 2\theta - \frac{T^2[\cos(2\theta - 2r) + R\cos 2\theta]}{1 + R^2 + 2R\cos 2r}\right\} = \frac{nP}{c}Q_s, \tag{10}$$

$$F_g = \frac{nP}{c}\left\{R\sin 2\theta - \frac{T^2[\sin(2\theta - 2r) + R\sin 2\theta]}{1 + R^2 + 2R\cos 2r}\right\} = \frac{nP}{c}Q_g, \tag{11}$$

Where n is the refractive index from the particle, P is the laser power, c is the light velocity, θ is the incidence angle, and r is the refractive angle. The total force can be calculated by following the Eq. 12.

$$F = F_s + F_g = \frac{nP}{c}Q, \tag{12}$$

where Q is

$$Q = \sqrt{(Q_g{}^2 + Q_s{}^2)}. \tag{13}$$

The coefficients *R* and *T* represent the reflectivity and transmissivity, respectively, and can be calculated as in Eq. 14 and 15.

$$R(\theta, r) = \frac{1}{2}\left[\frac{\sin(\theta - r)}{\sin(\theta + r)}\right]^2 + \frac{1}{2}\left[\frac{\tan(\theta - r)}{\tan(\theta + r)}\right]^2, \tag{14}$$

$$T(\theta, r) = 1 - R(\theta, r). \tag{15}$$

However, if suppose the samples are formed by spherical particles with a size smaller than the wavelength of the light, the regime will be ruled by the Rayleigh scatterer whose forces of gradient and scattering occur by the polarizability response of the particles after interaction with an electromagnetic light. These forces can be calculated using the electric dipole approximate, so the gradient force can be calculated by an induced dipole force, where:

$$\vec{p}(\vec{r}, t) = \alpha\, \vec{E}(\vec{r}, t), \tag{16}$$

and

$$\vec{F}(\vec{r}, t) = (\vec{p}(\vec{r}, t).\nabla)\, \vec{E}(\vec{r}, t), \tag{17}$$

α is the polarizability, and *E* is the electric field of the laser light. Therefore, the force calculation gives gradient force (Eq. 18), Figure 3-11b).

$$\vec{F}_g(\vec{r}) = \frac{1}{2n\varepsilon_0 c}\alpha\nabla I(\vec{r}). \tag{18}$$

I is the light intensity and ε_0 is the permittivity of the vacuum. The scattering force can be calculated by the Poynting vector of the beam, as can be seen in Eq. 19. Where σ is a particle cross-section containing the contribution of absorption and scattering and the time-averaged of the Poynting vector $\langle\vec{S}\rangle$.

Typically, optical tweezer measurements are realized in a solutions environment. Therefore, the particles will stay in a Brownian motion. For modeling, this problem can be used to approximate mass and spring problems using the Hooke Law to calculate the trap stiffness.

The optical tweezers equipment used consists of a linearly polarized infrared laser operating in the usual Gaussian (TEM00) mode, wavelength λ = 1,064 nm, with an (8.80 ± 0.08) mm beam waist measured at the objective entrance (whose aperture diameter is 6.0 mm). The tweezers are mounted on a NikonTi-S inverted microscope with a 100×N.A. 1.4 oil-immersion objective. The equipment is available in the Laboratório de Física Biológica of the Physics department in the UFV.

Figure 3-12. Optical Tweezers available in the Laboratório de Física Biológica on the physics department in the UFV. Adapted from the Website from Physics Department at UFV access by the link http://www.posfisica.ufv.br/?page_id=81#ER.

3.2.6 Electrochemical Analysis

The electrochemical analysis is a set of experimental techniques available in a potentiostat equipment that permits the evaluation of the chemical response of some samples by using electrical stimulation. The experimental setup in most electrochemical techniques comprises three electrodes: the working, counter, and reference. All the electrodes are connected to a potentiostat and immersed in an electrolyte solution, Figure *3-13*. The sample is deposited in the working electrode where the oxidation/reduction reactions occur, giving information about the material; typically, the working electrode is constructed with composite of carbon. The reference electrode is used to obtain an electrical potential fixed and defined between the reference and the working electrode; usually, the material used is silver or silver

chloride (Ag/AgCl). The counter electrode is used to avoid the electrolysis process; typically, the material used is platinum (Pt).

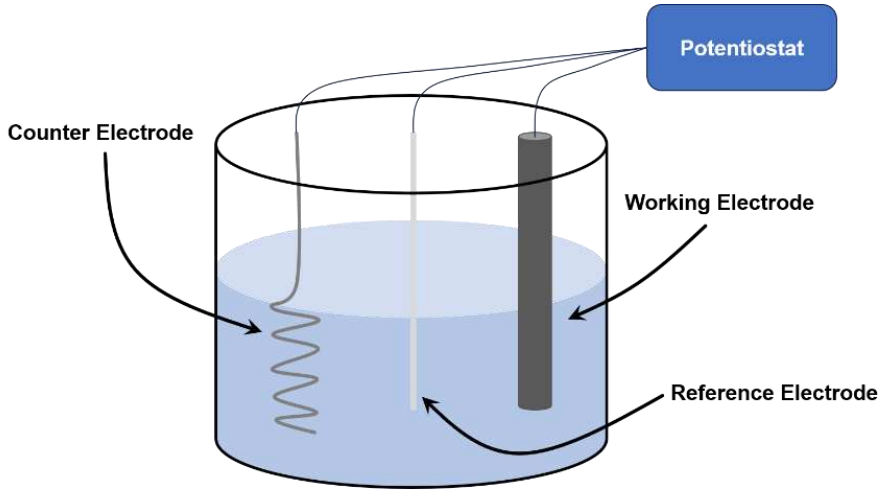

Figure 3-13. Illustration of the organization of the electrodes in a typical electrochemical measurement.

Figure *3-14* presents a scheme of the principal dynamic electrochemical techniques used to characterize polymer materials. This work used techniques in which the potential is controlled, such as cyclic voltammetry (CV), chronoamperometry (CA), charge-discharge measurements, and electrochemical impedance spectroscopy (EIS). These methods have the experimental set shown in Figure *3-13* and it is possible to obtain the following information about the samples:

- Cyclic voltammetry: the current is measured changing the applied voltage in the time. The parameters of the experiment are the maximum and minimum voltage, the voltage scan rate (V/s) and number of cycles. The results are generally plotted in a curve of current vs potential that gives information about: oxidation/reduction by peaks and gravimetric capacitance by the curve area; variations of the intensity of the peaks with the scan rate, which give informations about the diffusion of the ions, the capacitance contribution of the layers (trasatti's method analysis) and can be used to calibrate curves of electrodes used as sensors. The cyclic voltammetry measurements also provide information about the stability of the samples for a long number of cycles, which is essential in the characterization of supercapacitors and batteries.
- Chronoamperometry: This is method that the applied voltage follows a step curve and the variation of the current is evaluated in time. Because of this, the technique is usually

applied to produce the calibration curve of the sensor through the study of the variation of the current by the increment of some material in the solution.

- Galvanostatic charge-discharge: The galvanostatic charge/discharge (GCD) evaluates the sample's electric potential variation by applying a consecutive constant positive and negative current to charge and discharge them. This process corresponds to one cycle of the measurements. Therefore, GCD usually is used to evaluate energy storage materials such as batteries and supercapacitors.
- Electrochemical impedance spectroscopy: unlike the other methods described above, Electrochemical Impedance Spectroscopy (EIS) uses an alternating current (AC). With this, changing the frequency of the sine wave of the potential possibility makes it possible to scans the samples from high to low frequencies and obtains the complex impedance (Z). The imaginary and complex parts of Z are analyzed with the frequency. Other analysis can be made as the Nyquist Plot (-Im Z vs. Re Z). To analyze the data, an electrical equivalent circuit is created with electrical elements such as resistors (R), capacitors (C), constant phase element (CPE), and inductance (L), which permits fitting the equation and obtaining the information about the process interface electrode-electrolyte.

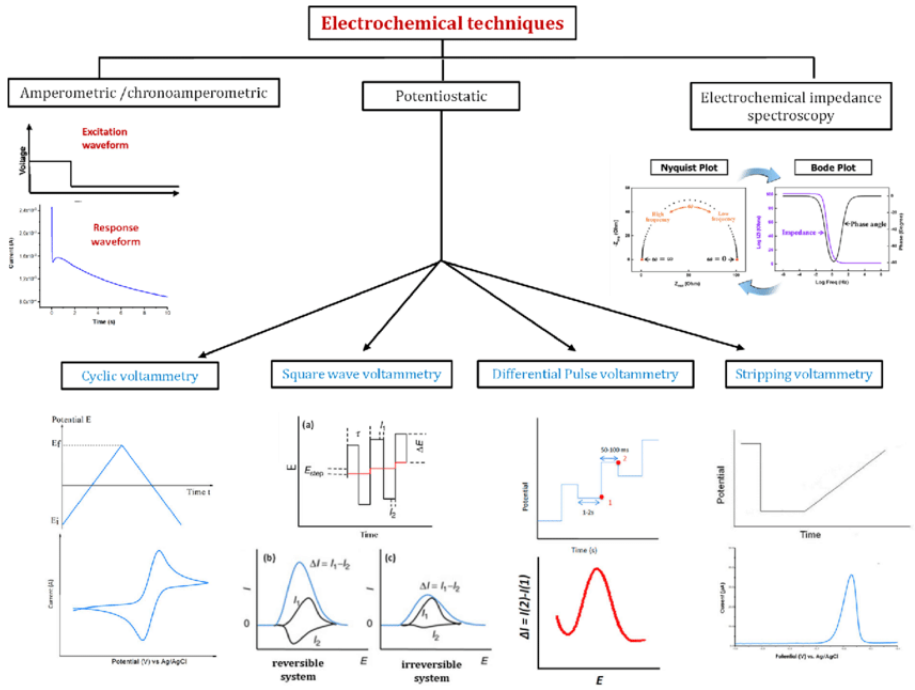

Figure 3-14. Scheme of standard electrochemical techniques used for polymer characterization. Adapted from the reference [(ZHENG *et al.*, 2021)].

This technique can be used to study materials' electrochemical properties and apply them in sensors, batteries, and supercapacitors. The equipment used was a Bio-Logic SAS VSP-300 potentiostat available at the Institute of Macromolecular Chemistry (Czech Academic of Science) in the conducting polymer department in Prague, Czech Republic.

Figure 3-15. Equipment used was a Bio-Logic SAS VSP-300 potentiostat available at the Institute of Macromolecular Chemistry (Czech Academic of Science) in the conducting polymer department. Image adapeted from the website acess from the link: https://cromocol.se/en/produkter/vsp-300/.

3.2.7 X-ray Diffraction

X-ray diffraction (XRD) is a non-destructive technique used to study the crystalline structure of samples. The method consists of focusing a beam with an x-ray frequency in a sample and analyzing the elastic light scattering from the sample. The scattering happens when the electromagnetic wave interacts with an atom in a crystalline plane of the sample. However, the beam will interact with some crystalline planes of the sample, not just one, causing destructive or constructive interference in the reflected light, creating an interference pattern in the samples, Figure *3-16*. As the incident angle (θ) of the crystalline plane by the electromagnetic wave will be the same as the reflected one, the distance (d) between two atom planes can be calculated using Bragg's law (Eq. 19), where λ is a wavelength and n is the

number of wavelengths. This law correlates the constructive peak with the respective interatomic distance.

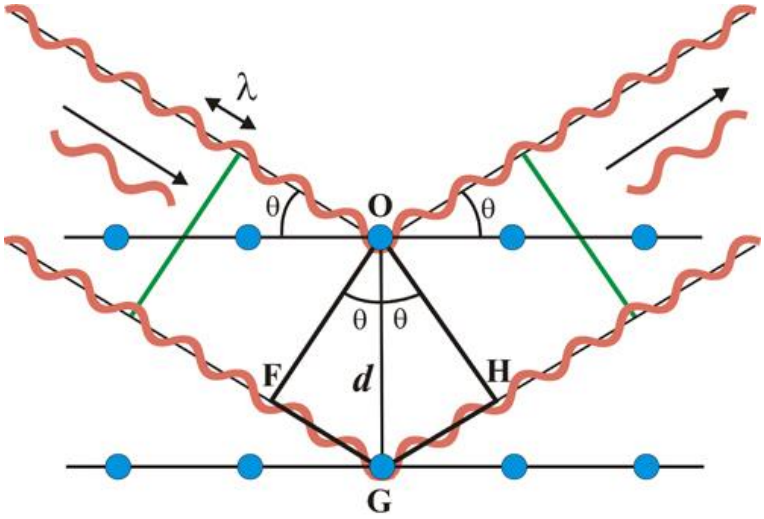

Figure 3-16. Bragg's diffraction in a crystal material. Adapted from the reference [https://www.xtal.iqf.csic.es/Cristalografia/parte_05_5-en.html].

$$n\lambda = 2d \sin\theta. \tag{19}$$

Using X-ray light with wavelengths in the range of 1 to 100 Å can improve the intensity of diffractions since they are close to the distances between atoms. Therefore, this equipment was used in this work to understand the crystallinity of the materials. The equipment used is D8 Discover, available in the Laboratório de Difração e Espalhamento de Raios-X at the Department of Physics in UFV, and Bragg-Brentano geometry was performed under the CuKα radiation (wavelength λ = 1.54 Å) using a high-resolution diffractometer GNR Explorer (Italy) with a Mythen 1K strip detector available in the Institute of Macromolecular Chemistry (Czech Academic of Science) in Prague, Czech Republic.

Figure 3-17. D8 Discover, available in the Laboratório de Difração e Espalhamento de Raios-X at the Department of Physics in UFV. Adapted from the Website from Physics Department at UFV access by the link http://www.posfisica.ufv.br/?page_id=81#ER.

Figure 3-18. High-resolution diffractometer GNR Explorer (Italy) with a Mythen 1K strip detector available in the Institute of Macromolecular Chemistry (Czech Academic of Science). Adapted from the Website from Institute of Macromolecular Chemistry access by the link https://www.imc.cas.cz/en/research/research-departments/.

3.2.8 Elemental Analysis

Elemental Analysis is a technique that provides reliable measurements of the amounts of carbon (*C*), hydrogen (*H*), nitrogen (*N*), sulfur (*S*), and chloride (*Cl*) present in a sample; the equipment is also known as CHNS or CHN analysis. To obtain this information, the equipment consists of controlled combustion of the samples in an inert atmosphere and the detection of the oxide gases resulting from the material, such as (H_2O, CO, CO_2, N_2, SO_2, SO_3, and N_xO_y) by reducing them catalytically and separated in chromatography columns for be detect by a thermally conductive detector. Different from techniques such as EDX, the Elemental analysis gives the exact percentage of the elements in the sample that can be used to understand the composition of the samples and the ratio of the components in the samples. The equipment used was the CHNS/O FlashSmart Elemental Analyzer, manufactured by Thermo Scientific and available at the Institute of Macromolecular Chemistry (Czech Academic of Science) in Prague, Czech Republic.

Figure 3-19. CHNS/O FlashSmart Elemental Analyzer, manufactured by Thermo Scientific and available at the Institute of Macromolecular Chemistry (Czech Academic of Science). Adapted from the Website from Institute of Macromolecular Chemistry access by the link https://www.imc.cas.cz/en/research/research-departments/.

3.2.9 Maldi-TOF

Matrix-assisted laser desorption/ionization (MALDI) and mass analyzer time of flight (TOF) is a mass spectrometry technique used to evaluate the ratio of mass/charge (*m/z*) of the samples. The measurements happen by diluting the powder samples in organic solvents and adding a matrix solution. The final solution will be added to the sample holder. A laser reaches the sample and ionizes it in charged molecules. These molecules will be accelerated by a differential of potential (Electric field). Because of the difference in the ratio of mass/charge, the molecules will be dispersed along the time of flight. Therefore, the detector can identify the different m/z molecules in the materials and provide information about the presence of oligomers and non-react molecules in the samples. The equipment used was MALDI-TOF/TOF mass spectrometer UltrafleXtreme, manufactured by Bruker Daltonik and available at the Institute of Macromolecular Chemistry (Czech Academic of Science) in Prague, Czech Republic.

Figure 3-20. MALDI-TOF/TOF mass spectrometer UltrafleXtreme, manufactured by Bruker Daltonik and available at the Institute of Macromolecular Chemistry (Czech Academic of Science). Adapted from the Website from Institute of Macromolecular Chemistry access by the link https://www.imc.cas.cz/en/research/research-departments/.

3.3.10 Thermogravimetric Analysis (TGA)

Thermogravimetric Analysis (TGA) is another mass spectrometry technique where the variation of the mass percentage is analyzed by constantly varying the temperature over time. The equipment is composite from a high-precision balance inside an oven. The sample is inserted over the balance, and the temperature constantly increases from 15 °C to 900 °C in the air or N_2 atmosphere. The results from the equipment are mass in different temperatures that can be studied by the variation of mass percentage with temperature. These results give information about thermal stability, oxidation, combustion, thermogravimetric kinetics, and the components present in the material. The equipment used was a Thermogravimetric analyzer Pyris 1 TGA (PerkinElmer) coupled with an FTIR spectrometer for online analysis of developed gases (TGA-FTIR) available in the Institute of Macromolecular Chemistry (Czech Academic of Science) in Prague, Czech Republic.

3.3 METHODS

3.3.1 Conductometry and pH meter

Conductometry and pH meter measurements were performed during the synthesis process of the sample PANI-SDS 1000 mM. For this, the electrodes were inserted into the solution every 15 minutes and waited for 5 minutes to take the measurements. The electrodes were cleaned using deionized water before the next measurement.

3.3.2 Dynamic Light Scattering

Dynamic Light Scattering measurements were performed for the PANI-PVP particles at different pHs. The PANI-PVP particles dedoped (pH 14) were filtrated using a paper filter and cleaned using an acetone and water solution until the solution coming out of the filter

became colorless. These powders were dissolved in a NaOH aqueous solution with different concentrations to obtain the pH of 14.0, 13.0, 11.4, 9.2, and 7.6. For redispersed the particles in the solutions, the samples were sonicated for 8 minutes.

3.3.3 Raman spectroscopy

PANI-PVP particle measurements were performed by deposition of the particle powder (pH 14) in the silicon using the argon ion laser ($\lambda = 514$ nm) and an objective 50x magnification. For comparison, measurements were also performed in the same conditions for the polyaniline polymer powder in the emeraldine base cleaned using filter paper and acetone.

PANI-SDS samples the Raman Spectroscopy was performed by deposition of the clean powder in a cover slip using three different wavelength beams: 488 nm, 514 nm, and 633 nm. The measurements were performed in different positions of the samples to observe the homogeneity of the composites using an objective of 50x magnification. In the Polarized analysis, the measurements were performed over one rod and using an objective with a magnification of 100x for the rod deposited by the stamping process in a cover slip. These measurements use a support to have precision when changing the orientation of the samples.

3.3.4 Optical Tweezers

The solutions used in the Optical Tweezers measurements were produced by diluting the synthesis product of PANI-PVP sample in a (1 M) NaOH solution by 1/5 to obtain particles at pH 14. From this solution was take an aliquot of 200 μL to fill the o-ring into two cover slips setup for the measurements. The laser used was the infrared 1064 nm.

3.3.5 Electrochemical Analysis

For Electrochemical Analysis, the PANI-SDS samples were filtrated using a paper filter and cleaned using HCl (0.2 M) solution and ethanol. The clean powder was ground using a mortar and pestle to produce a fine powder; 10 mg of the sample powder was added to an eppendorf with 400 μL isopropanol, 590 μL milli-Q water, and 10 μL Nafion solution is added to facility the aggregation of the composites in the electrode, and the mixture was two times stirred during 15 minutes. 1 μL of this solution was drop cast in a commercial carbon glass electrode (working electrode). The working electrode was cleaned and polished using soft paper and deionized water, a diamond pad with 1 μm polishing diamond solution, and an alumina pad with 1 μm polishing alumina solution.

4 RESULTS AND DISCUSSIONS OF PANI-PVP PARTICLES

In this chapter, we will show the PANI-PVP particles obtained from the synthesis described in Chapter 4 and their characterization using SEM, EDS, DLS, Raman spectroscopy, UV-vis, and optical tweezers.

4.1 Scanning Electron Microscopy (SEM)

To characterize PANI-PVP particles using SEM, 200 μL of PANI-PVP particle dispersion was diluted in a 1 mL NaOH (2.5 M). This process was made to analyze particles in an alkaline condition (pH ≈ 14), which is ideal for optical tweezer studies. The samples were deposited in a copper substrate by a drop cast method and dried for one day. The images obtained are shown in Figure *4-1*. Particles of reasonable narrow size distribution was obtained with 2.4 μm mean diameter and around 12% width.

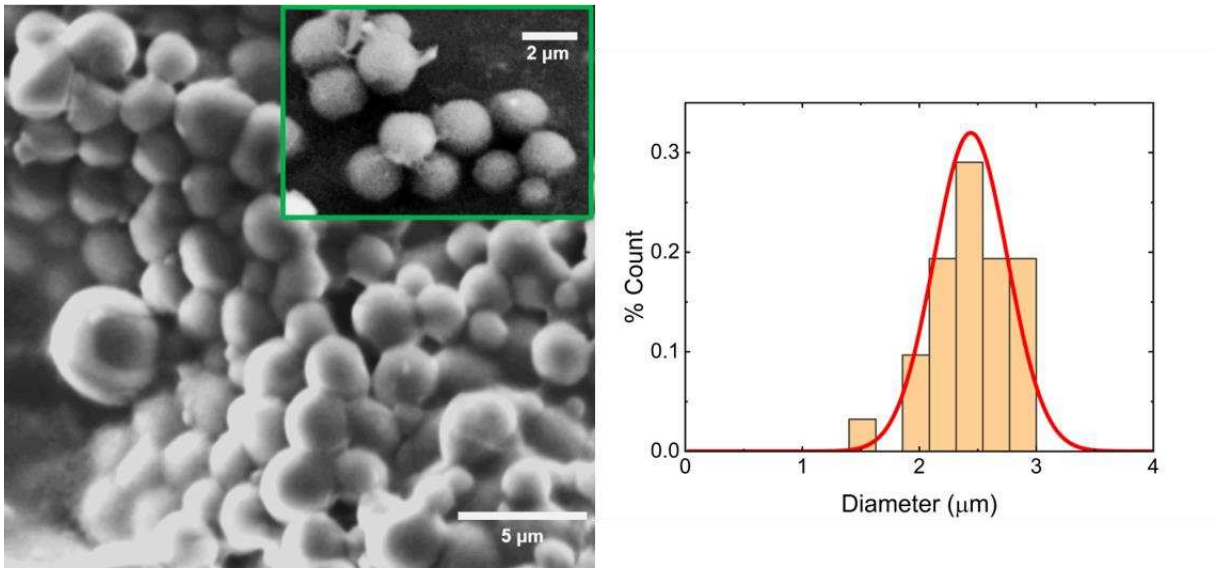

Figure 4-1. At the left: SEM images from PANI-PVP particles in pH ≈ 14. At right: histogram for the particles. The continuous line is the fit using a Gaussian distribution.

Figure *4-1* shows that the synthesis successfully produced particles with a spherical shape, excellent stability, and sizes around 1 to 3 micrometers. The fact that the particles

maintain its structural integrity is an evidence that the dedoping process works and the polymers stay in an emeraldine base. To evaluate the chemical elements in the particles we used Energy-dispersive spectroscopy (EDS) and the result is shown in Figure *4-2*. The presence of carbon (*C*), nitrogen (*N*), oxygen (*O*), and sulfur (*S*) in the particles can be noted. The carbon, nitrogen, and oxygen are associate to the aniline and PVP (Figure *4-3*). However, Figure *4-2* also shows a peak related to the sulfur not present in PANI or PVP molecules. The sulfur in the particles probably comes from the remnant APS in the solution after the cleaner process. It is important to note that, even if the information on the chemical components in the material is reliable the quantitative analysis of the results from EDS are not.

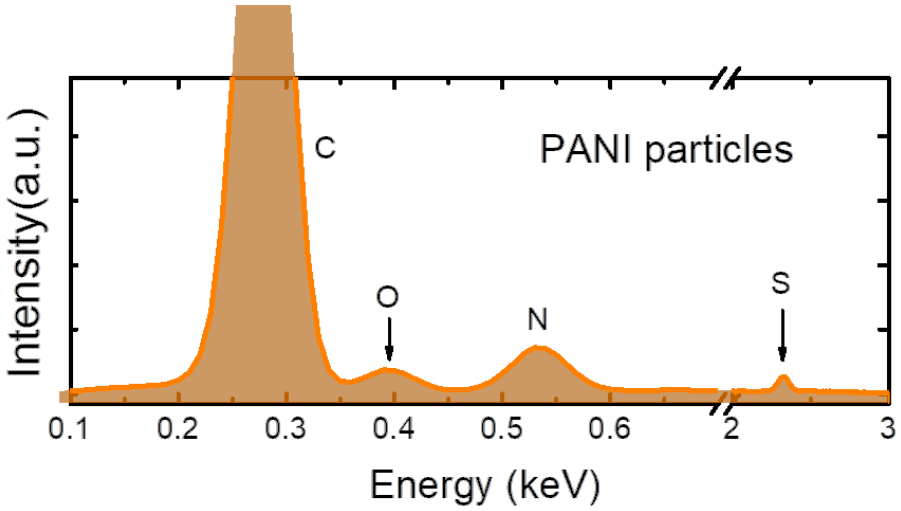

Figure 4-2. EDS spectra from PANI-PVP particles were obtained from SEM equipment.

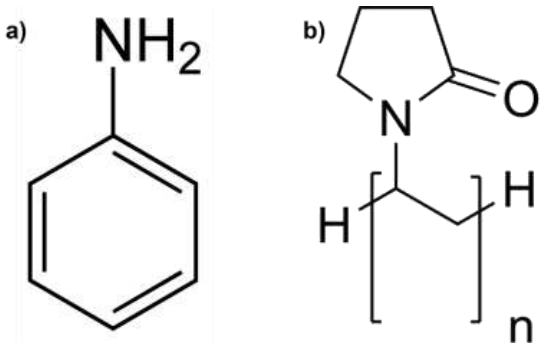

Figure 4-3. Illustration of monomer molecules of a) Aniline and b) Poly(vinyl pyrrolidone).

4.2 DLS analysis

The DLS technique allowed us to investigate the hydrodynamic diameter of the particle while in the dispersion state with different degrees of doping obtained by changing the pH of the solution. For this, the samples were cleaned following the process described in the section; the powder of PANI-PVP particles was redispersed in 5 solutions with pH equal to 14, 13, 11.4, 9.2, and 7.6, and sonicated for 8 minutes. Figure *4-4* shows the autocorrelation function normalized from the scattering intensity of the light $\left[g^{(2)}(\tau) - 1\right]/\beta$.

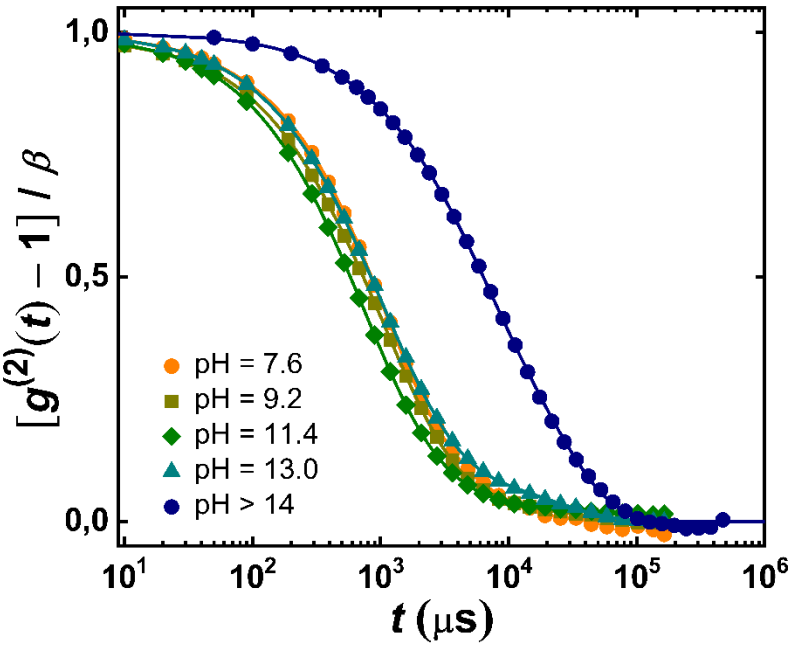

Figure 4-4. Autocorrelation function of intensity scattering normalized, obtained from PANI-PVP particles in different pH. The continuous line is the fit using a CONTIN model. (OLIVEIRA *et al.*, 2023)

In Figure *4-4*, the autocorrelation function was normalized by the β which can aslo be interpreted as the square of the scattered electrical field autocorrelation function, $\left[g^{(1)}(\tau)\right]^2$ (extrapolation of the curve to $\tau \rightarrow 0$) from each curve to make the visualization of the phenomenon easy. This graph shows us that the size of the particles changes with the pH because the exponential decay rate Γ is changing. The dark blue curve represents the particles in a solution with a pH close to 14. This curve has a lower decay rate, then the biggest

hydrodynamic radius. Also, it can be seen that the curves cannot be fit by just one exponential because the samples are more than one size of particle distribution, as shown in Figure *4-1*. Therefore, to analyze the data, a CONTIN method was used to fit the curve. Different from the analysis shown in the Material and Methods that for a monomodal distribution (one size of particle distribution), the CONTIN method is a non-monomodal distribution that can be applied to fit curves for samples with more than one particle distribution size. Figure *4-5* exhibits the size distribution of particles obtained from the CONTIN method fit to the different pH.

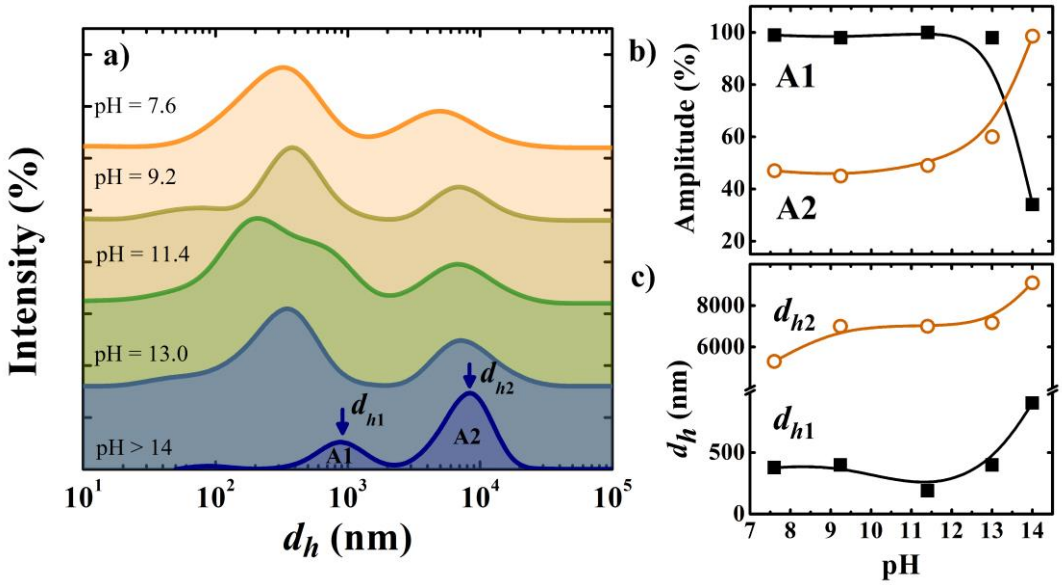

Figure 4-5. (a) Size distribution of the PANI beads (hydrodynamic diameter D_h) obtained using the CONTIN method to fit the autocorrelation functions obtained from the dynamic light scattering (DLS) measurements. (b) Amplitude and (c) hydrodynamic diameter as a function of the pH of the solution, showing that this parameter can modulate the effective size of the PANI particles.

From Figure *4-5* a), it is possible to observe that the samples have two different distributions of particle population independent of the pH. A smaller one with a hydrodynamic diameter (D_h) is an order of hundredths of nanometers to a few micrometers (population 1), and a larger one with one or two magnitudes higher (population 2). The larger particles, with diameters ranging from a few micrometers to tenths of micrometers, are within the limit of the sizes to have a reliable result using a DLS analysis since particles that big would probably sink or flocculate and give an underestimated value of D_h. However, it can be seen in Figure *4-4* that the results are smooth, well-behaved, and reproducible, showing us that the alteration in the obtained size is not critical.

Upon analyzing Figure *4-5* b) and c), we noticed that the hydrodynamic diameter of all the particles decreases as the pH level decreases. Also, there is an increase in the population of small particles (population 1) and a decrease in the population of oversized particles. The protonation in the PANI chains could explain this effect. At higher pH, the protonation of polymers is lower or nonexistent, making polymer aggregation into particles possible and decreasing the PANI solubility in an aqueous solution. When the pH decreases, the polymer starts to be protonated, which increases the solubility of the PANI in solution, decreasing the particle size. Due to the affinity of PVP with aniline compounds, the particles are probably formed by the association of PANI polymers and PVP inside the particles and a richer layer of PVP macromolecules outside, covering the particles to stabilize. Variation in the PANI chain protonation will change the conformation of the polymers inside the particles, making it possible for the big particles to break into small ones. Also, this can explain the fact that the width of the peaks, Figure *4-5* a), increases when decrease of the solution pH. Because of their size, particles with pH > 14 are the best samples for optical tweezer experiments using the setup available in our department.

4.3 Raman spectroscopy

Raman spectroscopy was performed using an argon ion laser (λ = 514 nm) and a microscope objective with a 50x magnification. The sample measurements were PANI-PVP particles and PANI polymers in a powder state deposited in a silicon substrate. Analyzing the spectra of the particles of PANI-PVP we observe the presence of the peaks at 1598 cm^{-1} (C-C stretching); 1510 cm^{-1} (N-H deformation); 1328 cm^{-1} (C-C stretching mode of the quinoid ring); 1206 cm^{-1} (C-N stretching); 1170 cm^{-1} (C-H deformation); 780 and 751 cm^{-1} (ring deformation in the PANI emeraldine base); 533 and 417 cm^{-1} (out-of-plane ring deformations in the PANI emeraldine base). The same peaks are present in PANI polymers, evidencing that the PANI in the particles have the same properties as PANI polymers and can be doped (undoped) like the polymer. This is evidence that the synthesis of the particles does not influence the quality of the polymer. The Raman spectra also show proof that PANI and PVP composite the particles.

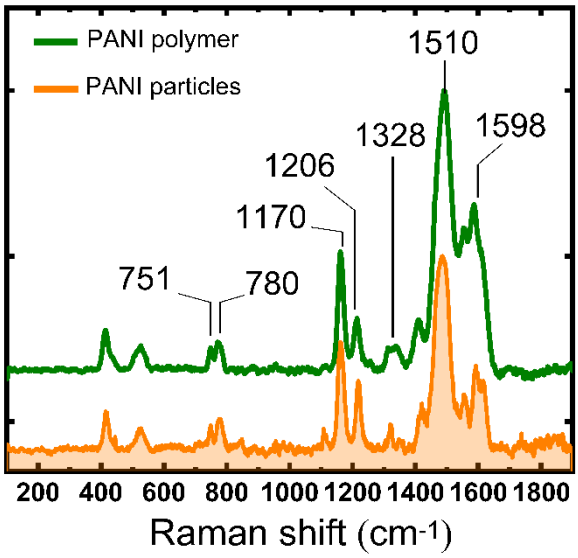

Figure 4-6. Raman spectra from the powder of PANI-PVP particles and PANI polymers in pH 14 using an argon ion laser (λ = 514 nm) and an objective 50x magnification.

4.4 Optical Tweezers

The setup of optical tweezers available is described in the Materials and Methods section. The optimal size of particles to be used in this technique is a few micrometers. The results of DLS show us that the samples in pH > 14 are the best because these particles are bigger and in this range. Also, the polymers are in an emeraldine base (isolator) where the particles are more easily trapped because the scattering force is lower. The sample was prepared by diluting 200 µL of PANI-PVP particles in 1 mL NaOH solution (2.5M). Figure *4-7* illustrates the experimental setup, where 200 µL of the final solution was added in a chamber formed by sandwiching an O-ring into two glass coverslips.

Every particle utilized in the measurements has the radius obtained by video microscopy of the free particle in solution in a Brownian motion (laser off). Bigger and more spherical particles were chosen to conduct the experiment. The trap stiffness κ was obtained from Brownian fluctuations (laser on) of the positions of trapped particles by an optical potential using a CMOS camera (Basler ac1920-155uc) with video microscopy during one minute following the methodology described in the reference (ANDRADE; GARCIA; ROCHA, 2021). The first analysis studied the influence of the laser power at the focus in the particles' trap stiffness in the direction traverses to the beam propagation. We consider the laser propagation

direction z and the particle trap stiffness in the x and y directions. This coordinate system is shown in Figure *4-7*. This measurement was performed using a PANI-PVP particle with a radius $a = 3.17 \pm 0.02$ μm and a position of 10 μm above the surface of the bottom coverslip. The laser power was varied from 1.6 to 5 mW. The results are shown in Figure *4-8*.

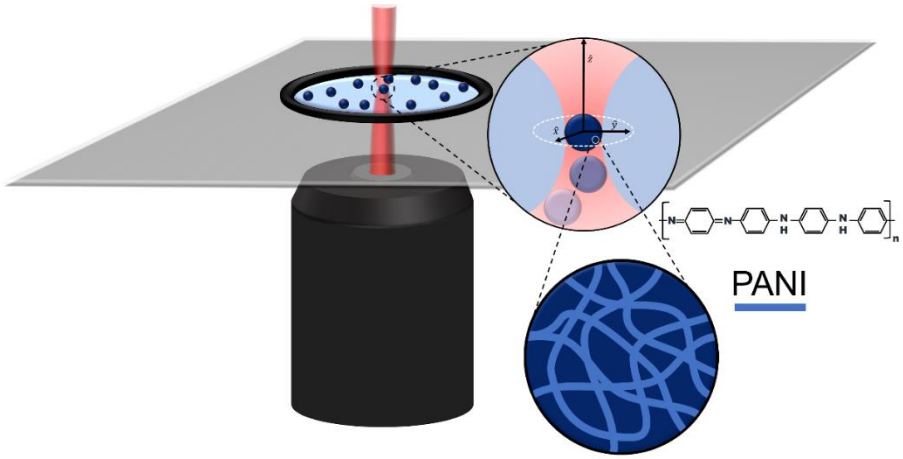

Figure 4-7. Illustration of an optical tweezers setup used to measure the PANI-PVP samples.

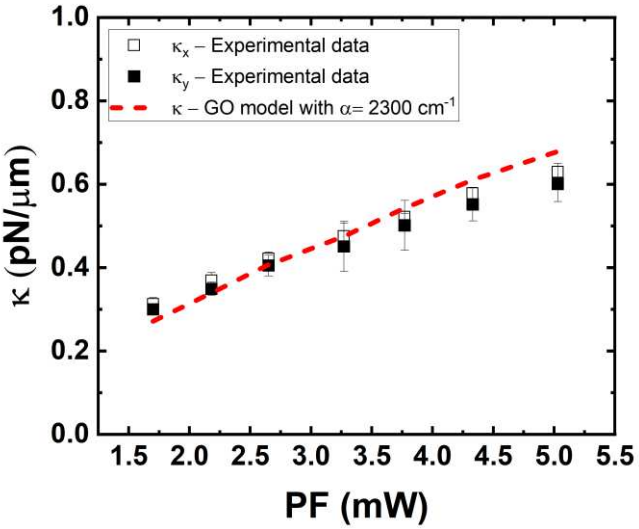

Figure 4-8. The squares represent the transverse trap stiffness κ for two perpendicular directions (x and y) as a function of the laser power at the focus PF. The dashed red line represents the GO model prediction for particles with an absorption coefficient $\alpha = 2300$ cm^{-1}. Both experimental and theoretical data were obtained for a bead with radius $a = (3.17 \pm 0.02)$ μm at a height $h = 10$ μm above the coverslip.

Figure *4-8* shows the trap stiffness for the axes x (κ_x) and y (κ_y), and the dashed red line is a theoretical result predicted by the geometrical optics model (GO) (ROCHA, 2009) based

on Ashkin's model for spherical particles under optical forces and generalized to include the effect of absorption of the materials. The absorption coefficient used for PANI-PVP particles was α = 2300 cm^{-1}, referenced by the literature (DE PAIVA *et al.*, 2021), and the refractive index used was 1.8 by the literature (FARAG; ASHERY; RAFEA, 2010). The GO model is used to produce the theoretical curve that neglects the spherical aberration of the particles. Analyzing Figure *4-8*, the experimental results agree with the GO model, showing us that considerations are valid and the absorption coefficient confirms that particles have a considerable absorbance at 1064 nm wavelength. Also, it can be noted that the trap stiffness slightly deviates from the theoretical curve. For powers less than 3.5 mW, the experimental points are slightly bigger than the theoretical curve and for powers higher than 3.5 mW the experimental points are slightly smaller. Therefore, the absorption coefficient of the particles is slightly lower than 2300 cm^{-1} in low power and slightly higher for high power. For power higher than 3.5 mW, the experimental points are slightly lower than the theoretical curve. Therefore, the absorption coefficient of the particles is slightly higher than 2300 cm^{-1}. This shows us that the particles' absorption coefficient depends on laser power, such as in some semiconductors like germanium or silicon (MEYER; BARTOLI; KRUER, 1980; MEYER; KRUER; BARTOLI, 1980). This happens because the increasing laser intensity could increase the rate of generation of free charges carries in semiconductors, which increases the absorption coefficient by the free carrier absorption mechanism (FOX, 2002; MEYER; KRUER; BARTOLI, 1980).

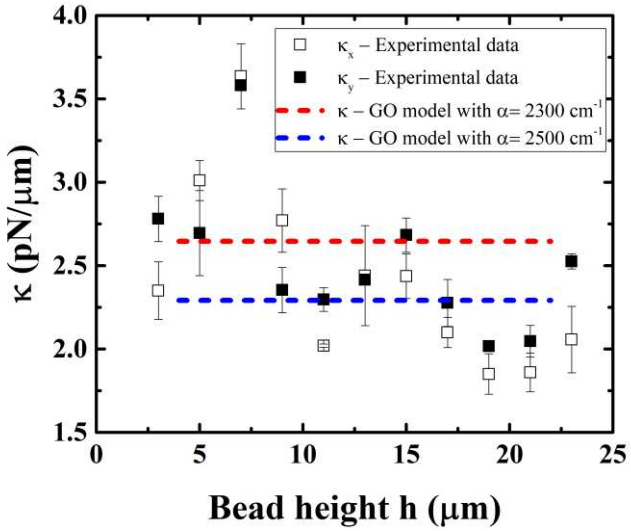

Figure 4-9. The squares represent the transverse trap stiffness κ for two perpendicular directions (x and y) as a function of the bead height h relative to the coverslip. The dashed red line represents the GO model prediction for particles with an absorption coefficient α = 2300 cm^{-1}. The dashed blue line is a similar theoretical prediction for α = 2500 cm^{-1}. Both experimental and theoretical data were obtained for a laser power at the focus of PF = 9.65 mW and bead radius a = (2.50 ± 0.03) μm.

Figure *4-9* shows the results of the influence of the bead height (particle height from the bottom coverslip) in the trap stiffness κ. This measurement was performed using a PANI-PVP particle with a radius a = 2.50 ± 0.02 μm and a laser power constant equal to 9.65 mW. Through the experimental data, we could verify that for both directions, the trap stiffness slightly decreases with the increase of the bead height. However, the GO model predicts that the expected behavior of the κ does not change with the height of particles, which could be seen for the dashed line blue (α = 2500 cm^{-1}) and red (α = 2300 cm^{-1}). Therefore, the slightly decrease of the trap stiffness in the experimental data suggests that the system is not completely free from spherical aberration effects because these effects usually decrease the trapping efficiency with the laser focus for beams with Gaussian geometry. However, the effect is minimal because the variation is lower. Comparing the GO model curves with different absorption coefficients is more evidence that the absorption coefficient of the particles changes with the laser power because, in this experiment, it is two times bigger than the results shown in Figure *4-8*.

Now, we investigated the influence of the radius of the particles in the κ. The GO model is applicable to systems where the particles have a radius bigger than the wavelength of the laser ($a >> \lambda$). The results of these measurements are shown in Figure *4-10*, where it can be noted that the experimental data have a hyperbolic curve behavior, such as that of the GO

model. However, the values of κ for the experimental data are smaller than the GO model for particles with a radius lower than 2.5 μm ($a < 2.5$ μm). Also, we can note that the photophoretic effects do not affect the PANI-PVP particles because the experimental results agree with the GO model for larger particles, where the photophoretic effects are expected to influence these particles.

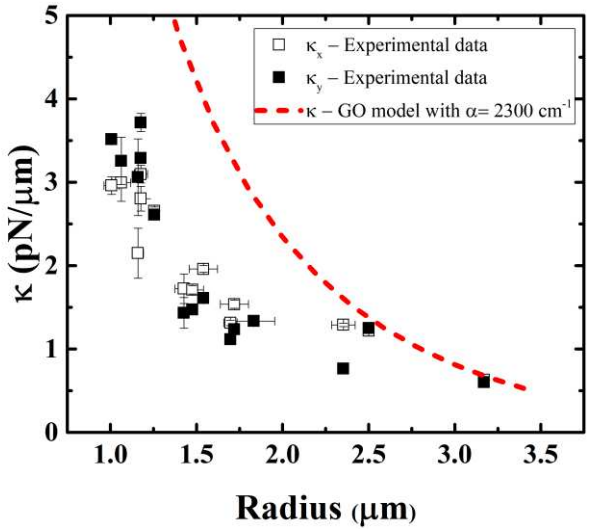

Figure 4-10. The squares represent the transverse trap stiffness κ for two perpendicular directions (x and y) as a function of particle radius and maintaining a fixed height h = 10 μm and a fixed laser power at the focus PF = 4.97 mW. The dashed red line represents the GO model prediction for particles with an absorption coefficient α = 2300 cm^{-1}.

5 RESULTS AND DISCUSSIONS OF PANI-SDS SAMPLES

In this chapter we will show the results of the characterization and application of the PANI-SDS composites obtained by the synthesis described in Chapter 4. The characterization techniques used were Scanning Electron Microscopy (SEM), Transmission Electron Microscopy (TEM), Energy dispersive X-ray spectroscopy (EDS), Raman spectroscopy, Fourier-Transform Infrared Spectroscopy (FTIR), X-ray diffraction and Small Angle X-Ray Scattering (SAXS), Elemental analysis, Maldi-TOF, and Electrochemical analysis.

5.1 Microscopy images

The study of PANI-SDS samples starts with a synthesis described in the **3.1.3 Synthesis rods/plates of PANI-SDS**. Firstly, we used the standard concentration of aniline, APS, and HCl to produce the PANI emeraldine salt, where the ratio of [APS]/[Aniline] equals 1. The sample produced is shown in Figure *5-1*, where the concentration of APS is equal to 1000 mM.

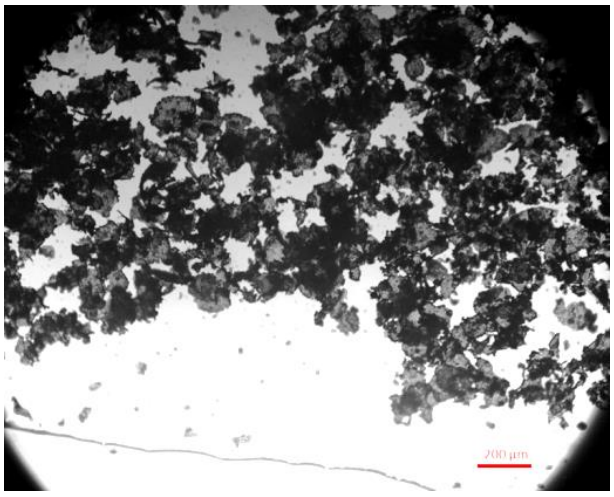

Figure 5-1. Microscopy optics image of PANI-SDS plate using a [APS] = 1000 mM.

In Figure *5-1* we can see the formation of PANI-SDS plates with size of hundreds of micrometers. Flexible and long rods were synthesized by adding an aliquot of 600 μL of the previous solution to 2 mL soluction with the same concentration of SDS and HCl. The results

are shown in Figure *5-2*, (a) after 10 minutes of the beginning of the synthesis and (b) after 30 minutes.

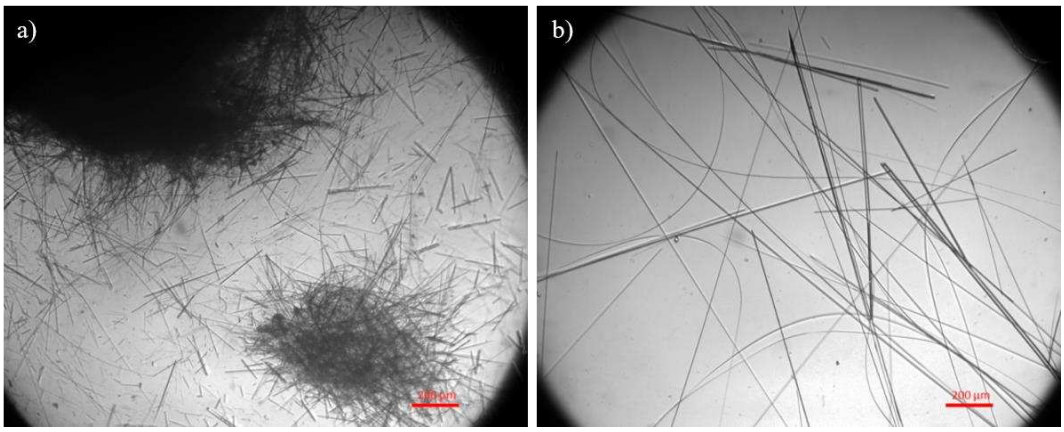

Figure 5-2. Rods are produced by diluting an aliquot with 600 µL in an aqueous acid solution with SDS (20 mM) with different periods after the synthesis beginner: a) 10 minutes and b) 30 minutes.

It can be noted that the samples from the aliquots produce rod-like structures with morphology different from the plates (Figure *5-1*) synthesized in the stock solution. Therefore, the change of aniline and APS concentration can produce different morphology of the samples. To understand the influence of the variation of APS in the morphology of the samples, we synthesized samples with APS concentration in the injection solution of 5, 20, 50, 100, 200, and 500 mM, corresponding to a ratio [APS]/[Aniline] of 0.005, 0.02, 0.05, 0.1, 0.2, and 0.5 respectively. The concentration of SDS and HCl was kept the same equal to 17.5 mM and 100 mM, respectively. The microscopic optic images of these samples are shown in Figure *5-3*, where we can evaluate the change in the morphology of the samples with the change in the [APS]/[Aniline]. Figure *5-3* shows images from the sample for different concentrations of the APS to evaluate the influence of the components in the morphology and the evolution of the samples over time. It can be seen that the sample changes the morphology with the concentration of APS and that structures have evolved with time and become the final structures after 60 hours of the beginner synthesis. Figure *5-3* a) and b) for 5 mM APS concentration, ensure the formation of rods 20 hours after the beginning of the synthesis, and the rods continue for 60 hours. However, we can see the evolution of the rods from irregular (crisp) to a regular shape after 60 hours. Also, it can be verified that the "dirt" in the solution (made of oligomers and polymers in amorphous and non-associate state) reduces throughout the time by its association to the growing structures.

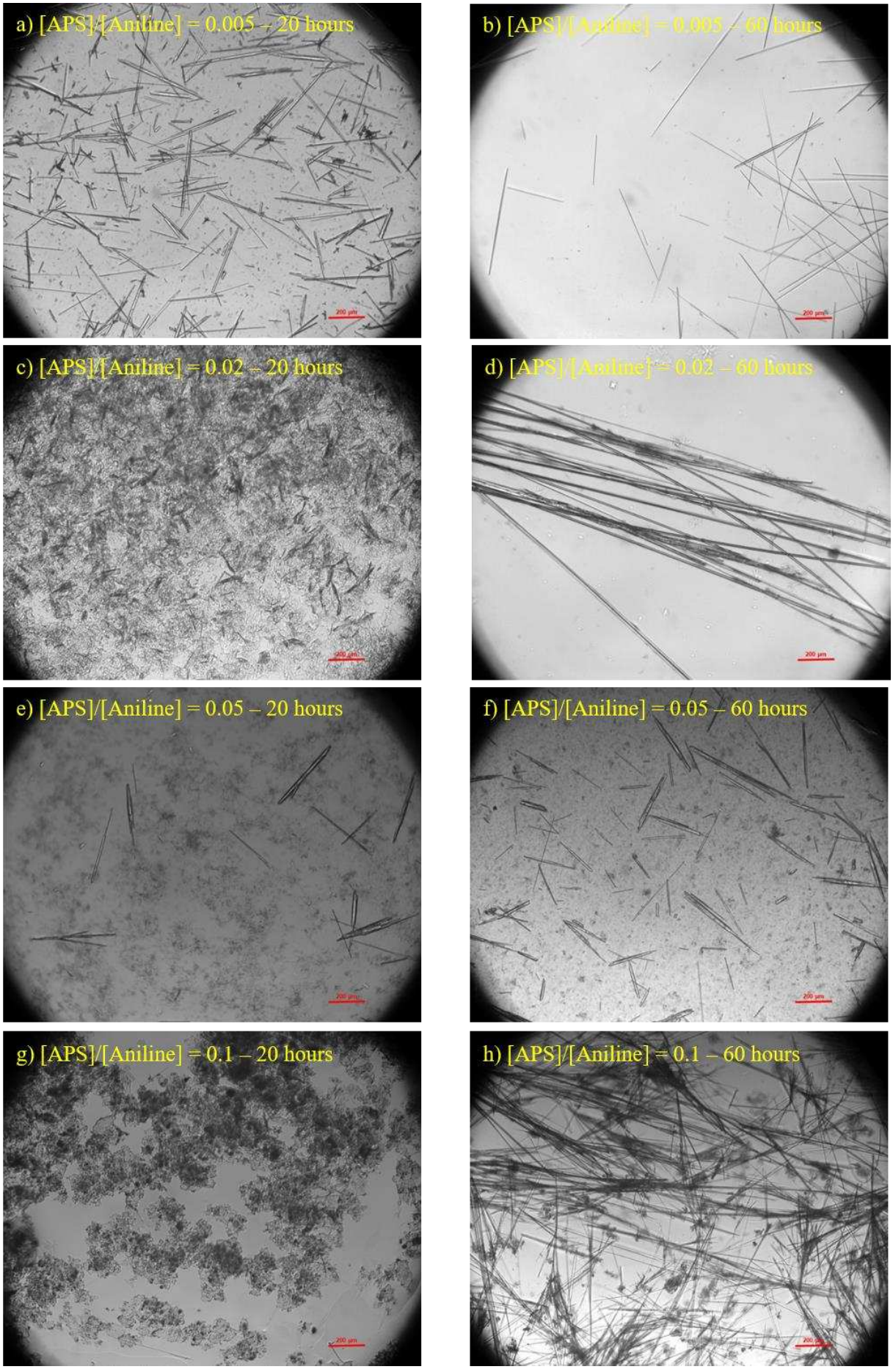
a) [APS]/[Aniline] = 0.005 – 20 hours
b) [APS]/[Aniline] = 0.005 – 60 hours
c) [APS]/[Aniline] = 0.02 – 20 hours
d) [APS]/[Aniline] = 0.02 – 60 hours
e) [APS]/[Aniline] = 0.05 – 20 hours
f) [APS]/[Aniline] = 0.05 – 60 hours
g) [APS]/[Aniline] = 0.1 – 20 hours
h) [APS]/[Aniline] = 0.1 – 60 hours

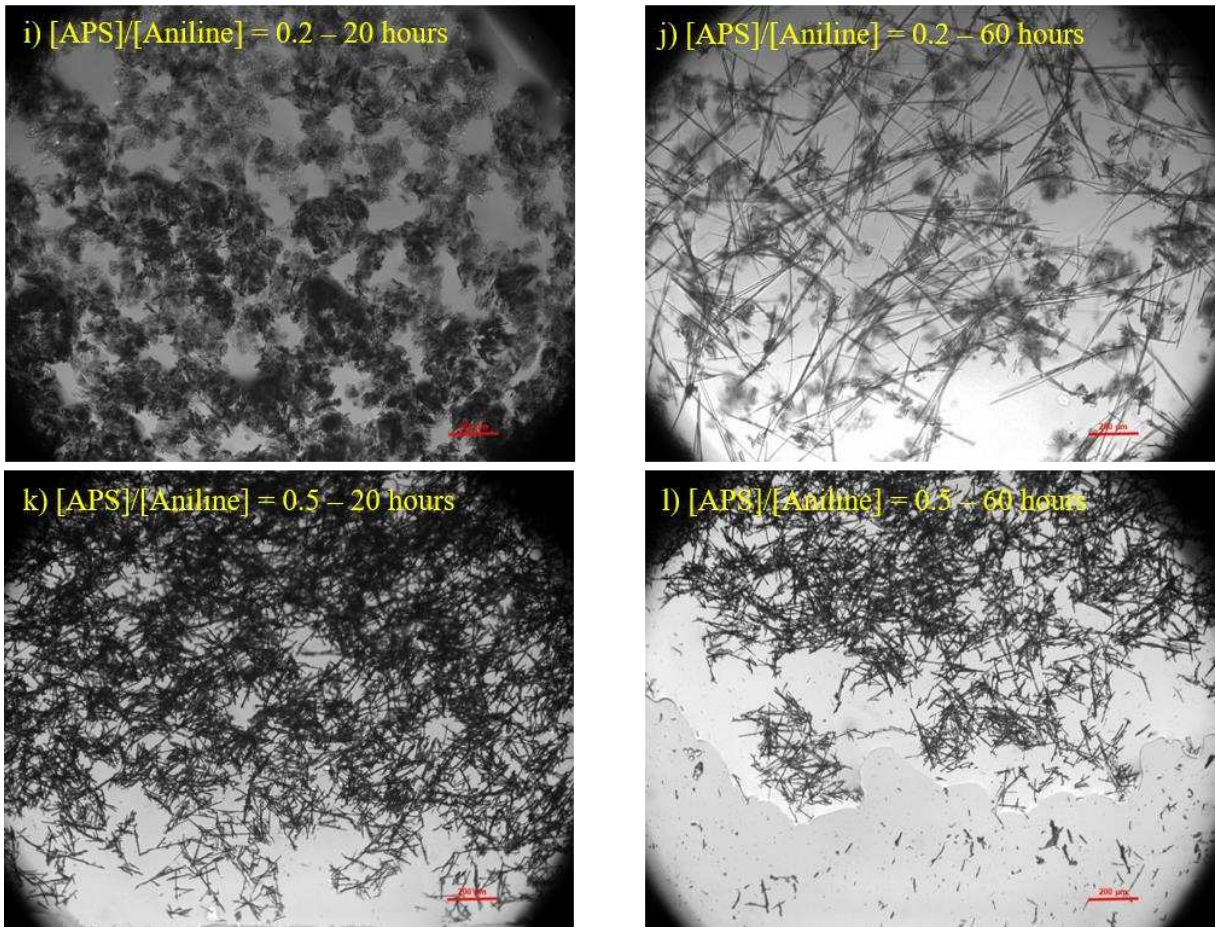

Figure 5-3. Microscopy optics images from PANI-SDS samples with SDS concentration of 20 mM changinge the [APS]/[Aniline] rate ratio and analyzing the evaluation in the time a) 0.005 after 20 hours, b) 0.005 after 60 hours, c) 0.02 after 20 hours, d) 0.02 after 60, e) 0.05 after 20 hours, f) 0.05 after 60 hours, g) 0.1 after 20 hours, h) 0.1 after 60 hours, i) 0.2 after 20 hours, j) 0.2 after 60 hours, k) 0.5 after 20 hours, and l) 0.5 after 60 hours.

For 20 mM of APS concentration, Figure *5-3* c) for 20 hours, it can be noted that the formation of some irregular structures, such as some leaf-like structures, is present. Although, for 60 hours, Figure *5-3* d), the system evolves to regular giant rods with some micrometers of diameter and some millimeters of length and also can verify the "dirt" become lower with the time agreement with the explanation above. The synthesis using 50 mM of APS, Figure *5-3* e) and f), can verify that shape of rods does not change with the time. However, the "dirt" decrease with the time and the population of rods increases, suggests that the system stays in evolution and the formation of the rods occurs by the aggregation of these smalls structures. Now, for 100 mM APS concentration, Figure *5-3* g) and h) have the formation of micrometer plate-like structures for small intervals, and these structures evolve into micrometer rod-like structures with "dirt" close to them.

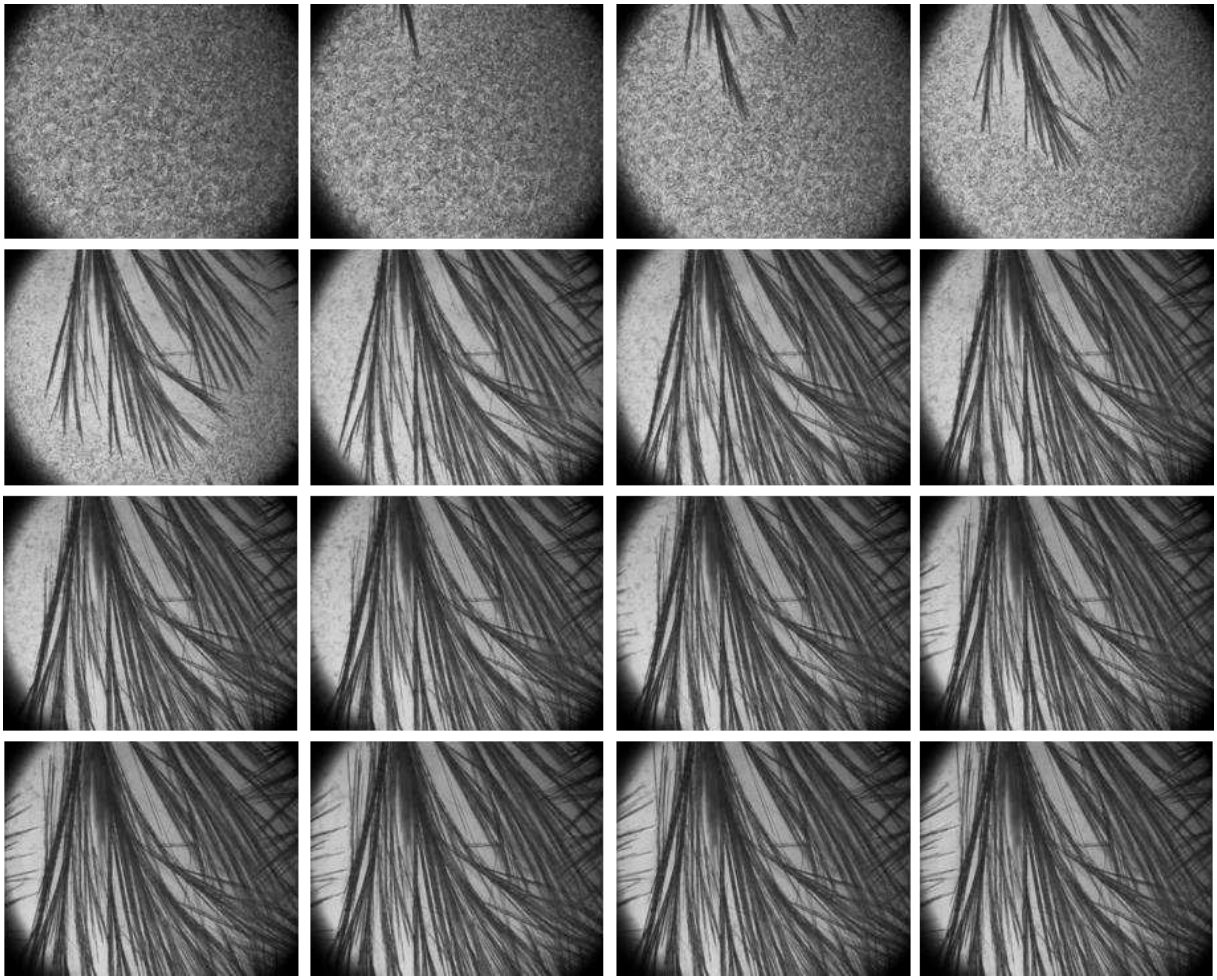

Figure 5-4. Microscopy optics images from PANI-SDS samples with SDS concentration of 20 mM with [APS]/[Aniline] = 0.02. The first picture was taken 1 hour after the synthesis start. The time interval between successive pictures was 10 minutes. The association of the non-soluble polymer/oligomer in the growing rods can be clearly seen.

The same behavior is observed in the samples synthesized using 200 mM of APS, Figure *5-3* i) and j). Finally, for the APS concentration of 500 mM, Figure *5-3* k) and l), we can observe the formation of aggregation of rod-like structures forming a rod lattice, and they do not change over time. Therefore, with these images, we can conclude that APS concentration influences the morphology of the structural changes from plates, rod lattice, and rods when we decrease the APS concentration. This can be explained because APS is responsible for the oxidation of monomers and initialization of the polymerization reaction; when the concentration of APS decreases, the number of the reactive monomers oxidated also decreases. As the oligomers and polymers are formed by the ligation of monomers oxidated, a lower concentration of APS supports the formation of oligomers that are small molecules and can be easily solvated for SDS molecules. Some reports (STEJSKAL *et al.*, 2006) show that oligomers can form rod-like structures, which could explain the formation of these structures for lower concentrations of

APS. For an APS concentration of 1000 mM, we have the [APS]/[Aniline] ratio equal to 1; for this condition, we expected the formation of larger size polymers. Therefore, the number of reactive monomers and the size of the polymers are responsible for the changes in morphology. Monitoring the synthesis with a microscopy optic video, it could be noted that non-associate oligomers/polymers in the images is absorbed by the rod or plate structures when they start growth. This confirms that "dirt" is formed by oligomers/polymers, with SDS forming an elemental structure to form the final samples.

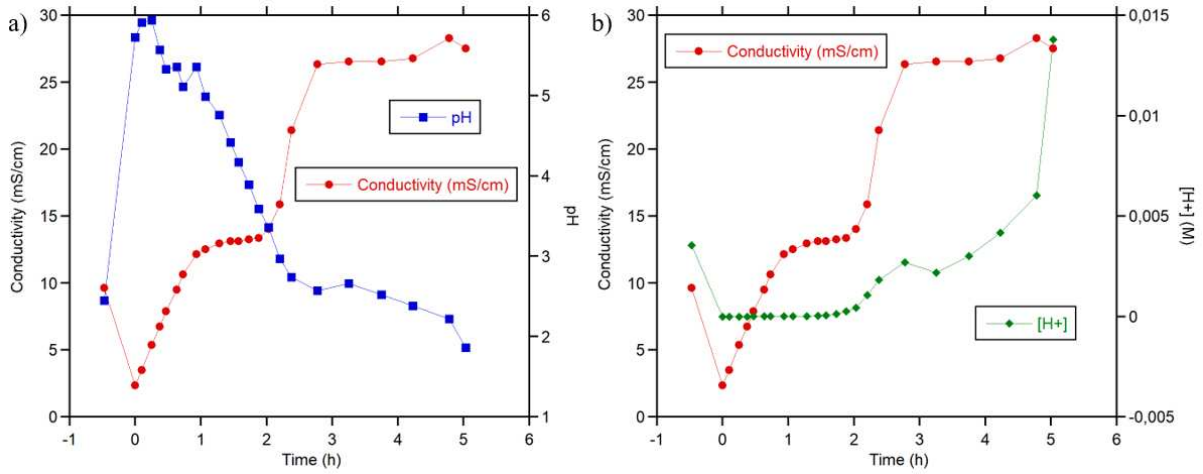

Figure 5-5. a) Conductometry and pH with the polymerization time during the synthesis of PANI-SDS and b) Conductometry and [H^+] for 20 mM of SDS, [APS]/[Aniline] = 1, and 0°C.

We also monitor the pH and conductometry of the samples during the synthesis, and the results are shown in Figure *5-5*. In the figure the time lower than zero corresponds to the conductivity and pH values before adding aniline to the solution. The time equal to zero marks the addition of the aniline and the APS to the solution. Just after the adition of the aniline its oxidation in an acid solution can be observed, absorbing the free H^+, increasing the pH of the solution, and decreasing the conductivity. The APS is countinously injected for one hour, which causes an linear increase in conductivity in the solution. Between 1 and 2 hours, the conductivity curve is stabilized, and the pH curve continues to decrease, which could be explained by the release of H^+ in the oligomer process formation (KHALID; HONORATO; VARELA, 2018). Between 2 and 3 hours, the increase in the conductivity and pH is observed and could be explained by the formation of the polymer chain and the start of the formation of rods/tubes and plate structures. After 3 hours, the stabilization of the conductivity and pH related to the end of the polymerization reaction.

5.2 Solubility test

The solubility test was used to understand the rods composition; for this, the rods were obtained using 50 mM of APS. The first analysis was diluted at 1:5 V/V in water, acetone, and N-methyl-pyrrolidinone (NMP), as shown in Figure *5-5*.

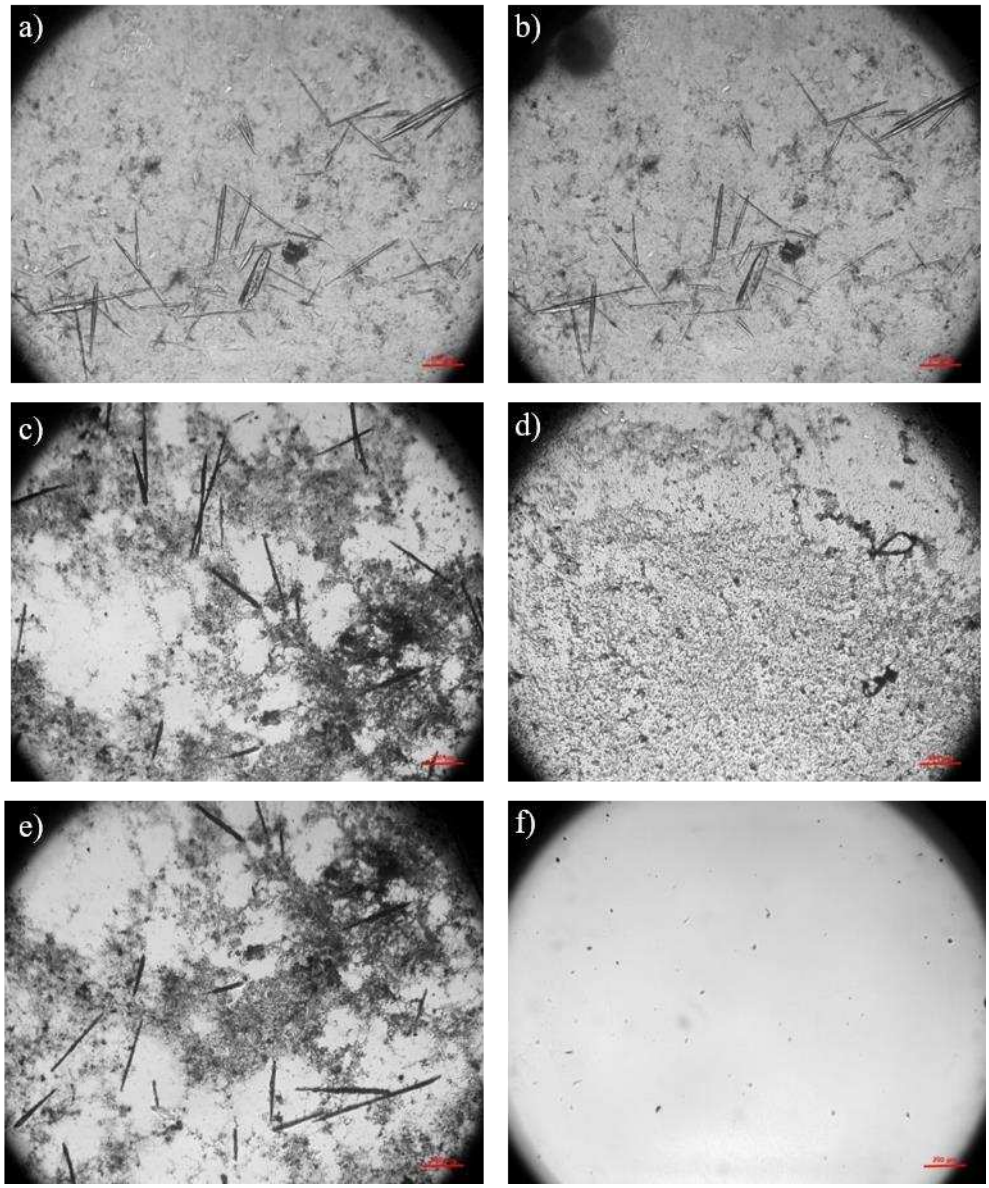

Figure 5-6. Solubility test for rods using [APS] = 50 mM in different solutions: a) before and b) after water dilution; c) before and d) after acetone dilution; e) before and f) after NMP dilution. After the dilution, the samples were kept for 5 minutes until the image was taken.

The water dilution, Figure *5-6* a) and b) the rod's morphology and has a minor degradation on the surface, probably because the water washed the surfactants on the surface of the rods. The acetone dilution is shown in Figure *5-5* c) and d) the rods are broken, which can be explained because acetone is typically used to wash oligomers and small polymers. Therefore, the acetone can wash the surfactants and polymers. Also, the acetone can break the hydrophobic interactions because of the variation in the dipole moment compared with the water, which explains the presence of non-associate oligomers/polymers after the dilution. NMP dilution is shown in Figure *5-6* e) and f), where it could be noted that adding the solution breaks the rods and dissolves the polymers and the surfactant. NMP is a well-known PANI solvent that proves that rods are formed by PANI and SDS interactions. As in the emeraldine salt, the PANI has a positive charge in the chain, and the SDS in the solution has a negative charge in the surfactant head; it is expected that these two molecules can interact by ionic forces. To evaluate this supposition, microscopic videos were made while washing the solution using water and HCl (100 mM), Figure *5-7*.

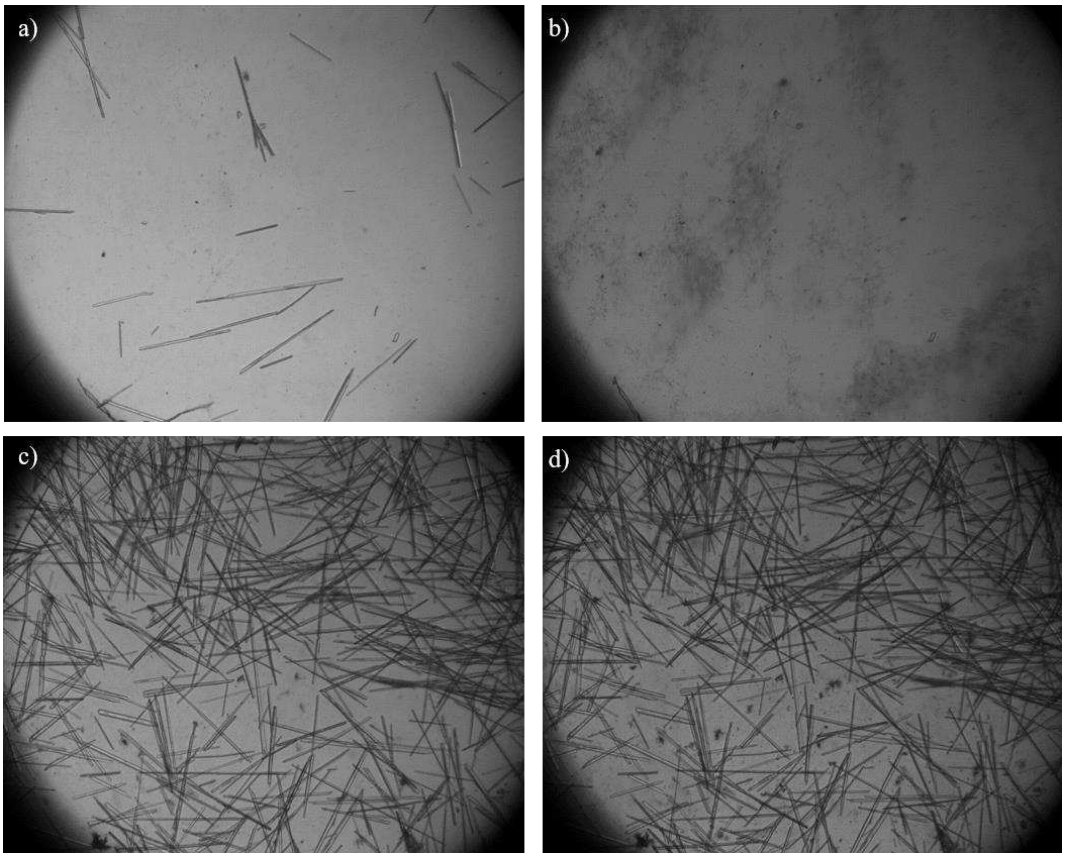

Figure 5-7. Solubility test for rods produced by [APS] = 10 mM with a continued flow rate of 1 μL/min: a) before and b) after the water solution; c) before and d) after the HCl (100 mM) solution.

Figure *5-7* a) and b), the dilution using a water solution with a flow rate of 1 μL/min can cause the rods to vanish and appear as non-associate oligomers/polymers in the solution. This happens because adding water increases the pH of the solution, changing the PANI conductive characteristics and breaking the rods, proving that rods have an ionic interaction between PANI and SDS. Also, the polymers inside the rods will go to the solution after breaking them, making the non-associate oligomers/polymers appear. The dilution using an HCl solution proves that statement because the rods remain intact after hours; in this case, we do not have a change in the pH and the PANI conductive characteristics.

5.3 Scanning electron microscopy (SEM) and transmission electron microscopy (TEM)

The characterization using optics microscopy gives us essential knowledge of the samples for continuing the characterization. As seen in Figure *5-3*, some samples have a final morphology close to the other, and because of this, we choose some concentration to continue the characterizations. Therefore, for the characterization after this point, the concentration of APS analyzed was 5, 20, 500, and 1000 mM and we also studied the influence of the temperature in the synthesis by the polymerization at 0 °C and room temperature (RT) around 25 °C. The SEM images of these samples are shown in Figure *5-8*. The nomenclature of the samples are show in Table *5-1*.

Table 5-1. Nomenclature of the samples PANI-SDS samples

Sample	Name
PANI	PANI
PANI-SDS 5 mM	PS5
PANI-SDS 20 mM	PS20
PANI-SDS 20 mM RT	PS20RT
PANI-SDS 500 mM	PS500
PANI-SDS 1000 mM	PS1000
PANI-SDS 1000 mM RT	PS1000RT

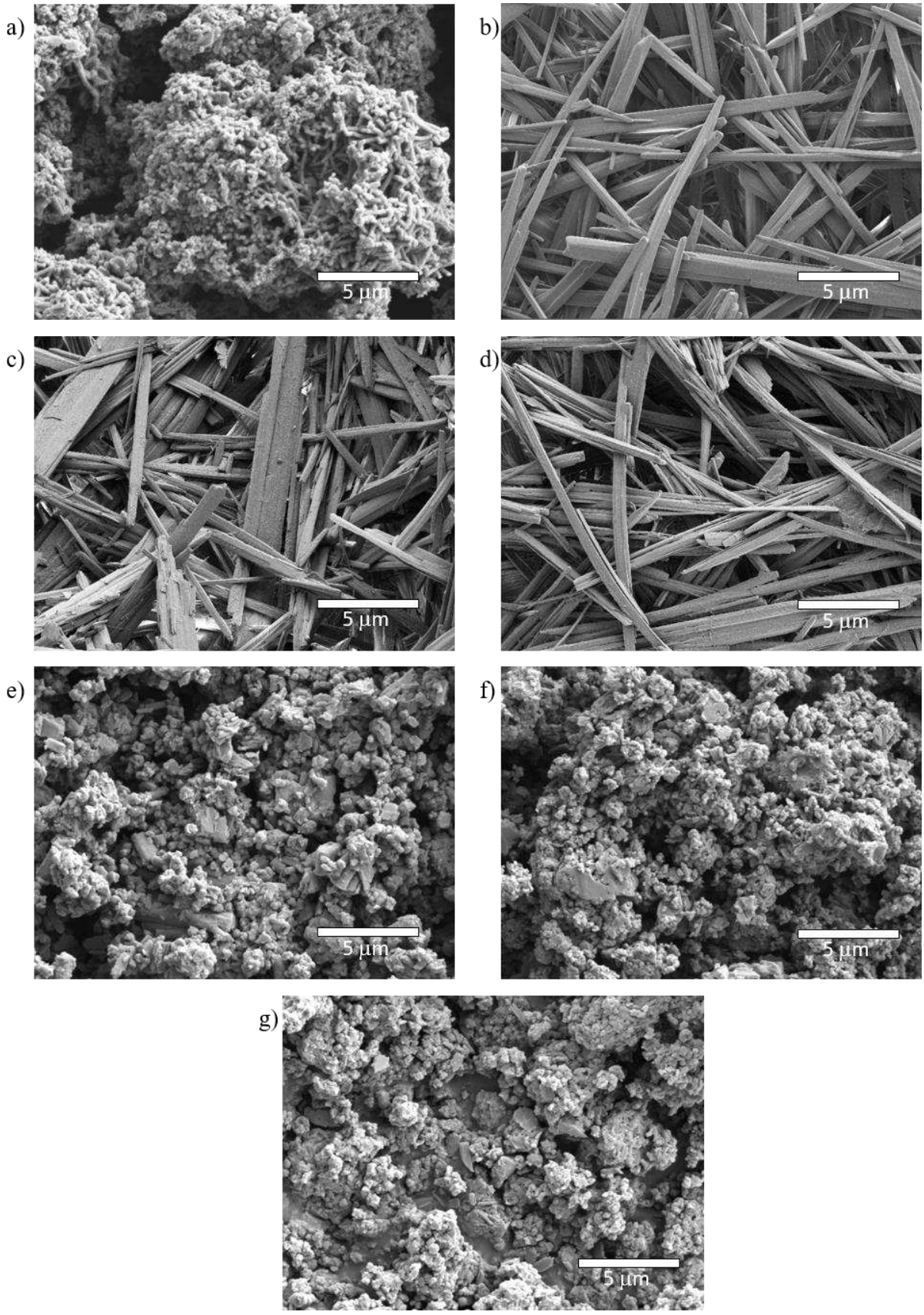

Figure 5-8. SEM images of PANI and PANI-SDS samples with different temperatures and APS concentrations: a) PANI polymer; b) PS5; c) PS20; d) PS20RT; e) PS500; f) PS1000; g) PS1000 RT.

Comparing the image of the pure PANI polymer (Figure *5-8* a)) with the other samples, the influence of SDS in the samples is evident. The pure PANI are amorphous and the SDS increases the crystallinity of the samples. In PS5, PS20, and PS20RT micrometer rods are formed in agreement with the microscope optical images and the synthesis temperature does not influence the morphology of the samples. In PS500, PS1000, and PS1000RT it could be noted the presence of small pieces of the plates and rods. However, the samples seem the same and do not change with the influence of temperature. To continue the analysis, we use the TEM equipment for images with lower dimensions to study the morphology of the samples. The results are shown in Figure *5-9*.

The TEM images are in agreement with the microscope image results shown above. In Figure *5-9* b), c), and d), the formation of flexible rods with micrometers of length can be seen. Again, the influence of temperature is not noted. Now, for high concentrations of APS (500 and 1000 mM) we can see the formation of rods and plates and the increase temperature, in these cases, influences the morphology inhibiting plate formation.

Figure *5-10*, EDS analysis, shows us the presence of SDS because of the peaks *S*, *Na*, *O*, and *C*, and PANI because of the peaks *C* and *N* in the rods. Also, the *Cl* signal can be associated with the polymers staying in the conductive base (emeraldine salt). The rod is formed by PANI and SDS molecules.

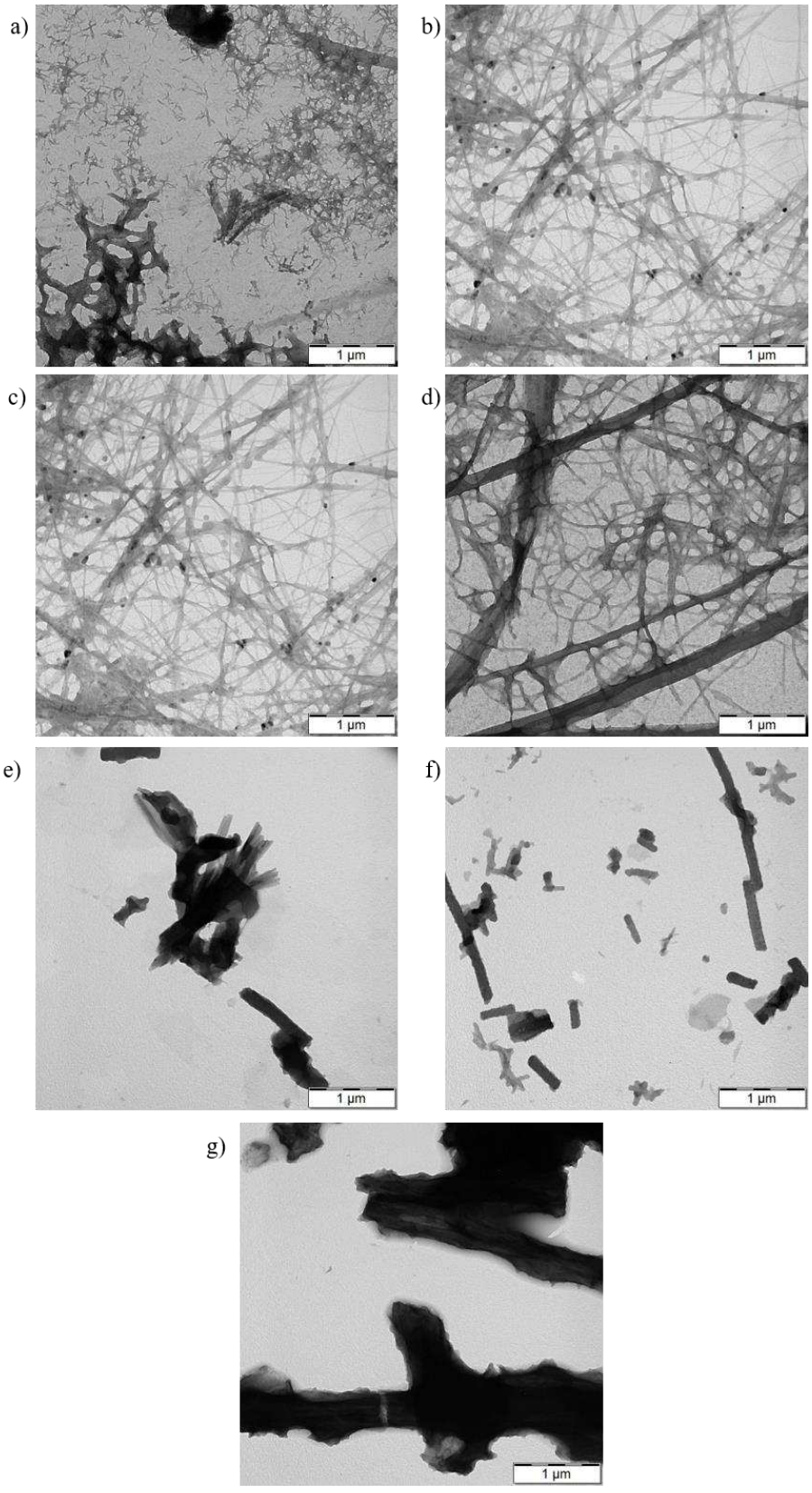

Figure 5-9. TEM images of PANI and PANI-SDS samples with different temperatures and APS concentrations: a) PANI polymer; b) PS5; c) PS20; d) PS20RT; e) PS500; f) PS1000; g) PS1000 RT.

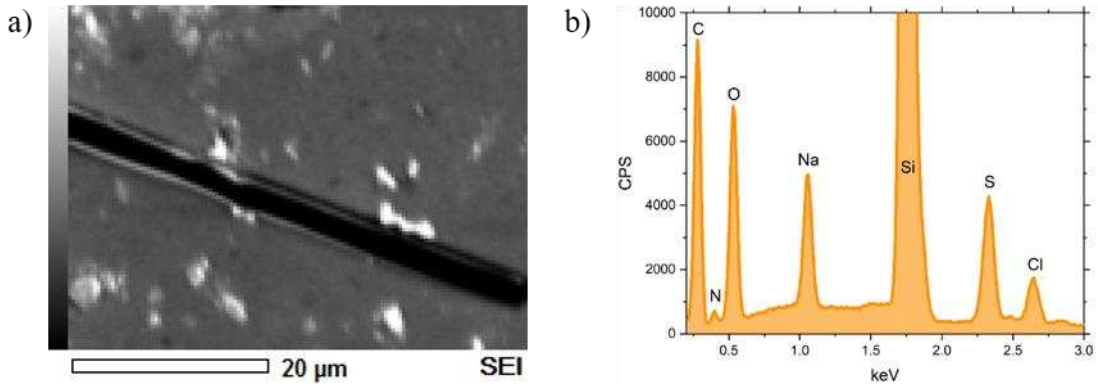

Figure 5-10. EDS analysis for a PANI-SDS 20 mM rod was obtained by drop cast deposition in a silicon substrate.

5.4 Elemental Analysis

The elemental analysis results from PANI and PANI-SDS samples are shown in Table *5-2*, where we obtained the percentage of the mass of each chemical element in the sample with precision.

Table 5-2. Results from Elemental Analysis of PANI and PANI-SDS samples. The under-detection limit (UDL) is lower than 0.03.

Sample	% C		% H		% N		% S		% Cl
PS5	60.15	60.15	9.22	9.23	4.05	4.18	8.98	9.06	UDL
	60.14		9.23		4.31		9.13		
PS20	59.94	60.02	9.17	9.18	4.74	4.75	9.05	9.03	UDL
	60.10		9.18		4.76		9.01		
PS20RT	60.88	60.82	9.17	9.20	4.60	4.52	9.07	9.06	UDL
	60.75		9.23		4.44		9.05		
PS500	61.18	61.08	6.81	8.28	8.19	8.09	5.81	5.93	1.70
	60.98		9.74		7.98		6.04		
PS1000	60.45	60.46	6.66	6.56	7.74	7.77	5.52	5.62	2.40
	60.46		6.46		7.80		5.71		
PS1000RT	59.29	59.30	6.64	6.75	7.65	7.60	5.50	5.49	3.10
	59.31		6.86		7.54		5.48		
PANI	56.68	56.68	4.60	4.80	10.84	10.80	2.74	2.80	8.60
	56.67		4.99		10.76		2.86		

Using the results shown in Table *5-2*, we analyze to understand the proportion of monomers of polyaniline (*N*) and molecules of SDS (*S*). These results are displayed in Table *5-3*, where we calculated the ratio N/S_{SDS} and $N/S_{SDS}(C_{SDS})$. In the last one, we calculate the

number of mols of *S* to remove the signal from some remaining impurities after cleaning. For this calculus, we use the concentration of *S* present in the PANI sample. As these samples do not have SDS, the presence of *S* is associated with APS molecules dopant the polymer. Therefore, to have the signal of *S* only from the SDS, we subtract from the total signal of Sulfur (S_T) the concentration of Sulfor from APS absorbed by PANI. For this, we use weighted by the concentration of N_{PANI} from the sample with just PANI and the samples with SDS (N_T), using Equation 20.

$$S_{SDS} = S_T - \frac{N_T S_{PANI}}{N_{PANI}}. \quad (20)$$

With the S_{SDS} permits, obtain the concentration of C_{SDS} by the multiplication for 12.

Table 5-3. Analysis of the Elemental Analysis of PANI and PANI-SDS samples.

Sample	C_{SDS} (mol)	H (mol)	N (mol)	S_{SDS} (mol)	Cl (mol)	N/S_{SDS}	N/S_{SDS} (C_{SDS})	N/Cl
PS5	3,217	9,154	0,298	0,249	0,000	1,200	1,113	---------
PS20	2,962	9,104	0,339	0,243	0,000	1,394	1,374	---------
PS20R	3,127	9,129	0,323	0,246	0,000	1,312	1,238	---------
PS500	1,622	8,211	0,577	0,119	0,048	4,834	4,270	12,038
PS1000	1,705	6,509	0,555	0,112	0,068	4,940	3,904	8,194
PS1000RT	1,684	6,698	0,542	0,110	0,087	4,938	3,864	6,201
PANI	0,092	4,758	0,771	0,000	0,243	--------	---------	---------

From Table *5-3*, the $N/S_{SDS}(C_{SDS})$ ratio is close to 1 for the samples with APS concentrations lower than 20 mM and close to 4 for samples with concentrations bigger than 500 mM. This means that the rod-like structures for each aniline molomeric unit there is one SDS molecule. For APS concentrations bigger than 500 mM (plate structures) for each aniline monomeric unit there is around 4 molecules of SDS. This difference in the ratio is caused by the fact that high concentrations of APS facilitated the formation of larger PANI polymers, decreasing the number of molecules of SDS interacting with the PANI; low concentrations of APS facilitate the formation of oligomers and increase the number of SDS molecules interact with the samples. This also can be observed because the molar concentration of nitrogen is two times bigger in the synthesis with a high concentration of APS.

The ratio of aniline and SDS added to the solution was 114 mM/17.4 mM, or 6.5 aniline molecules per SDS molecule. For samples using less than 20 mM of APS in the synthesis, the proportion of aniline and SDS is around 1 ($N/S_{SDS}(C_{SDS})$ in Table *5-3*). The lower concentration of APS could explain the difference, further the formation of oligomers or small polymers. Therefore, the solution has a considerable concentration of non-react monomers, washing them in a clean process. For samples using more than 500 mM of APS in the synthesis of the samples, we have the proportion around 4 ($N/S_{SDS}(C_{SDS})$ in Table *5-3*). This difference could be explained by the fact that some aniline molecules do not react or form oligomers and they were washed during the cleaning process. The difference between the N/S_{SDS} and $N/S_{SDS}(C_{SDS})$ is that the first was calculated by taking out the signal of *S* in the PANI, referent just about APS residual, and the second was taking out the signal of *C* from aniline, and with this, all remain carbon was associated to the SDS molecules. Finally, the temperature did not influence the results as the number of aniline and SDS molecules.

5.5 Maldi-TOF

To continue studying the chemical structures of the PANI-SDS samples, the Maldi-TOF analysis was made in the samples of PANI polymers using 1000 mM of APS, PANI oligomers using 20 mM of APS, PS5, PS20, PS20RT, PS500, PS1000, and PS1000RT. These results are shown in Figure *5-11*. The peak at 114 *m/z* can be related to APS molecules that remain after the cleaning process, corroborating the Elemental analysis results (Table *5-2*), where we can verify the presence of some APS molecules. The synthesis of PANI ([APS]/[Ani] = 1), Figure *5-11* a) expects the presence of only polymers with high molar weight, although the results show the presence of oligomers more specific with 3 and 5 anilines. Figure *5-11* b), the synthesis of PA 20 mM ([APS]/[Ani] = 0.02), the results show the presence of oligomers as expected. Comparing Figure *5-11* g) with h) shows that the influence of temperature does not change the formation of the polymer. The behavior of the PANI polymer curves, Figure *5-11* a) is the same for higher concentrations of APS (higher than 500 mM), demonstrating that SDS does not influence the formation of the polymer, Figure *5-11* f), g), and h). However, for low APS concentrations, shown in Figure *5-11* c), d), and e), the signal is reasonable until 4 anilines, showing that for this concentration of APS, the SDS influence in polymer formation favors the formation of oligomers with low molar mass.

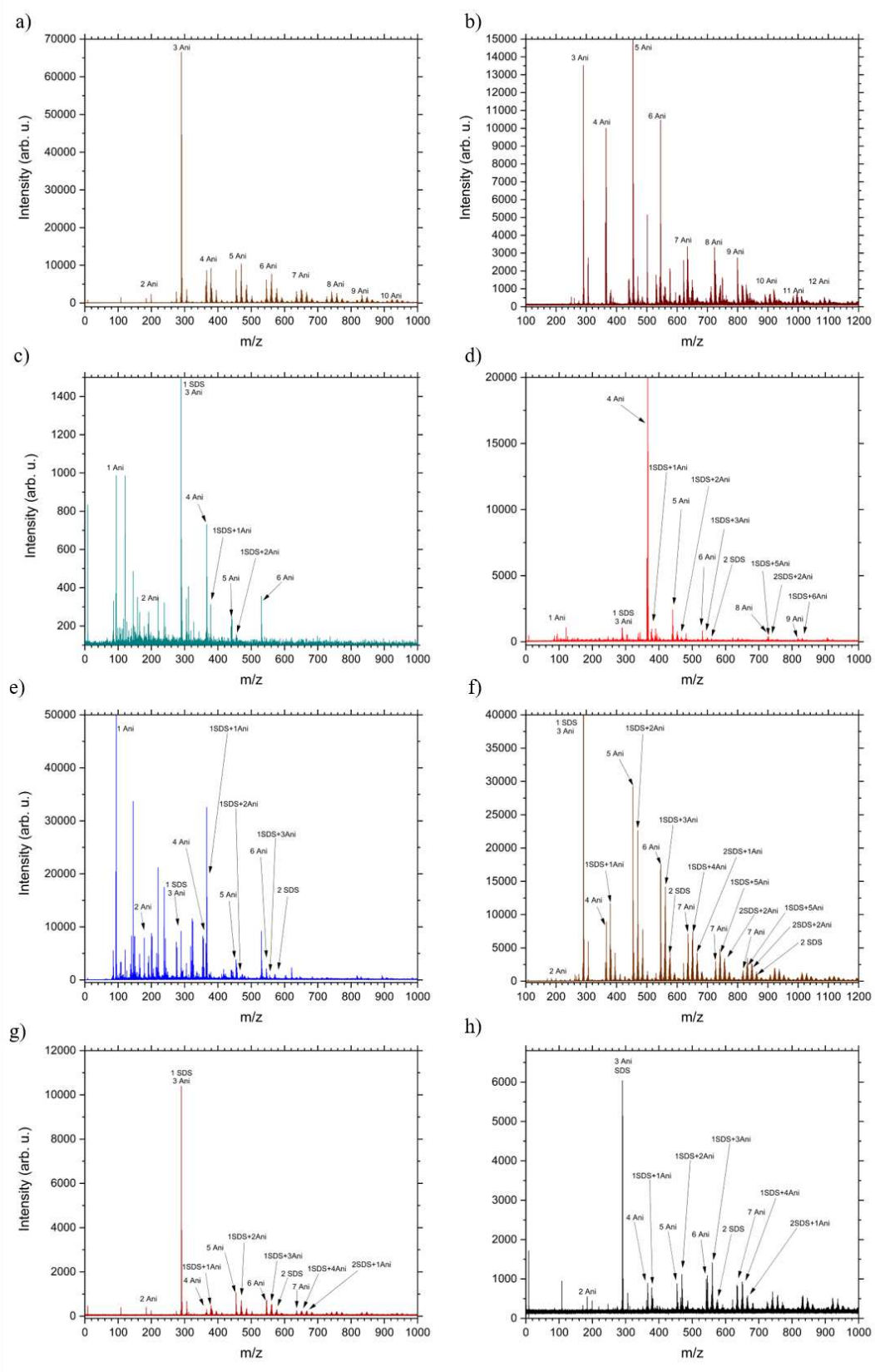

Figure 5-11. Maldi-TOF results for a) PANI polymers, b) PANI oligomers 20 mM; c) PS5; d) PS20; e) PS20RT; f) PS500; g) PS1000; and h) PS1000 RT. Where the arrow represents the configuration of molecules that can represent the peak.

5.6 Fourier-Transform Infrared spectroscopy

To continue the sample characterization, we must have information about the molecular structures in the rods/tubes and plates. FTIR spectroscopy is a powerful technique that reveal the molecular structure and significant components present in the sample. The samples were prepared in KBr pellets for the transmission measurements. The first characterization was to study the influence of the APS concentration on the molecular structures of the sample. The samples used were aniline (114 mM) and SDS (20 mM), varying the APS inject concentration from 0 mM, 5 mM, 20 mM, 500 mM, and 1000 mM, where the results are shown in Figure *5-12*.

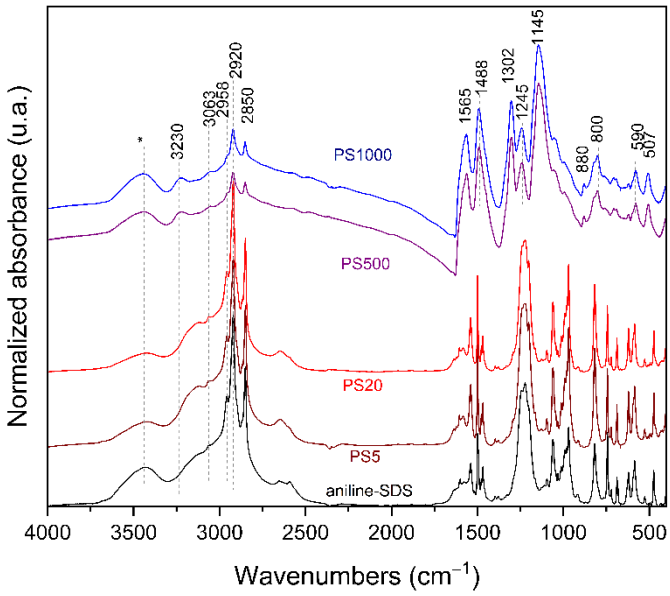

Figure 5-12. FTIR spectra of the PANI-SDS samples varying concentration of the APS and a mixture of aniline monomer with SDS for comparison. An OH stretching band of residual moisture in the KBr pellets is marked with an asterisk.

From Figure *5-12*, it is observed that SDS is a significant component in all the samples by the intense peak of the CH stretching band at 2850, 2920, and 2958 cm^{-1}, in agreement with other characterization shown above the rods/tubes and plates composite by SDS and PANI. It is evident that spectra from samples with low concentration ([APS] $\leq$ 20 mM, samples PS5 and PS20) are different from those with higher concentration ([APS] $\geq$ 500 mM, samples PS500,

PS1000); the difference between the two groups of samples are noted in the SEM and TEM images such as in the elemental analysis and Maldi-TOF characterization.

The spectra of the samples prepared at higher concentrations of oxidant (500 mM and 1000 mM) correspond to protonated PANI with its typical bands at 3230 cm^{-1} (NH stretching); 3063 cm^{-1} (CH stretching); 1565 cm^{-1} (quinonoid ring stretching); 1488 cm^{-1} (benzenoid ring stretching); 1302 cm^{-1} (skeletal vibration related to π-electron delocalization); 1245 cm^{-1} (C~N stretching in protonated semiquinonoid structure); 1145 cm^{-1} (-NH^{+}= structure stretching); 880 cm^{-1} (out of plane CH deformation of 1,2,4- and 1,2,4,5-substituted rings); 800 cm^{-1} (out of plane CH deformation of 1,4- and 1,2,3,4-substituted rings); 590 cm^{-1} (ring deformation); and 507 cm^{-1} (ring deformation of 1,4-substituted rings) (MORÁVKOVÁ; ŠEDĚNKOVÁ; BOBER, 2020; SOCRATES, 2004; TRCHOVÁ *et al.*, 2014). The low-wavenumber region also indicates the presence of oligomers with various ring-substitution patterns. However, the typical phenazine-like oligomer bands at 1444 and 1414 cm^{-1} (TRCHOVÁ *et al.*, 2012) are missing; thereby, the oligomers of the Michael-adduct (Figure *5-14*) type are probably more prominent. The spectra of the samples prepared at lower concentrations of oxidant (5 mM and 20 mM) are identical to the spectrum of a mixture of aniline and SDS. FTIR detected neither PANI nor aniline oligomers; thereby, the oligomers can only be present in the sample in low concentrations

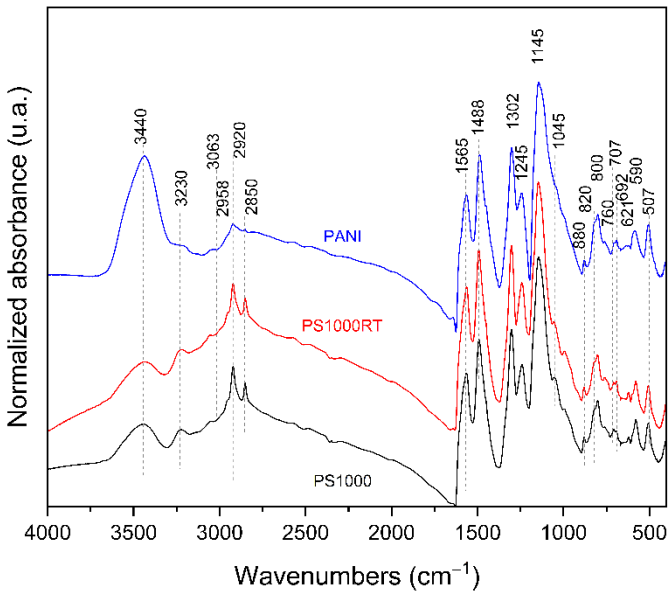

Figure 5-13. FTIR spectra of the PANI-SDS 1000 mM at low and room temperature and comparison with the PANI polymer.

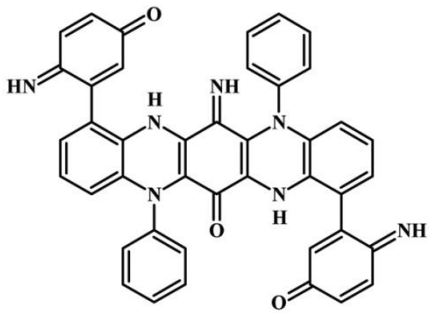

Michael-type adduct

Figure 5-14. Michael-type adduct with aniline molecules is a kind of oligomers.

The analysis of temperature influence was studied in the samples of PS1000 at low temperature (0 °C) and room temperature (25 °C), as shown in Figure *5-13* and comparing them with the sample with just the PANI polymer. The results show that in the sample with the PANI polymer, the contribution of SDS absorption is missing at 2920, 2850, 1245, 1045, and 621 cm^{-1}, as expected. The PS1000 samples do not differ from each other according to their FTIR spectra, proving that temperature does not influence the molecular structure of the samples. Thus, in all cases, the main component is the protonated PANI and the content of oligomers in these samples is similar.

5.7 Raman spectroscopy

Raman spectroscopy is also a technique that permits obtaining information about the molecular structures to complement the results from the FTIR. We also used polarized Raman spectroscopy to get information about the orientation of the molecules in our sample. Unlike the FTIR, Raman spectroscopy allows selective observation of minor components of mixtures thanks to the resonance enhancement mechanism. To evaluate the doping of the PANI in the structures more accurately, a laser wavelength of 633 nm was used (Figure *5-15*), which resonantly enhances the Raman scattering from quinonoid and charged phenazine-like structures. In contrast, the vibration modes of doped C~N^+ structures are still well observed. Also, this excitation line permits evaluating oligomers presence in the sample.

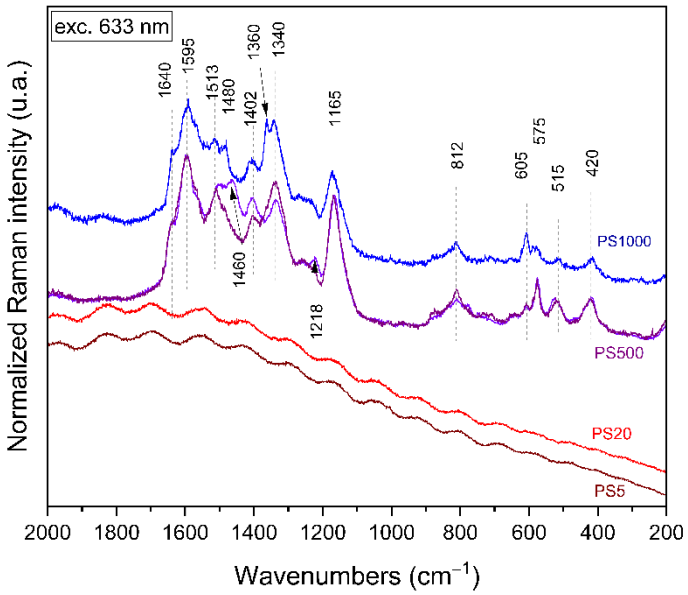

Figure 5-15. Raman spectra of PANI-SDS samples with different concentrations of APS in synthesis were excited using a laser beam with a wavelength of 633 nm.

The spectrum of PS1000 (blue curve) consists of bands at 1595 cm^{-1} (semiquinonoid ring stretching) with a shoulder at 1640 cm^{-1} (C=O stretching in benzoquinonoid structure); 1513 cm^{-1} (NH deformation); 1480 cm^{-1} (C=N stretching of bipolaronic quinonoid structure); 1402 cm^{-1} (neutral phenazine-like structure ring-stretching, highly localized C~N^{+} stretching); 1360 cm^{-1} (C~N^{+} stretching in localized polaron structure, e.g. in charged phenazine-like structure); 1340 cm^{-1} (C~N^{+} stretching in delocalized polaron structure); 1165 cm^{-1} (CH deformation); 812 cm^{-1} (benzenoid ring deformation); 605 cm^{-1} (end-group benzenoid ring stretching, typical N-phenyl phenazinium cation); 575 cm^{-1} (neutral phenazine-like ring stretching); 515 cm^{-1} (quinonoid ring stretching); and 420 cm^{-1} (ring deformation) (DE SANTANA *et al.*, 2006; DO NASCIMENTO; SILVA; TEMPERINI, 2006; MORÁVKOVÁ; DMITRIEVA, 2017; MORÁVKOVÁ; ŠEDĚNKOVÁ; BOBER, 2020; TRCHOVÁ *et al.*, 2014). The spectrum corresponds to a PANI containing both phenazine-like and benzo quinonoid oligomers. For PS500 samples (violet curve) the spectra differ from the PS1000 by the shift of the C=N stretching to 1460 cm^{-1}, a position typical for emeraldine base; the lack of localized polaronic C~N^{+} stretching; decrease of the end-group-ring stretching band at 605 cm^{-1}; and increase of the neutral phenazine-like and quinonoid ring stretching bands at 575 and 515 cm^{-1}. These changes indicate lower protonation of both polymer and oligomer fractions. Now, the samples with low concentrations of APS in synthesis, PS20 and PS5 display only

fluorescence when excited with a laser wavelength of 633 nm, as is typical for aniline oligomers (MORÁVKOVÁ *et al.*, 2013; TRCHOVÁ *et al.*, 2014).

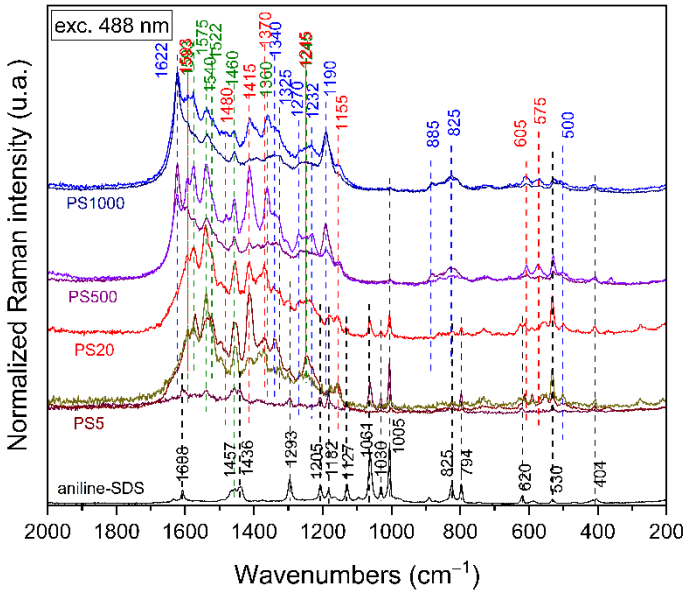

Figure 5-16. Raman spectra of PANI-SDS samples in different positions of the powder varying the concentration of APS, excited using a laser beam with a wavelength of 488 nm.

To evaluate the presence of some types of oligomers in the samples, Raman spectroscopy using a laser beam with a wavelength of 488 nm is indicated because some of these oligomers have the resonance of the molecular vibrations in this excitation frequency. Oligomers of type Michael-adducts, it is a component of the oligomer mixture obtained at neutral and alkaline media, have bands typical of 1,4-Michael type segment at Raman shift equal to 1593, 1575, 1540, 1460, 1360, and 1240 cm^{-1} (DOS SANTOS; TEMPERINI, 2020; FERREIRA; PIRES; TEMPERINI, 2011), were observed in all samples in Figure *5-15*, marked with green lines. Oligomers of type phenazine-like structures can be observed in bands at 1593, 1480, 1415, 1370, 1245, 605, and 575 cm^{-1} in all samples in Figure *5-16*, marked with red lines.

PANI polymer peaks are observed in the Raman spectra of PANI-SDS 1000 mM and PANI-SDS 500 mM represented with a blue line for the bands at 1622 cm^{-1} (benzenoid ring stretching); 1340 and 1325 cm^{-1} (C~N^{+} stretching in delocalized polaron structures); 1270 cm^{-1} (C-N stretching in quinonoid structure); 1232 cm^{-1} (C-N stretching in benzenoid structure); 1190 cm^{-1} (CH deformation); 885 cm^{-1} (benzenoid ring deformation); 825 cm^{-1} (out of plane CH deformation); and 500 cm^{-1} (ring deformation) (BOYER *et al.*, 1998; COCHET

et al., 2000; LOUARN *et al.*, 1996). Although, bands of the aniline-SDS mixture are observed in samples of PS5 and PS20, indicating the presence of just oligomers. These bands are marked in black lines.

Figure *5-16* exhibits more than one curve for each concentration to evaluate the heterogeneity of the samples in different positions. The spectra show high heterogeneity in the samples for other regions of the sample, in agreement with the morphology observed by SEM images, Figure *5-8*. The presence of polymers and oligomers free with the supramolecular structures could explain this. Evaluating the rod structures, it is evident the constitution of these materials are prevalently oligomers and aniline-SDS stacks, depending on the oxidation level, in agreement with the elemental analysis results that show the presence of 1 SDS molecule for 1 monomer molecule.

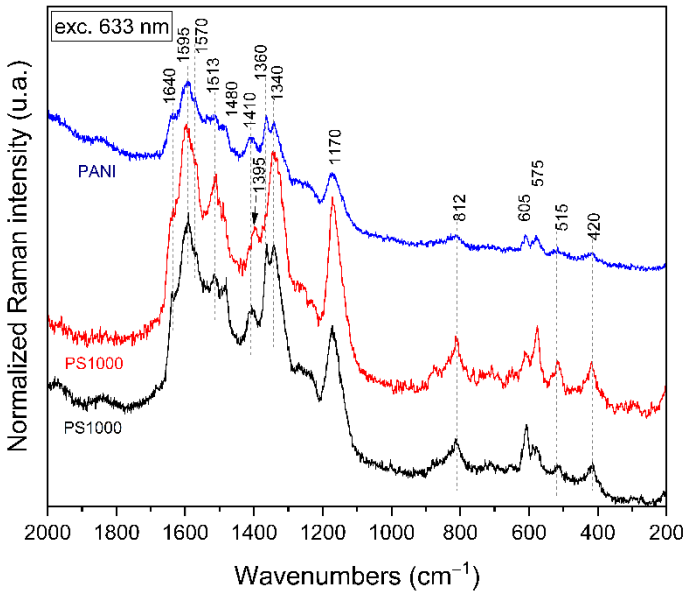

Figure 5-17. Raman spectra of PS1000 samples were prepared at temperatures different from the PANI polymer and excited using a laser beam with a wavelength of 633 nm.

The temperature influence in the synthesis of the samples was studied using a laser beam with a wavelength of 633 nm, resonance for quinonoid, and charged phenazine-like structures vibrations, Figure *5-17*. The spectrum of the sample prepared at room temperature, PS1000RT, differs from the sample prepared at 0 °C, PS1000, by the absence of C=N stretching band at 1480 cm^{-1} and C~N^{+} stretching band at 1360 cm^{-1}; and a decrease of the benzenoid ring-deformation band at 605 cm^{-1}, all being a fingerprint of protonated phenazine-like structure

(TRCHOVÁ *et al.*, 2014). On the other hand, a band connected with π-dimerized polaron structures (MORÁVKOVÁ; DMITRIEVA, 2017) at 1395 cm^{-1} replaces the neutral phenazine-like ring stretching highly localized C~N^+ stretching band at 1410 cm^{-1}. The PANI neat sample displays a higher fluorescence background than PANI-SDS samples, indicating lower protonation of the oligomer fraction (MORÁVKOVÁ *et al.*, 2013; TRCHOVÁ *et al.*, 2014) and the decreased benzenoid ring stretching band at 605 cm^{-1}, typical of charged phenazine-like (BOYER *et al.*, 1998).

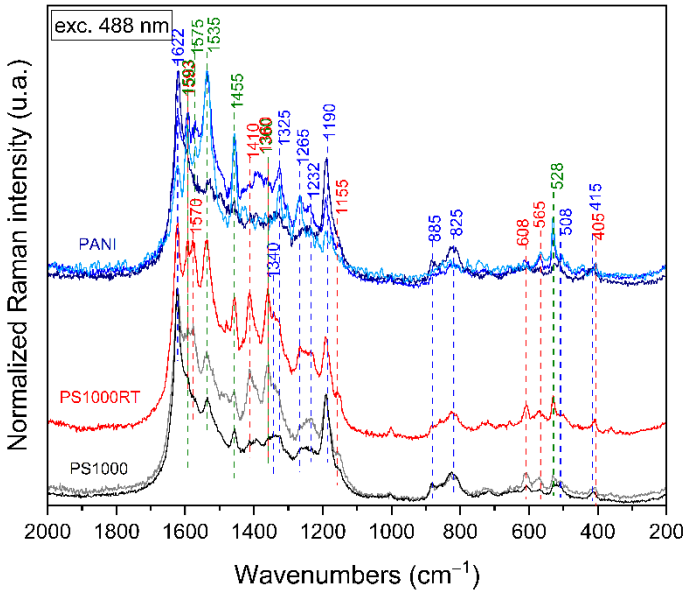

Figure 5-18. Raman spectra of PS1000 samples were prepared at temperatures different from the PANI polymer and excited using a laser beam with a wavelength of 488 nm.

The temperature influence in PANI-SDS 1000 mM samples was also studied in a laser beam with a wavelength of 488 nm to evaluate the presence of oligomers (Figure *5-18*). For each oligomer described in Figure 5-16, the same color was used to demonstrate its peak in Figure 5-18. It noted that oligomers' presence is not homogeneous in the sample, and they are more present in the residues of rods and plates in the sample agreement with the SEM images in Figure *5-8*, where the presence of broken structures in the samples can be noted. This proves that crystallinity structures are formed by SDS and aniline oligomers, and for high concentrations of APS, the formation of polymers occurs herein with these structures. Therefore, the sample prepared at a low temperature looks like it has more concentration of oligomers compared with room temperature.

5.8 Polarized Raman spectroscopy

Polarized Raman spectroscopy is a technique that permits obtaining the orientation of the molecules present in a sample. The method uses polarizers to polarize the light that comes to the sample and also the light that goes to the detector. If the sample has preferential orientations in some molecule bounds a variation in the intensity when this sample is rotated on the plane traverse to the laser beam is observed. PANI-SDS 5 mM samples were studied using a laser beam with a wavelength of 514 nm. The measurements were performed by turning the samples at 360° and taking a measurement for each 15°. First, test measurements were made using a silicon (100) sample to verify the polarized setup, where the peak of 520.5 cm^{-1} was studied. The Raman spectra and the polar graph are shown in Figure *5-19*.

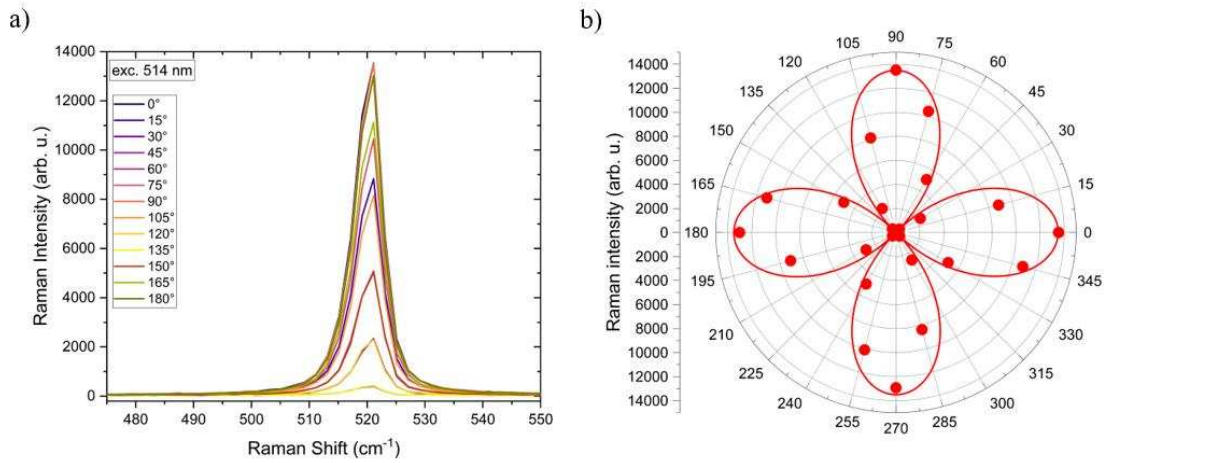

Figure 5-19. Polarized Raman spectroscopy for silicon (100) sample using a laser beam with wavelength 514 nm. a) Spectra of the 520.5 cm^{-1} peak from 0° to 180° and b) the polar graph for all the measurements from 0° to 360° where the straight line is an eye guide.

The silicon (100) sample was positioned for the cleaved part aligned with the 0°. As the cleaved part represents the orientation (100), the maximum intensity for this angle is expected. This can also be seen in Figure *5-19* a), which shows the change in intensity with the variation of the angle between the sample and the polarization of the light. For the silicon (100), the intensity is maximum over 90° rotation because this rotation takes back to the same orientation (YOO; HARIMA; YOSHIMOTO, 2015). The minimum is 45°, representing the orientation (110). Therefore, the setup works and can be applied to the PANI-SDS samples. In the Figure

5-19 b) have the polar graph plotting the intensity of the peak 520.5 cm^{-1} in function of the angle.

The PANI-SDS 5 mM rods were studied using a laser beam wavelength of 514 nm. Figure *5-20* a) shows the Raman spectra for this sample when excited for a laser beam of 514 nm. The bands 1607 cm^{-1} (C=C stretching vibration of the phenylene ring), 1206 cm^{-1} (C-N stretching in a benzenoid ring), 1182 cm^{-1} (C-H deformation vibrations of a semiquinonoid ring), 1004 cm^{-1} (C-C stretching), and 796 cm^{-1} (C-C ring deformation) are related to the aniline oligomers present in the rods. The bands 2800-3000 cm^{-1} (CH_2 bending modes and C-H stretching vibrations), 1300-1460 cm^{-1} (CH_2 bending modes), 1030 cm^{-1} (C-C stretching mode), and 824 cm^{-1} (RO-SO_3 vibrational modes) are related to the SDS presence in the sample (CAZZOLLI *et al.*, 2012; VALMALETTE *et al.*, 2014). Therefore, the results confirm that the rods are composoded of an association of aniline and SDS. To evaluate the orientation, measurements of polarized Raman spectra were obtained following the procedure described above, and the results are shown in Figure *5-20* b). It can be seen that some peaks change the intensity with the angle variation, showing that they have a preferential orientation of the molecules inside the rods.

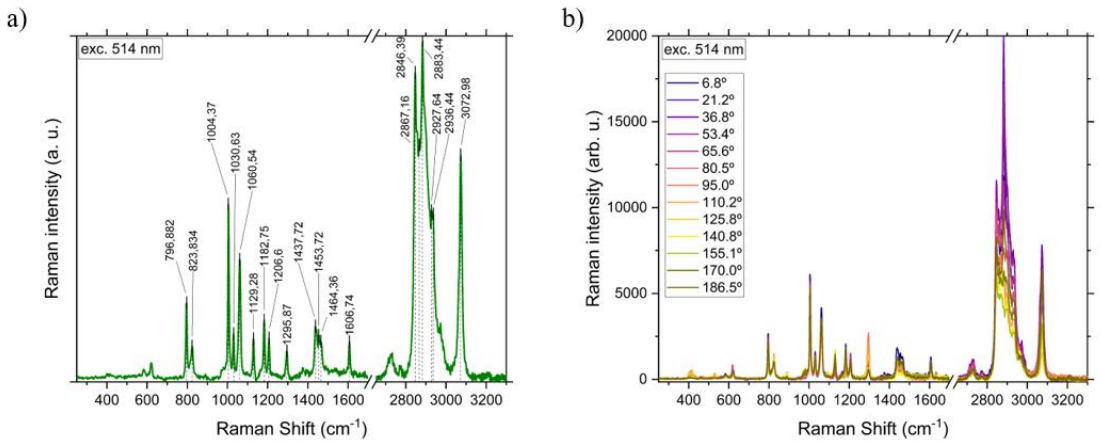

Figure 5-20. a) Raman spectroscopy for PS5 sample using a laser beam with wavelength 514 nm. b) Polarized Raman spectroscopy for PS5 sample using a laser beam with wavelength 514 nm varying the angle 0° to 180°.

Microscope optic images from the rod obtained from the Raman spectra are shown in Figure *5-21*, where the orientation variation can be seen. Figure *5-21* a) shows that 0° positions were chosen for the rod to be aligned with the polarization of the light.

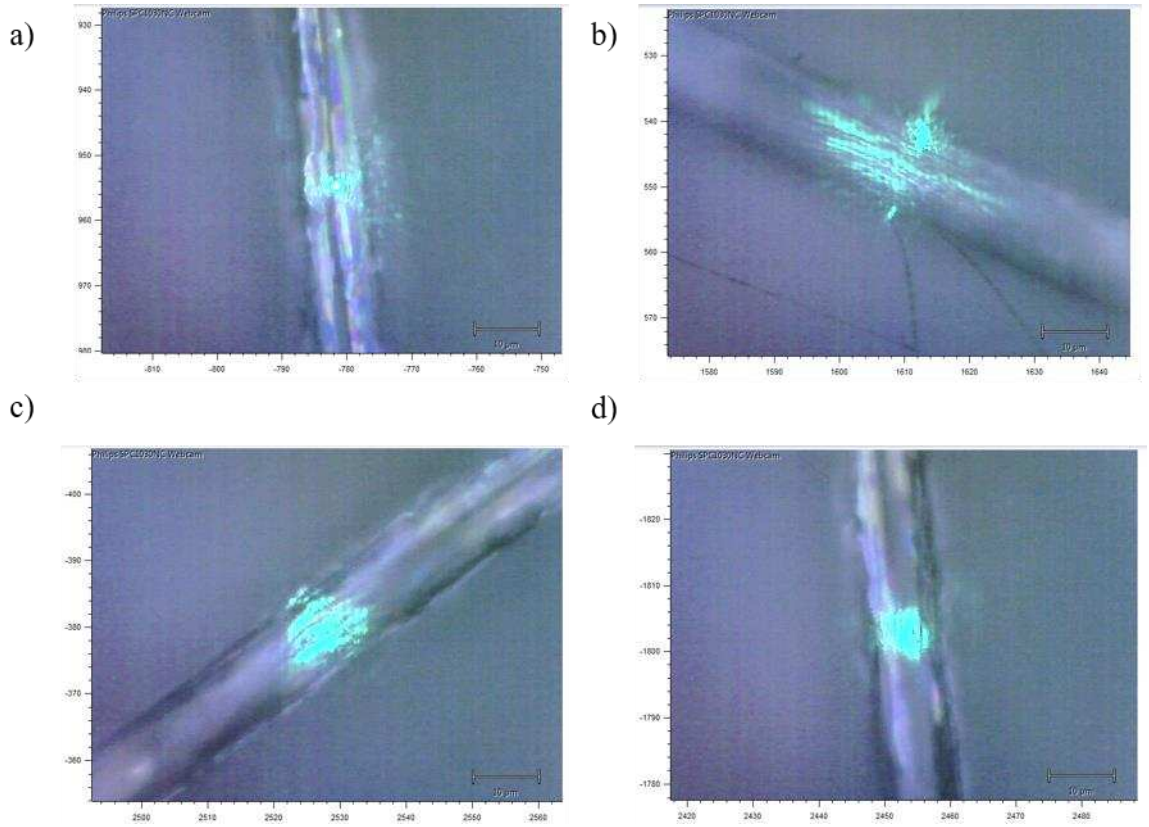

Figure 5-21. Microscope optics images from PS5 rods over glass slip for different angles: a) 0°, b) 60°, c) 120°, and d) 180°.

Using this technique we had hints about the molecular orientation of aniline (monomers and oligomers) and SDS molecules inside the rods. For PANI-SDS samples was analyzed the peaks of 1206 cm^{-1} (C-N stretching in a benzenoid ring), 1182 cm^{-1} (C-H deformation vibrations of a semiquinonoid ring), 1004 cm^{-1} (C-C stretching), and 796 cm^{-1} (C-C ring deformation) because the stretching of bounds C-C and C-N are aligned with the backbone of the oligomer molecule (PANI) and the peaks of 1030 cm^{-1} (C-C stretching mode) and 824 cm^{-1} (RO-SO_3 vibrational modes) because the stretching of bounds C-C are aligned with the backbone of SDS molecule. The angular difference between the SDS tail (carbon chain) and the head (RO-SO_3) is well-known, equal to 35.25°, and will be used to verify the results. The polar graph of these peaks is shown in Figure *5-22*.

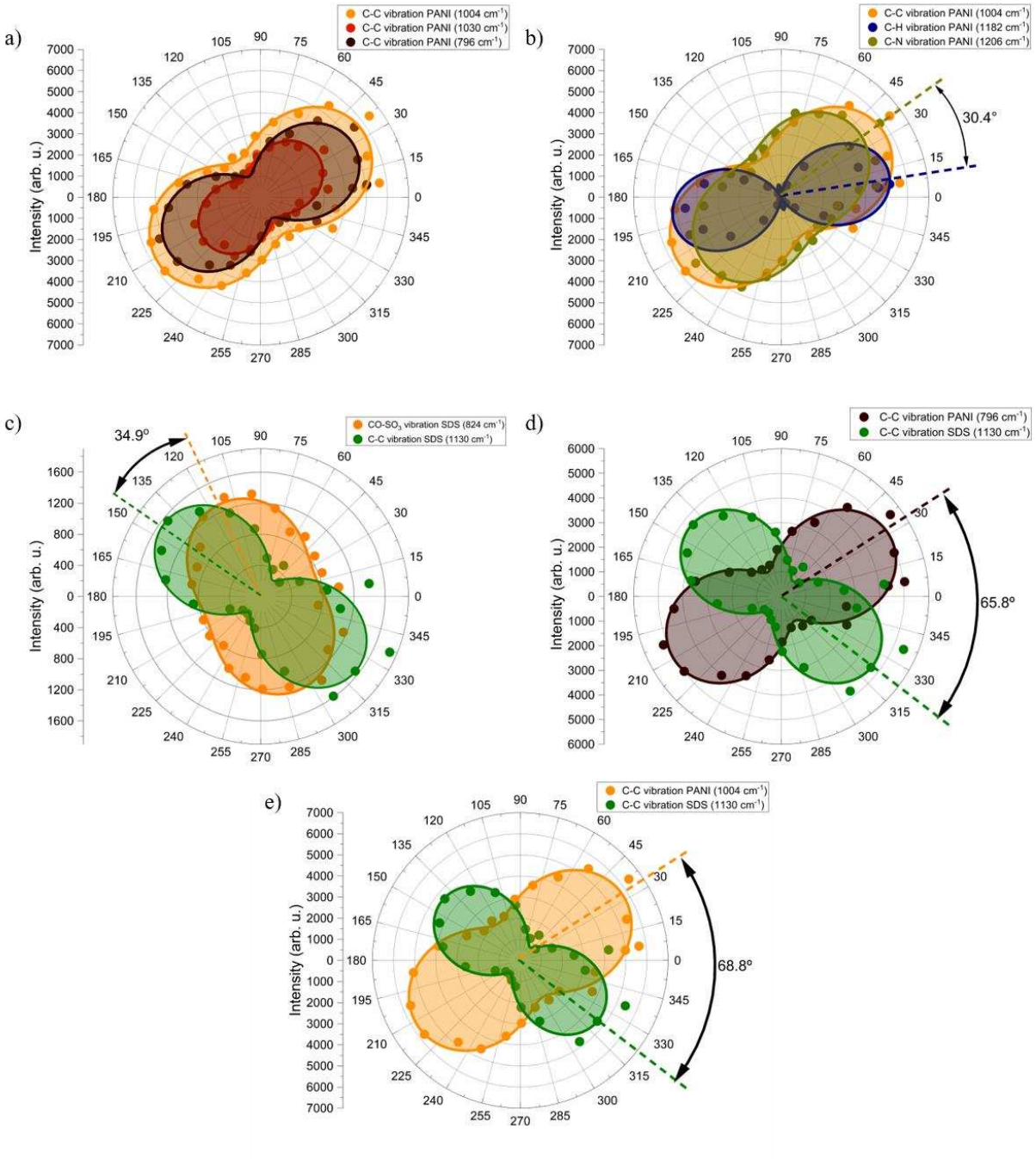

Figure 5-22. Polar graph with the intensity of Raman spectra using a laser beam with a wavelength of 514 nm for different peaks. a) Evaluation of peaks of the C-C stretching (1004, 1030, and 796 cm^{-1}) related to the backbone of aniline oligomers; b) Comparison of the angle between the backbone of aniline oligomers (1004 cm^{-1} C-C stretching) with the C-N stretching and C-H deformation; c) The angle between the backbone of SDS molecule (1130 cm^{-1} C-C stretching) with the surfactant head (CO-SO_3 vibration); d) Angle between the backbone of aniline oligomers (C-C stretching 796 cm^{-1}) and backbone of SDS molecule (1130 cm^{-1} C-C stretching); e) Angle between the backbone of aniline oligomers (C-C stretching 1004 cm^{-1}) and backbone of SDS molecule (1130 cm^{-1} C-C stretching).

All the polar curves were fitted using Equation 21 with $I \propto \cos^2\theta$ to obtain the orientation. Where A, B, and C are constants and θ is the angle of rotation of the sample. The polar behavior of these bounds vibrations follows some references observed in the $\cos^2\theta$.

$$I = A + B\cos^2(\theta + C) \tag{21}$$

Figure *5-22* a) shows that the peaks related to C-C stretching in the aniline or PANI oligomers have the same preferential orientation and cylindric symmetry (180° angle between the maximums or minimums) that correspond to the expected for a straight molecule-like oligomers; with this, we can conclude this orientation is the exact orientation of the backbone oligomers chain. Also, we can observe that the maximums have an angle of around 35°. As the rod is aligned with the horizontal (0°) we can conclude that the aniline/PANI molecules have an angle of around 35° with the principal axes of the rods. Figure *5-22* b) shows that the orientation of C-C stretching and the C-N stretching are aligned. This was expected because this two bonds are aligned with the backbone chain of the molecule. However, compared with the C-H deformation, it could be seen that the two are not aligned in agreement with what is expected. For the SDS molecules the peak related to C-C stretching of SDS and CO-SO_3 vibration, Figure *5-22* c), shows an angle of 34.9°, which is close to the theoretical angle between the backbone tail and the head of SDS that is equal to 35.25°. These results show the precision of the technique and the confirmability of the results. Finally, the orientation analysis between the aniline/PANI oligomers and SDS molecules is shown in Figure *5-22* d) and e), comparing the backbone orientation (C-C stretching) of the tail for SDS and the chain for the oligomers. We can see that the orientation between the two molecules inside the rod is 67°.

These results give us information about the rod's molecular orientation and allow us to schematic the unit cell that forms these crystalline samples, that is proposed in Figure *5-23*. The aniline/PANI oligomers are aligned in a straight line and the hydrophobic tail of SDS made an angle of 67° with the aniline/PANI oligomers. It is reasonable to assume that ionic forces must take place between the SDS head $–SO_3^-$ and the protonized $–NH^+$ in alinilne, connecting these two groups. From the Elemental Analysis results we know that the ratio of SDS molecule:aniline (N/S_{SDS} in Table *5-3*) is close to 1 meaning that for each aniline there would be one SDS molecule. Finally is thermodinamically unfavorable that the hidrophobic tail of the surfactante will be facing the solvente, so we propose a structure with double layers of SDS, and so of aniline/PANI oligomers, or one by one packing, as shown in Figure *5-23*.

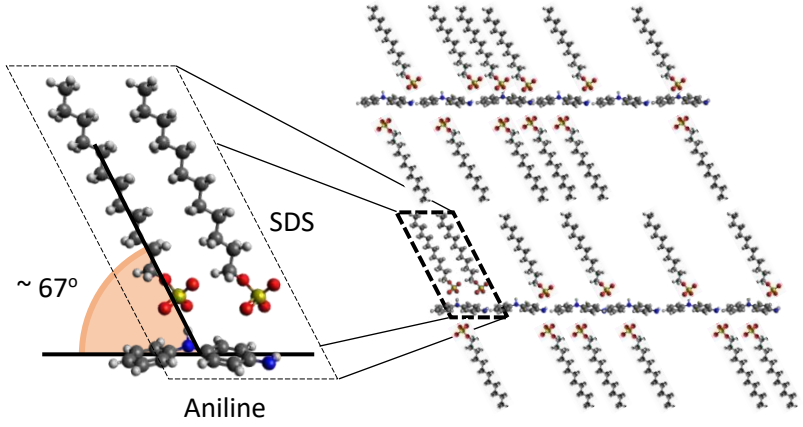

Figure 5-23. Illustration of a molecular orientation between the SDS molecules and aniline oligomers forming an angle of 67°. The images were obtained using the Avogadro software. Black spheres represent Carbon, red spheres represent Oxygen, yellow spheres represent Sulfur, and blue spheres represent Nitrogen.

5.9 X-ray diffraction (XRD)

X-ray diffraction (XRD) is another technique that permits evaluating the molecular structures that form the rods/tubes and plates. and will permit obtaining information about the characteristics of this crystal, such as the degree of crystallinity and the spacing between the crystalline planes. These results are essential for explaining the structural formation of these supramolecular structures.

Using the equipment high-resolution diffractometer, GNR Explorer acquired the XRD patterns for the samples PS5, PS20, PS500, PS1000, SDS, aniline oligomers, and PANI, to study the influence of the APS concentration, temperature synthesis, and the presence of SDS. The results are shown in Figure *5-24*.

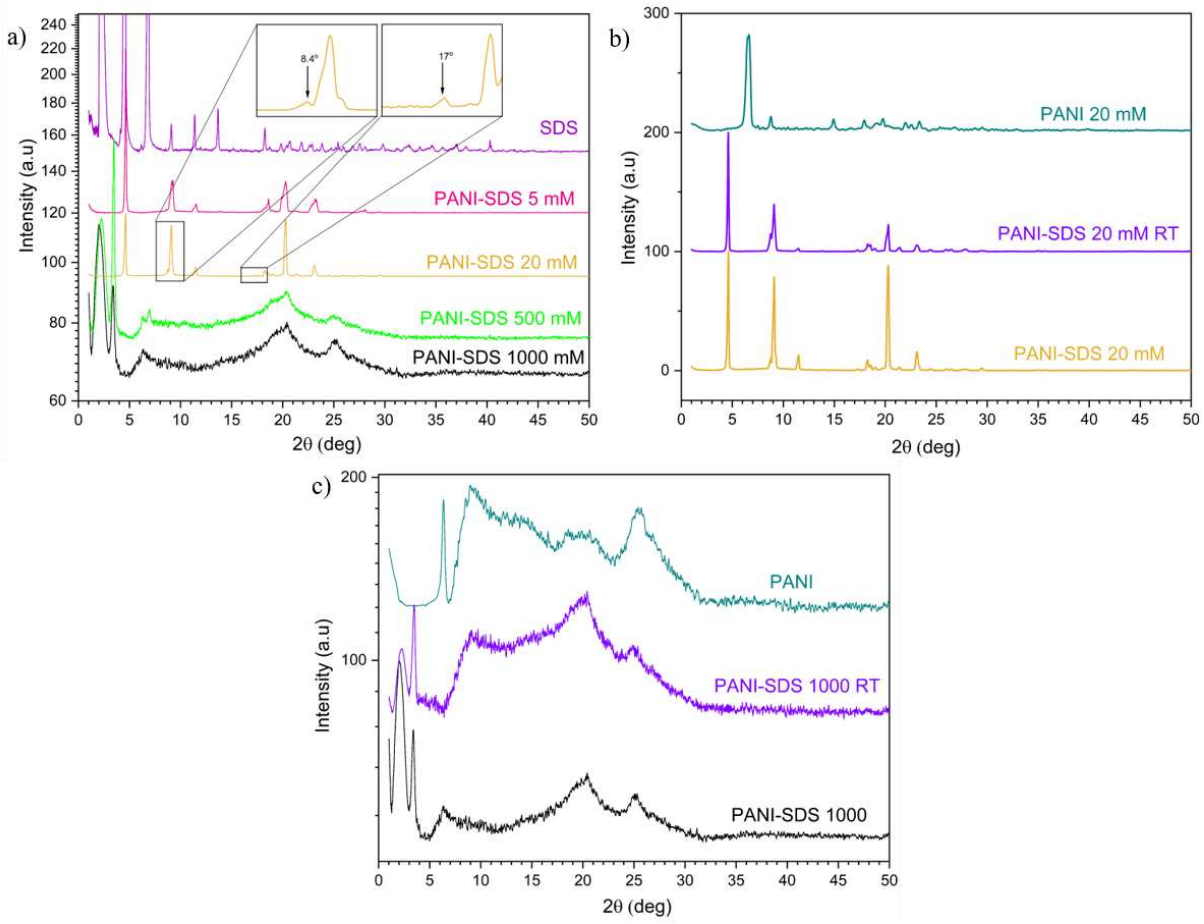

Figure 5-24. X-ray diffraction patterns of (a) SDS and PANI-SDS samples prepared with different amounts of APS, (b) PS20 samples prepared in different temperatures and without the SDS (aniline oligomer), and (c) PS1000 samples prepared in different temperatures and without the SDS (PANI polymer).

Figure *5-24* a), the most intense peaks of the SDS are positioned at 2θ = 2.29°, 4.55°, 6.17°, and 13.66° corresponding to (100), (200), (300), and (600) reflection planes, respectively, agree with the sodium dodecyl sulfate phase with a monoclinic P21/c space group (CCDC database, deposition number 750018). The samples obtained by synthesis using low concentrations of APS (PS5 and PS20) have structures with rod-like shapes, and the XRD patterns for the two samples have the same peaks, proving that the rods produced in the two samples have the same unit cell. Figure *5-24* a), the peaks present in this sample are positioned at 2θ = 4.63°, 9.20°, 11.52°, 8.60°, 20.32° and 23.10°. The peak at 4.63° is the strongest reflection corresponding to an interlayer space (d-spacing) of 1.91 nm. On the other hand the peak of anhydrous SDS, Figure *5-24* a) at 2θ = 2.29°, which corresponds to the double layer pack of SDS molecules of 3.89 nm , disappeared, indicading that this double layers of SDS is not present in PANI-SDS crystal, but only one layer, or a double layer with heterogeneous packing. This peak is positioned at an angle slightly larger than in the SDS samples, which can

be explained by the reduction of the angle of the SDS molecules from 93° (in the anhydrous form) to 67°, as shown in Depolarized Raman analysis. With these informations we are able to picture a probable organization of the aniline and SDS molecules: the rods are made of layers of one aniline/PANI molecules and two incomplete layers of SDS (Figure *5-23*). One other possible configuration of a one layer of aniline/PANI + one complete layer of SDS (meaning that for each aniline there will be one SDS) but this hypothesis was discarded since it is expected that about half of the nitrogen of the aniline will be protonated and only this half of nitrogen should interact with a SDS molecule. Other compelling evidence that supports the model of the two incomplete layers of SDS came from the results of AFM (to be shown later) which shows that the surface of rods has steps of ~3.1 nm height, which agrees with the size of two layers of tilted SDS molecules. Finally, two parallel SDS molecules that interacts with protonated aniline should have an orthogonal distance of ~ 0.54 nm (= distance between adjacent N in PANI × sin 67°) which correspond to a XRD angle of 2θ ~ 17°. Following the same reasoning, two SDS molecules should have 2θ ~ 8.4°. Small peaks at both angles are observed in PS20 (insets in Figure *5-24*).

Therefore, with the repetition of the unit cell proposed, the oligomers will have a better organization, with the distances between them equal to the length of angled surfactant molecules (MURUGESAN; SUBRAMANIAN, 2003; POUGET *et al.*, 1994). The peak at 20.32° is attributed to the scattering from oligomer chains due to π-π stacking interactions, and the peak at 23.10° appears due to the counter-ions (Cl^-) incorporated in the oligomers (BURON *et al.*, 2011). The high crystallinity of the samples is more evidence that the presence of oligomers in these samples is bigger than that of PANI polymers because the crystallinity of the samples decreases when the molecular weight of polymers increases (LUO *et al.*, 2009).

Samples produced using high concentrations of APS (PS500 and PS1000) are more amorphous and have the same pattern. The peaks present in these samples were 2θ = 3.24°, 6.40°, 19.37°, 20°, 20.50°, and 25.21°, indicating the formation of semi-crystalline PANI. Therefore, the samples have a large peak around 20° (amorphous) present in PANI neat samples, proving the presence of high molecular weight polymers. These spectra are similar to those obtained in the literature for PANI doped with SDS and sulfonic acid (KABABYA *et al.*, 1999; KIM *et al.*, 2001). The peak around 3.24° corresponds to an interplanar distance of around 2.6 nm. This peak may suggest the counter ion incorporation (Cl^-) for the PANI, seeing that the ratio of Cl/N increases for synthesis in high concentrations of APS (5.4 Elemental Analysis). Another explanation may be the SDS and PANI ordination change in the plate morphology. A

broad peak at 2.24° corresponds to an interplanar distance of 3.9 nm, which could be explained by a double SDS layer inter PANI chains/stacks, in agreement preposition in Figure *5-23*.

The influence of the temperature was analyzed for 20 and 1000 mM of APS. The XRD patterns of PS20 prepared at low and room temperature have the same peaks; the only difference appears in the intensity of the peaks, Figure *5-24* b). Because of the intensity decrease in the peaks at 9.20° and 20.32° for the PS20RT, this sample has a higher degree of crystallinity (DOC)(Table *5-4*). Therefore, the increase in the temperature does not influence the ordering of the crystalline oligomers and SDS, but only the crystallinity. The crystallinity of the oligomers can be seen in Figure *5-24* b) (PANI 20 mM) because the oligomers may form some supramolecular structures for this concentration. On the other hand, no change in DOC was observed for PS1000RT compared with PS1000, Figure *5-24* c). The change of peak positions occurs in the first two peaks are shifted towards lower angles and appear with less intensity, while the third peak (at 6.40° to PS1000) is shifted to 9.1° (PS1000RT). These modifications manifest a less close-packed arrangement of PANI chains/stacks.

Table 5-4. Degree of crystallinity (DOC) of PANI-SDS samples.

Sample	**DOC, %**	**Sample**	**DOC, %**	**Sample**	**DOC, %**
SDS	99.7				
PS5	88.8				
PS20	84.7	**PS20RT**	92.9	**PANI 20 mM**	59.8
PS500	43.2				
PS1000	44.2	**PS1000RT**	44.4	**PANI 1000 mM**	38.7

The bigger change in the degree of crystallinity is visible for the samples prepared without SDS; in the case of the PS20 sample, it decreases from 84.7 to 59.8%, and for the samples PS1000 it decreases from 44.2 to 38.7%. In both samples, the first intense sharp peak in the sample with SDS is shifted to $2\theta = 6.42°$ for the samples without SDS, corresponding to the interlayer distance of 1.38 nm. The shift towards lower distances evidences that in the case of the samples prepared with SDS, it is intercalated between polymer chains. Moreover, for both samples, there was a significant decrease in the peak intensity at 20.50°, suggesting much poorer ordering between adjacent PANI chains.

5.10 Electrochemical analysis

The idea of the project is to produce, characterize, and apply the PANI-SDS samples in electronic devices and/or electrochemical sensors. The characterization above allowed us to understand the formation of rods/tubes and plates and the composition of PANI-SDS structures. Now, the electrochemical analysis will be used to evaluate the electrochemical properties of the samples and apply them to supercapacitors and electrochemical sensors. For this, the samples must have a strong enough electric response to be measured. In the characterization of the molecular structures, it becomes clear that samples synthesized with low concentrations of APS (PS5 and PS20) have a formation of PANI oligomers that are not good conductors. On the other hand, the samples synthesized with high concentrations of APS (PS500 and PS1000) form PANI longer polymers in emeraldine salt that are good conductors. Thus, for the electrochemical analysis it will be used the samples synthesized with high concentrations of APS such as PS500, PS1000, PS1000RT, and PANI with no SDS.

To prepare the samples for electrochemical analysis, the clean powder was ground using a mortar and pestle to produce a fine powder; 10 mg of the sample powder was added to an eppendorf with 400 μL isopropanol, 590 μL milli-Q water, and 10 μL Nafion solution is added to facility the aggregation of the composites in the electrode, and the mixture was two times stirred during 15 minutes. 1 μL of this solution was drop cast in a commercial carbon glass electrode (working electrode). The working electrode was cleaned and polished using soft paper and deionized water, a diamond pad with 1 μm polishing diamond solution, and an alumina pad with 1 μm polishing alumina solution.

Cyclic voltammetry (CV) in HCl (0.2 M) solution was made for the samples PS500, PS1000, PS1000RT, and PANI, where the rate of [APS]/[Aniline] was equal to 0.5 (PS500) and was equal to 1 for the others samples. The measurements were performed using the samples deposited on a carbon glass electrode (CGE) (working electrode), platinum (counter-electrode), and silver chloride (reference electrode). Figure *5-25* shows the CV curves obtained for 4 cycles of measurements with the potential between (-0.2V to 0.8V) and for different scan rates of 10, 20, 50, 100, and 200 mV/s.

It is possible to see the presence of the peaks referent to oxidation (reduction) of the PANI. The peak around 0.2 V is related to the transition of the leucoemeraldine base (fully reduced) to the emeraldine salt (partially oxidized), and the peak around 0.5 V is associated with the transition from the emeraldine salt to the pernigraniline base (fully oxidized). The

second peak is smaller because of the presence of oligomers in the samples; this was observed in the Raman spectroscopy analysis. The presence of the two oxidation and two reduction peaks shows the quality of the polymer PANI synthesized. However, the sample with PANI neat has a bigger graph area than the other samples; it can be related to the gravimetric capacitance, meaning that the PANI neat has the biggest gravimetric capacitance (Table *5-5*). Therefore, the presence of SDS molecules in the sample decreases the gravimetric capacitance of the sample because the SDS is not a conductor and its presence in the sample does not contribute to the conductivity. As the capacitor is deposited by mass, the presence of SDS decreases the concentration of PANI molecules in the electrode, reducing the gravimetric capacitance. Finally, the temperature of the synthesis has a slight influence on the gravimetric capacitance where the low temperature is slightly greater. By analyzing the impact of the APS concentration, the sample of PS500 has a gravimetric capacitance around 30% lower than PS1000.

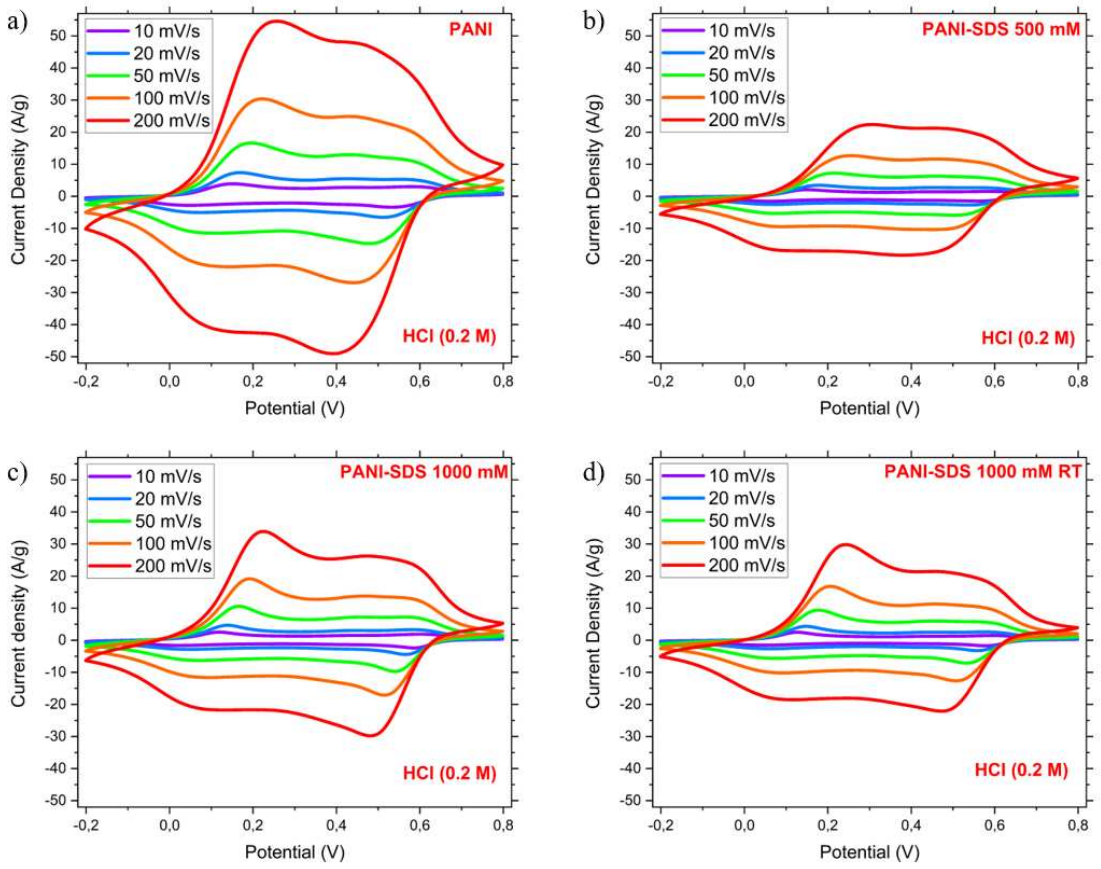

Figure 5-25. Cyclic voltammetry of PANI neat and PANI-SDS samples in HCl (0.2 M) solution, varying the scan rate of 10, 20, 50, 100, and 200 mV/s. a) PANI neat, b) PS500, c) PS1000, and d) PS1000RT.

Different electrolyte solutions were used to verify the influence of SDS molecules in the samples. Measurements in a neutral salt KCl (2 M) electrolyte are shown in Figure *5-26*. The gravimetric capacitance is bigger for the sample of PANI pure (Table *5-5*) for the scan rates larger than 20 mV/s. However, the samples with the SDS exhibit one oxidative peak, showing the SDS protects the samples, maintaining this process active in basic solutions. The gravimetric capacitance for the sample PS500 is lower than PS1000, showing the influence of the APS concentration in the samples. However, the synthesis temperature did not change anything in the shape curve, such as the capacitance in the KCl solution.

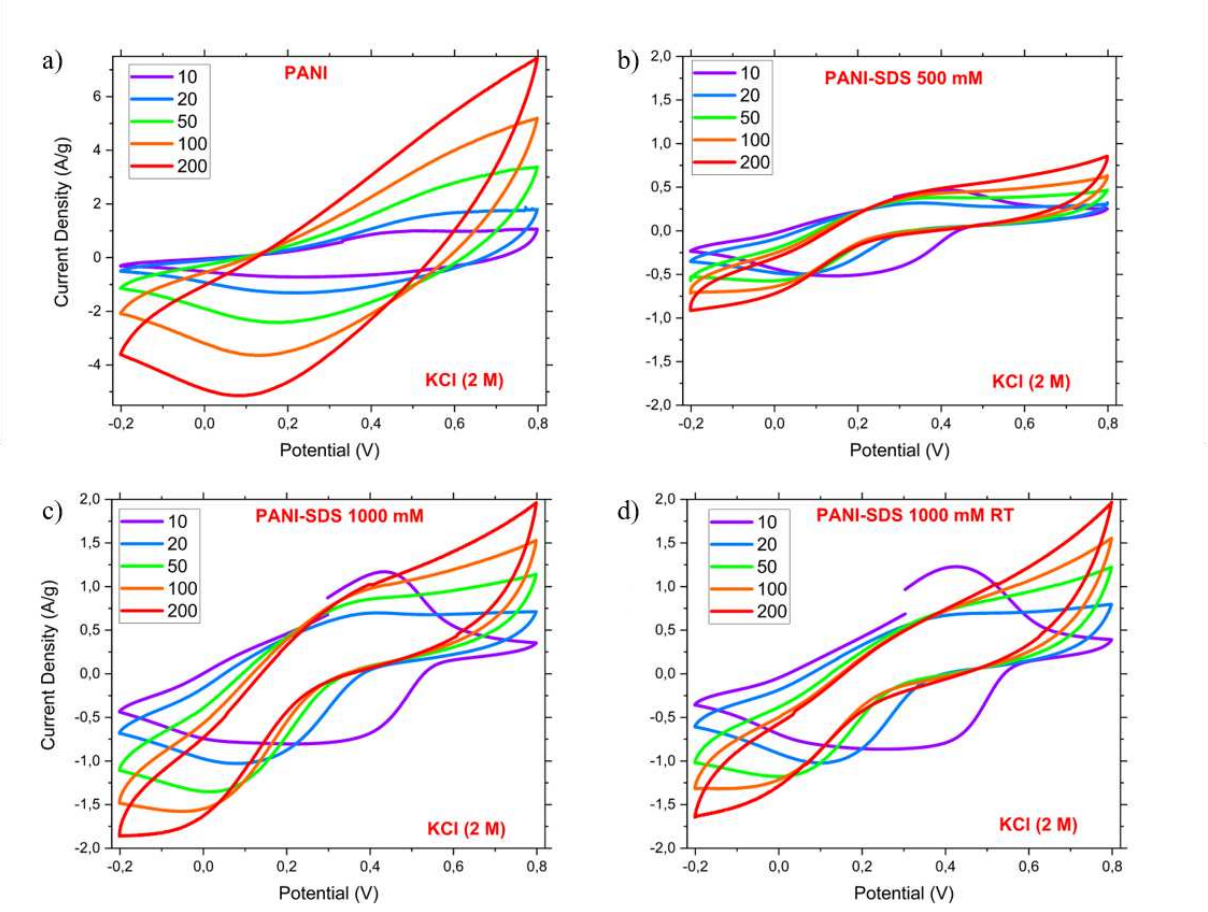

Figure 5-26. Cyclic voltammetry of PANI neat and PANI-SDS samples in KCl (2 M) solution, varying the scan rate of 10, 20, 50, 100, and 200 mV/s. a) PANI neat, b) PS500, c) PS1000, and d) PS1000 RT.

Measurements performed in a basic solution using KOH (6 M) electrolyte can be observed in Figure *5-27*. In this electrolyte, no oxidation peak is observed in those samples. However, the capacitance for the samples with SDS is more significant than PANI neat and the

weak signal from the samples of PANI in the basic solution is because the counter ion free in solution has the same charge as the polymer.

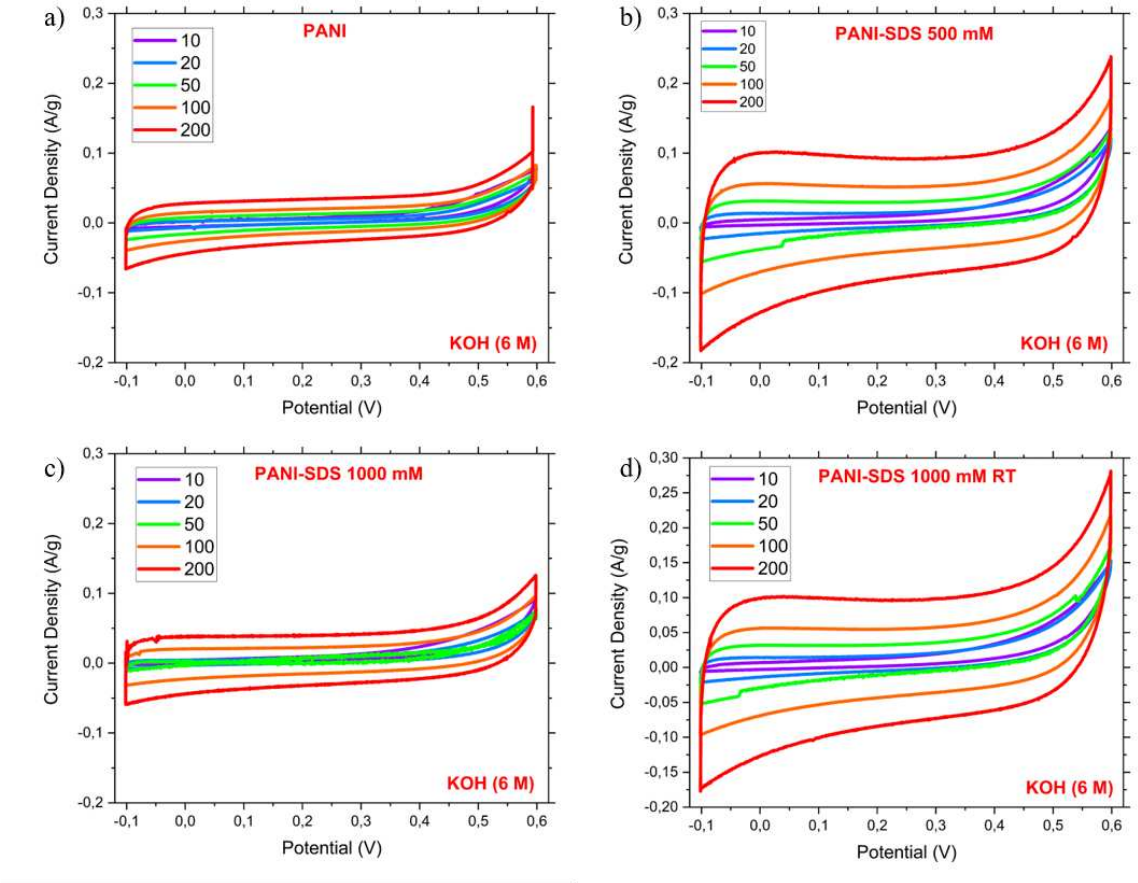

Figure 5-27. Cyclic voltammetry of PANI neat and PANI-SDS samples in KOH (6 M) solution, varying the scan rate of 10, 20, 50, 100, and 200 mV/s. a) PANI neat, b) PS500, c) PS1000, and d) PS1000 RT.

Another solution that was tested using the PANI and PANI-SDS electrodes was a PBS buffer solution. This electrolyte was chosen because it is essential to employ a buffer solution for electrochemical sensor characterizations to ensure that conductivity changes come from the interaction between the sensitive materials and not from changes in the solution characteristics. Figure *5-28* shows the CV curves obtained for the samples PANI, PS1000, and PS1000RT in a PBS solution (0.1 M), pH 7, changing the scan rate from 5 to 100 mV/s. The samples with SDS exhibit oxidative peak, showing that these samples have a better response in a neutral medium. Also, these samples have a bigger capacitance than the PANI (Table *5-5*). Thus, the SDS improves the PANI samples in basic or neutral mediums, making them stable in these

conditions and permitting the oxidation and reduction reaction to continue to occur in the PANI-SDS samples.

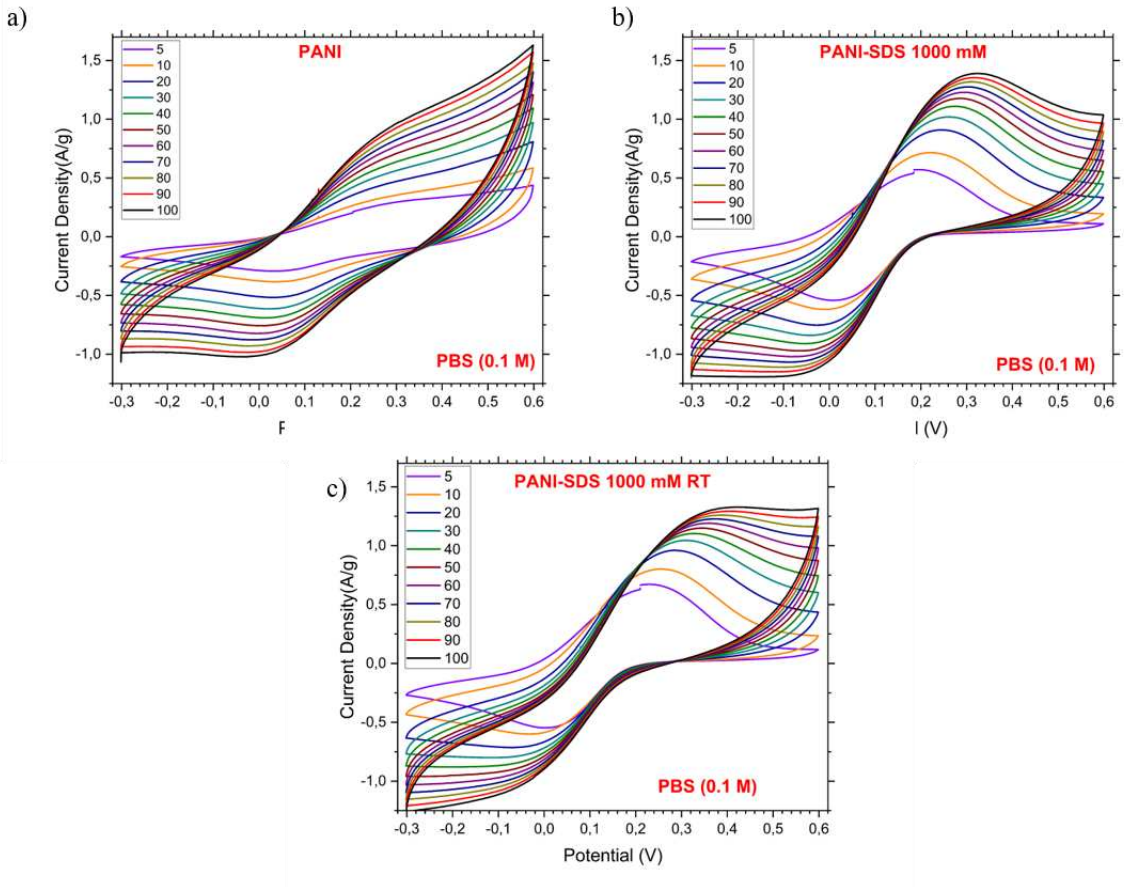

Figure 5-28. Cyclic voltammetry of PANI neat and PANI-SDS samples in KOH (6 M) solution, varying the scan rate of 5, 10, 20, 30, 40, 50, 60, 70, 80, 90, and 100 mV/s. a) PANI neat, b) PS1000, and c) PS1000 RT.

Table *5-5* shows the Gravimetric capacitance (F/g) calculated using the Eq. (22) and the results obtained from the samples of PANI neat, PANI-SDS 1000 mM (PANI-SDS LT), and PANI-SDS 1000 mM RT (PANI-SDS RT) in solutions of HCl (0.2 M), KCl (2 M), KOH (6 M), and PBS (0.1 M). The capacitance for samples with SDS is almost half lower than PANI neat in the HCl solution. However, for the other solutions the SDS increases the capacitance of the samples. The temperature of the synthesis did not show so much influence on the capacitance and the shape of the curves. The Gravimetric capacitance is calculate using the Eq. (22), where m is mass loaded on the electrode surface, ΔV is the potential window, v is the scan rate, I is the current, and V is the potential.

$$C = \frac{\int IdV}{2m\Delta Vv} \quad (22)$$

Table 5-5. Gravimetric capacitance (F/g) of PANI neat, PANI-SDS LT (1000 mM), and PANI-SDS RT (1000 mM).

Scan Rate (mV/s)	Gravimetric capacitance (F/g)		
	PANI-SDS LT	PANI-SDS RT	PANI
HCl (0.2 M)			
10	110.93	91.15	181.95
20	102.06	83.49	169.70
50	91.35	74.35	153.62
100	83.81	67.59	142.26
200	76.39	61.10	130.45
KCl (2 M)			
10	43.27	45.52	45.91
20	17.06	16.70	35.67
50	7.60	6.68	22.90
100	4.06	3.22	15.90
200	2.04	1.71	10.18
KOH (6 M)			
10	0.50	0.84	0.55
20	0.25	0.67	0.21
50	0.019	0.49	0.21
100	0.20	0.52	0.18
200	0.19	0.47	0.16
PBS (0.1 M)			
10	21.25	22.55	17.50
20	13.24	13.39	11.48
50	6.79	6.38	6.50
100	3.98	3.63	4.22
200	____	____	____

As the objective is to apply these samples in supercapacitors or electrochemical sensors, we will start the characterization focusing on the application of supercapacitors. The results from C.V. curves show a low capacitance for applying these samples in supercapacitors; however, another characterization can be used to evaluate other essential characteristics in a supercapacitor, such as the cycling stability and the time of charge and discharge. Cycling stability measurements were performed for the PANI neat, PANI-SDS 1000 mM (PANI-SDS LT), and PANI-SDS 1000 mM RT (PANI-SDS RT) during 5000 cycles, with a scan rate of 100 mV/s, in HCl (0.2 M) solution (Figure *5-29*). The samples of PANI-SDS have the capacitance

reduced by around 50% of the beginning after 5000 cycles, demonstrating that the samples do not have strong resistance for a significant number of cycles. For supercapacitors, it is expected that the capacitance does not decrease during 5000 cycles. PANI pure sample curve has an increase in capacitance at the beginning of the measurements, which can be associated with the swelling/shrinking problem caused by the ions accommodated into the conducting polymer. This effect does not happen in the samples with SDS, showing that SDS improves the release of ions in the samples because PANI-SDS samples have more crystallinity than the polymer.

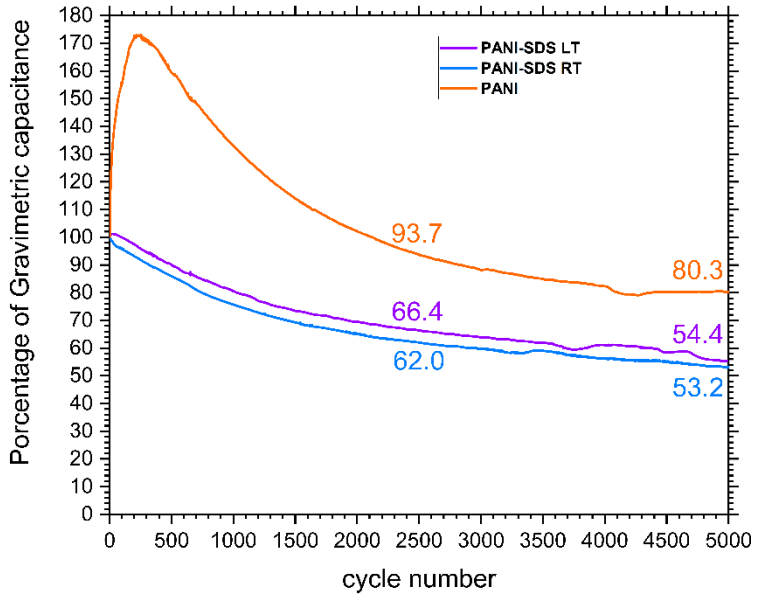

Figure 5-29. Percentage of Gravimetric capacitance for the samples PANI neat, PANI-SDS LT, and PANI-SDS RT, obtained by cyclic stability measurements during 5000 cycles, scan rate of 100 mV/s, in HCl (0.2 M) solution.

Gravimetric charge-discharge (GCD) curves measurements for samples of PANI neat, PANI-SDS 1000 mM (PANI-SDS LT), and PANI-SDS 1000 mM RT (PANI-SDS RT) were made (Figure *5-30*). It is shown that the time of charge of the samples is bigger than the time of discharge time, demonstrating that samples are unsuitable for applying for a supercapacitor and batteries. The gravimetric capacitance obtained by the discharge process shows the sample of PANI neat is bigger than SDS samples and the capacitance is not significantly affected by the temperature of the synthesis process.

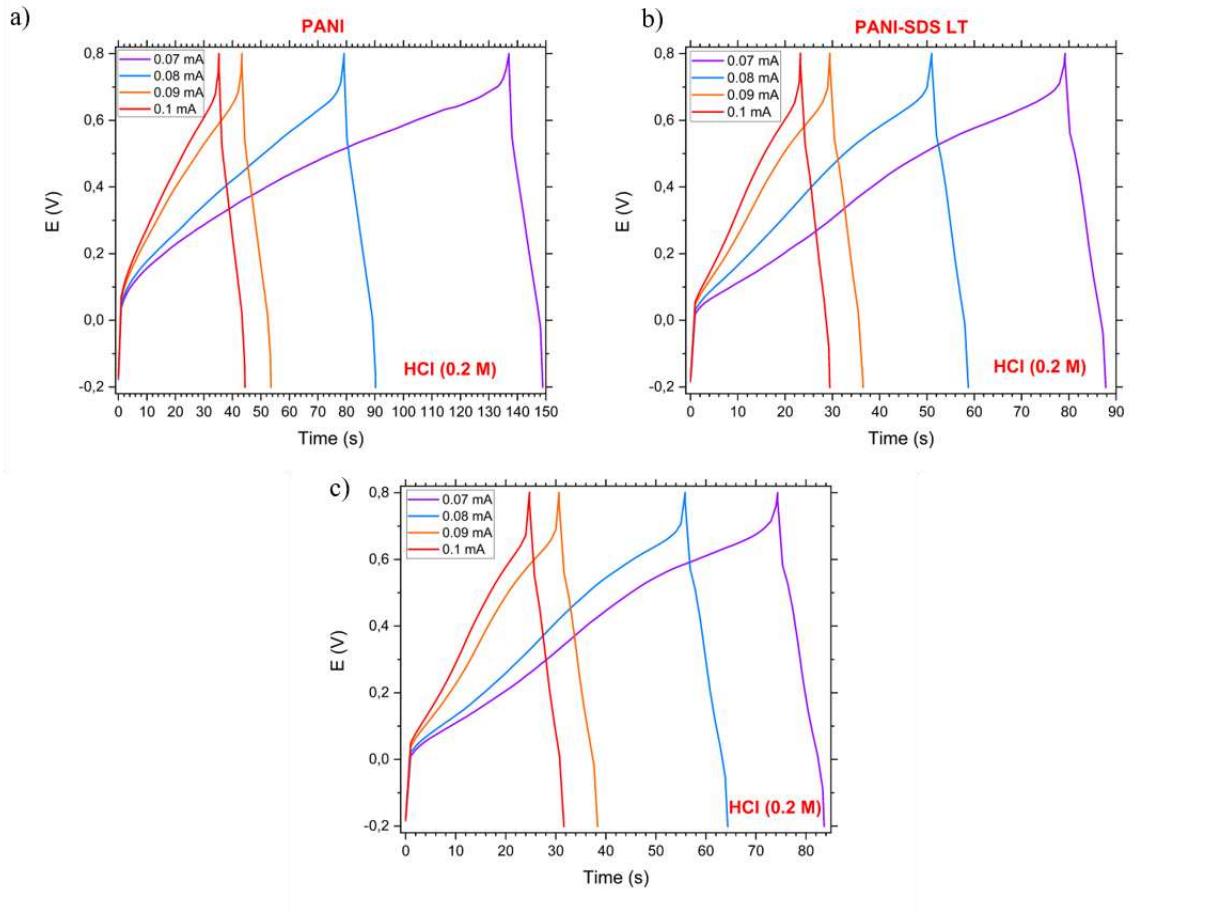

Figure 5-30. Gravimetric charge-discharge curves for the samples PANI neat, PANI-SDS LT, and PANI-SDS RT, obtained by a charge-discharge current with 0.07, 0.08, 0.09, and 0.1 mA in HCl (0.2 M) solution.

Table 5-6. Gravimetric capacitance (F/g) obtained from the discharge curve.

Applied current (mA)	**Gravimetric capacitance (F/g)**		
	PANI-SDS 1000 mM	PANI-SDS 1000 mM RT	PANI
0.07	60.2	65.1	82.9
0.08	61.8	68.0	88.5
0.09	63.2	69.4	91.6
0.1	62.4	68.8	91.0

The samples of PANI neat, PANI-SDS 1000 mM (PANI-SDS LT), and PANI-SDS 1000 mM RT (PANI-SDS RT) do not present good results to be applied in supercapacitors. Therefore, we testes the applicability of these samples to be used as an electrochemical sensor. Ascorbic acid was the substance to be tested and the interest in these molecules comes from the fact it is important to monitoring the concentration of this molecule in the human metabolism, to prevent some diseases. Also, can be used this sensor to quality control in food and

pharmaceutical industry. Ascorbic acid sensor based in PANI is produced by some references, in this project the idea is studied the influence of SDS in the quality of the sensor. Cycling voltammetry using a 50 mM ascorbic acid in 0.1 M of PBS solution, Figure *5-31*, was used to evaluate whether the samples may be employed as sensors. It showed that SDS improved the sensibility of the samples in ascorbic acid solution. The response current is duplicated compared with the PANI neat and three times more than the Carbon Glass electrode. The ascorbic acid peak was 0.6 V in PANI neat samples, and CGE shifted to 0.4 V for the samples with SDS. This happens because of the adsorption of ascorbic acid for PANI-SDS molecules.

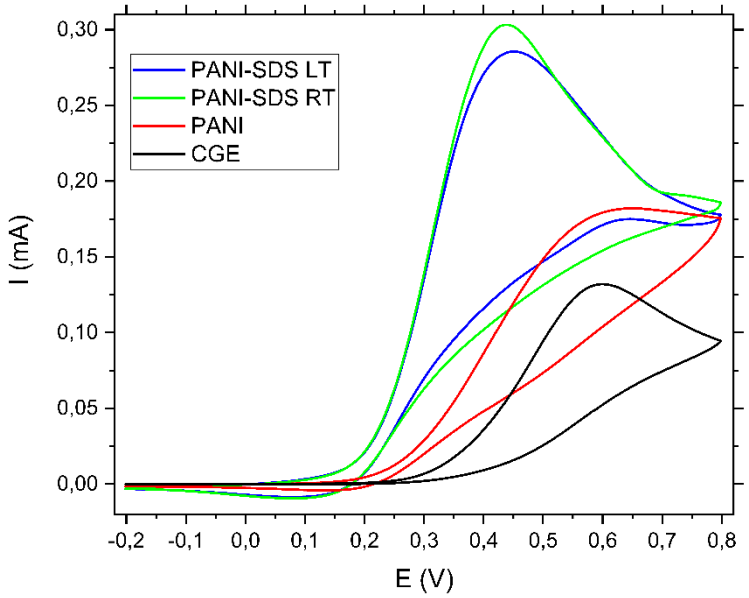

Figure 5-31. Cyclic voltammetry measurements of PANI, PANI-SDS LT, PANI-SDS RT, and carbon glass electrode (CGE) for 50 mM ascorbic acid pure in 0.1 M PBS solution for the scan rate equal to 10 mV/s.

To obtain information about the diffusion of ions in the layers of the sensors, cyclic voltammetry measurements of PANI, PANI-SDS LT, and PANI-SDS RT were performed for 50 mM ascorbic acid concentration, 0.1 M of PBS solution, and varying the scan rate from 5 to 100 mV/s, Figure *5-32*. In Figure *5-25*, we can note that samples with SDS have an oxidation peak and a higher response than PANI pure. The inset graph it show the peak intensity versus the square root of the scan rate ($v^{1/2}$), giving us information about the diffusion of the ions. The linear behavior shows the process is an electrochemically reversible electron transfer process involving freely diffusing redox species (ELGRISHI *et al.*, 2018).

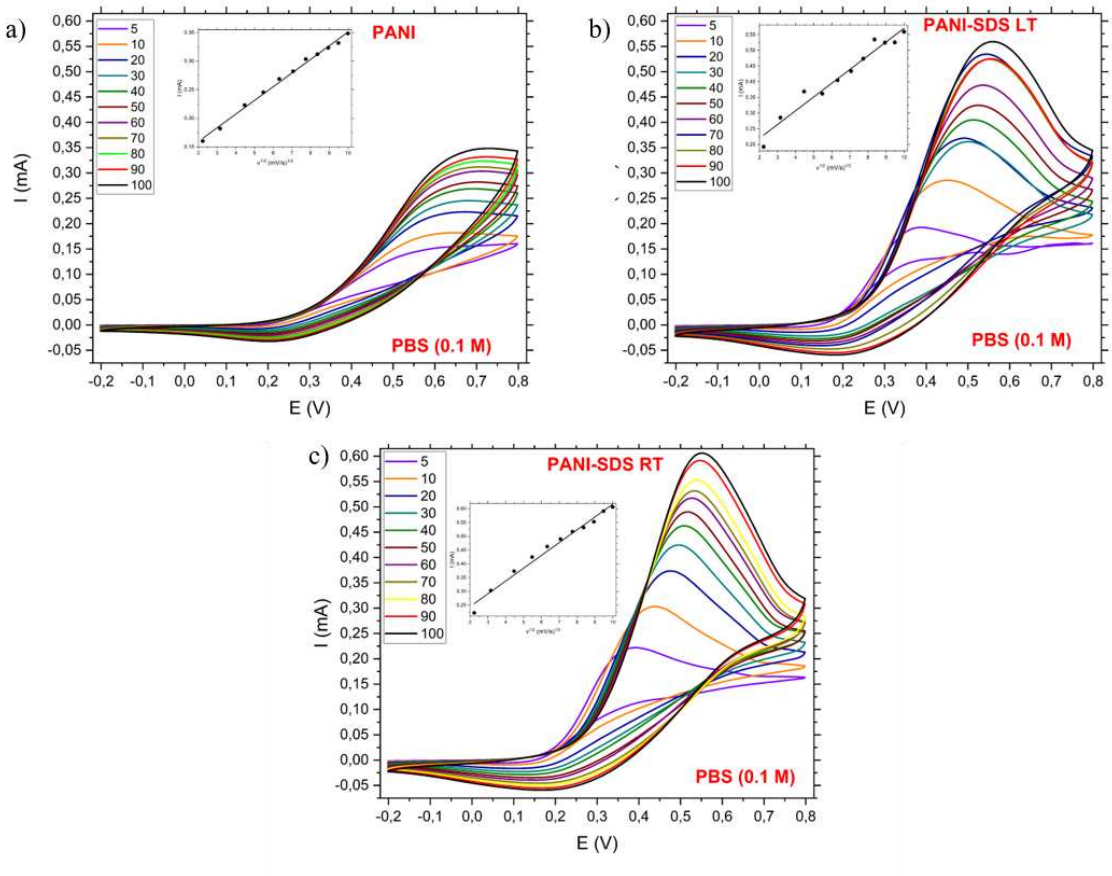

Figure 5-32. Cycling voltammetry of PANI, PANI-SDS LT, and PANI-SDS RT samples using 50 mM ascorbic acid neat and 0.1 M PBS solution, varying the scan rate from 5 to 100 mV/s.

We performed chronoamperometric measurments to obtain the calibration curves for the sensor with for PANI-SDS LT and PANI-SDS RT samples. Figure *5-33* a) shows the calibration curve to get the best potential applied (V). The potential choose was 0.6 V because have the higher current response. Figure *5-33* b) shows a measurement of PANI-SDS LT for 15 different concentrations of ascorbic acid from 0.02, 0.1, 0.2, 0.5, 1, 1.5, 2, 4.5, 7, 9.5, 12, 27, 50, 77, and 102 mM. The measurements were performed by after each addition of the ascorbic acid, the sample is stirring during 1 minute and waiting for 5 minutes, and the results read from the stabilization of the curve. Therefore, Figure *5-33* b) it is possible seen the peaks that represent each addition of solution.

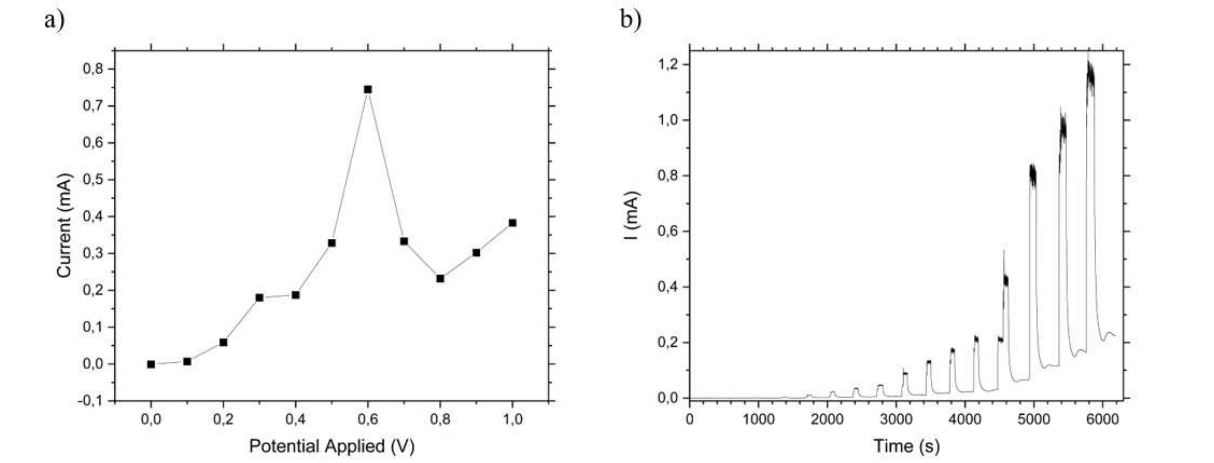

Figure 5-33. a) Calibration curve to find the better potential applied to be used in chronoamperometric. b) Measurement of chronoamperometric of PANI-SDS LT for 15 different ascorbic acid pure concentrations.

The calibration curves obtained using 3 repetitions of PANI-SDS measurements are show in the Figure *5-34*, where the inset graph is in logarithm scale to facility the visualization. It could be seen that the two samples have a straight line linear fit. The calibrations curves were obtained using an ascorbic acid pure chemical component. The sample of PANI-SDS RT shows a better result in terms of lower error bars at each point when compared with the error bars. The values for both the samples were almost the same very close showing that temperature of the synthesis does not significantly influence in the sensor performance. The calibration curve for the sample PANI-SDS LT and PANI-SDS RT can be obtained by a linear fit of the curves in Figure *5-34*. For the sample PANI-SDS LT the equation find was I(mA) = -0.00012(9) + 0.00296(8)*[AA](mM) and for PANI-SDS RT was I(mA) = -0.00011(2) + 0.00285(5)* [AA](mM), where *I* stand for the average current in mA and [AA] the concentration of ascorbic acid in mM.

The sensor test measurements were performed using a commercial orange juice to evaluate if the sensor can be selectively reutilized, and the results using a calibration curve are close to expected. The results are shown in Figure *5-35* a), where the specification of the orange juice is depicted in Figure *5-35* b).

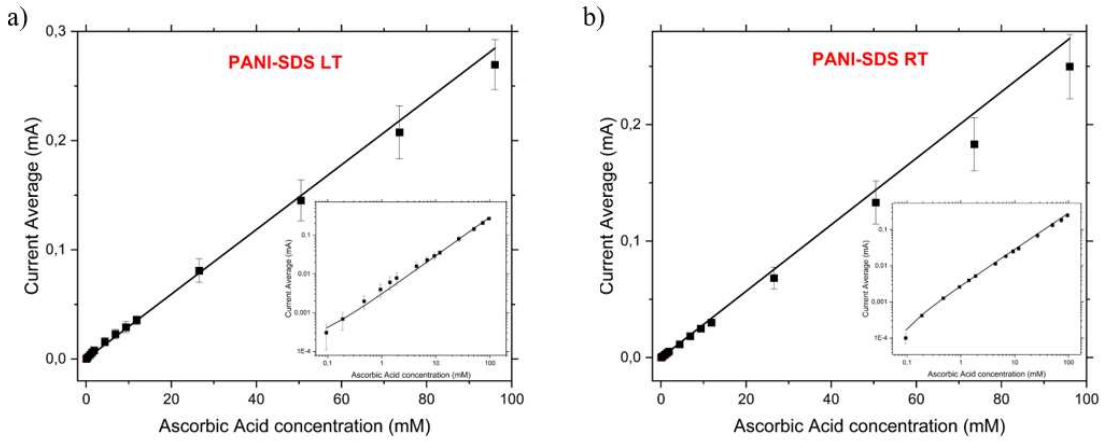

Figure 5-34. Calibration curve of the samples PANI-SDS LT and PANI-SDS RT for ascorbic acid sensor.

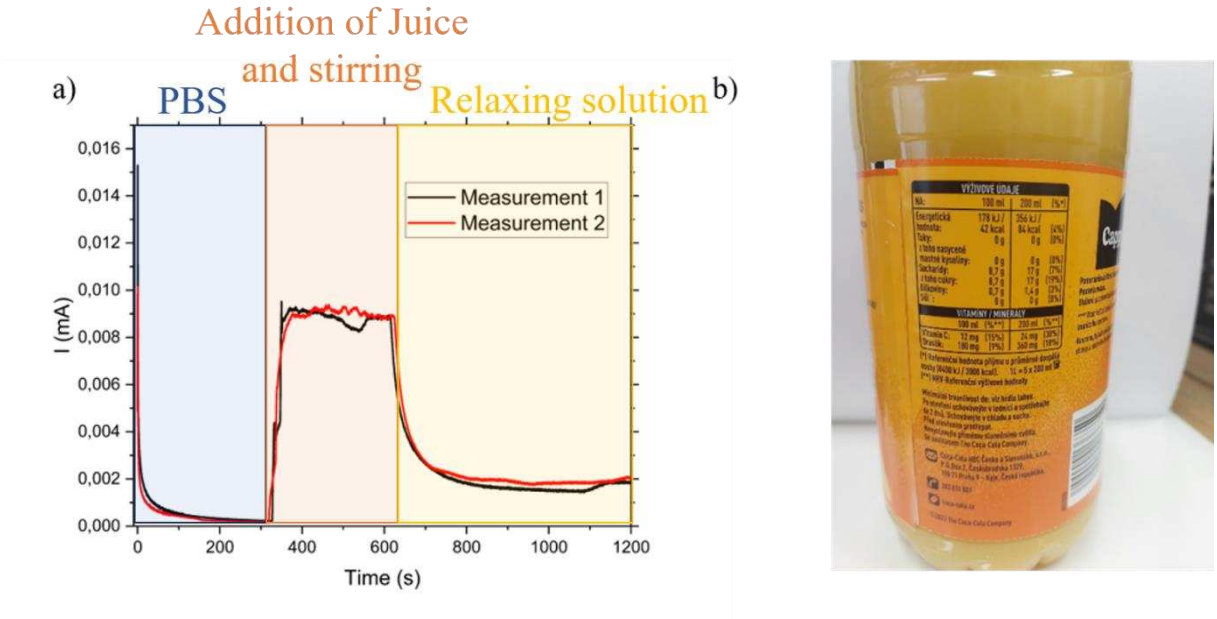

Figure 5-35. Sensor measurements testing using a commercial orange juice to detect the ascorbic acid in a PBS (0.1 M) solution. a) The chronoamperometric curves for the two measurements and b) the specification of the commercial orange juice.

The Figure *5-35* a) was performed to test using the same sensor. After measurement 1, the sensor was cleaned with deionized water and started measurement 2 using a new PBS solution. The solution of juice added was 8 mL in 4 mL of PBS solution. The two curves show a slight difference between them, proving that the sensor can be reutilized. This measurement was made using a commercial orange juice that shows us the selectivity of our sensor for sensing just the ascorbic acid. The current plateau in Figure *5-35* can be utilized to find the

concentration of the ascorbic acid in the juice; using this current to the calibration equation (0.0014 mA), the value measured of the ascorbic acid concentration was 0.51 mM, and the value expected (from the label) is 0.46 mM that represents a deviation of around 10%. The detection limit is 0.11 mM, and the quantification limit is 0.33 mM of Ascorbic acid for the PANI-SDS samples calculated following the rules of Agência Nacional de Vigilância Sanitária (ANVISA).

6 RESULTS AND DISCUSSIONS OF PDA/ANI-SDS SAMPLES

In this chapter we present the results from the characterization and application of electrochemical sensors of the copolymers and SDS composites. The copolymer samples were obtained by a radical synthesis using the same concentration of the monomer's aniline and PDA with the ratio of oxidant agent and monomers equal to 1 ([APS]/([Ani]+[PDA]) = 1). Also, it evaluated the influence of three different dopant acids such as HCl, H_2SO_4, and CSA. The following characterization techniques were employed: Scanning Electron Microscopy (SEM), Transmission Electron Microscopy (TEM), Raman Spectroscopy, Fourier-Transformed Infrared Spectroscopy (FTIR), X-ray Diffraction, Elemental Analysis, Maldi-TOF, and Electrochemical Analysis.

6.1 Electron microscopy

Microscopy analyses of the samples were made using SEM and TEM techniques. The samples of PDA/Ani and PDA/Ani-SDS produced with different dopants (HCl, H_2SO_4 and CSA) were cleaned following the process described in RESULTS AND DISCUSSIONS OF PANI-SDS SAMPLES. For all the characterization, the samples were ground befor used. Figure *6-1* represents the images of all samples. The nomenclature is presented in Table *6-1*. Also, the polymers' samples using only aniline (Ani) or PDA were synthesized using the same concentration of HCl, and the ratio of [APS]/[monomer] equal 1.

From Figure *6-1*, it is possible to see the difference in the morphology of the polymers produced by only the monomers of ANI and PDA. The ANI composites (Figure *6-1* a)) are more amorphous than the ones made for PDA (Figure *6-1* b)). The PDA samples have a plate-like morphology. Figure *6-1* c), e), and g) show the samples produced using copolymer synthesis, where the influence of PDA and different acids in the morphology becomes apparent, making them more crystalline. The sample in acid solution with the addition of PDA (Figure *6-1* c)) presents diverse crystalline structures. Now, with the addition of the SDS (Figure *6-1* d)) some rod-like structures can be observed and the samples become more crystalline. Figure *6-1* e), the composites produced using H_2SO_4 (PAH) are more crystalline than the polyaniline

(ANI), and the morphology of the structures is not well defined. However, the addition of SDS (PAHS) increases the crystallinity of the samples and the formation of rod structures, Figure *6-1*f). The CSA (biggest molecule) also leads to the formation of crystalline structures in the samples, Figure *6-1* g), probably because of the formation of structures with this CSA and the polymers. Adding SDS (PACS) facilitates the formation of micrometer structures with rod and plate morphology. TEM images were obtained for the same samples to continue the microscopy analysis (Figure *6-2*).

Table 6-1. Nomenclature of the samples characterized with SEM and TEM.

Monomer	Surfactant	Dopant	Name
Aniline	-	HCl	Ani
PDA	-	HCl	PDA
PDA+Aniline	-	HCl	PA
PDA+Aniline	SDS	HCl	PAS
PDA+Aniline	-	H_2SO_4	PAH
PDA+Aniline	SDS	H_2SO_4	PAHS
PDA+Aniline	-	CSA	PAC
PDA+Aniline	SDS	CSA	PACS

From Figure *6-1*, it is possible to see the difference in the morphology of the polymers produced by only the monomers of ANI and PDA. The ANI composites (Figure *6-1* a)) are more amorphous than the ones made for PDA (Figure *6-1* b)). The PDA samples have a plate-like morphology. Figure *6-1* c), e), and g) show the samples produced using copolymer synthesis, where the influence of PDA and different acids in the morphology becomes apparent, making them more crystalline. The sample in acid solution with the addition of PDA (Figure *6-1* c)) presents diverse crystalline structures. Now, with the addition of the SDS (Figure *6-1* d)) some rod-like structures can be observed and the samples become more crystalline. Figure *6-1* e), the composites produced using H_2SO_4 (PAH) are more crystalline than the polyaniline (ANI), and the morphology of the structures is not well defined. However, the addition of SDS (PAHS) increases the crystallinity of the samples and the formation of rod structures, Figure *6-1* f). The CSA (biggest molecule) also leads to the formation of crystalline structures in the samples, Figure *6-1* g), probably because of the formation of structures with this CSA and the polymers. Adding SDS (PACS) facilitates the formation of micrometer structures with rod and

plate morphology. TEM images were obtained for the same samples to continue the microscopy analysis (Figure *6-2*).

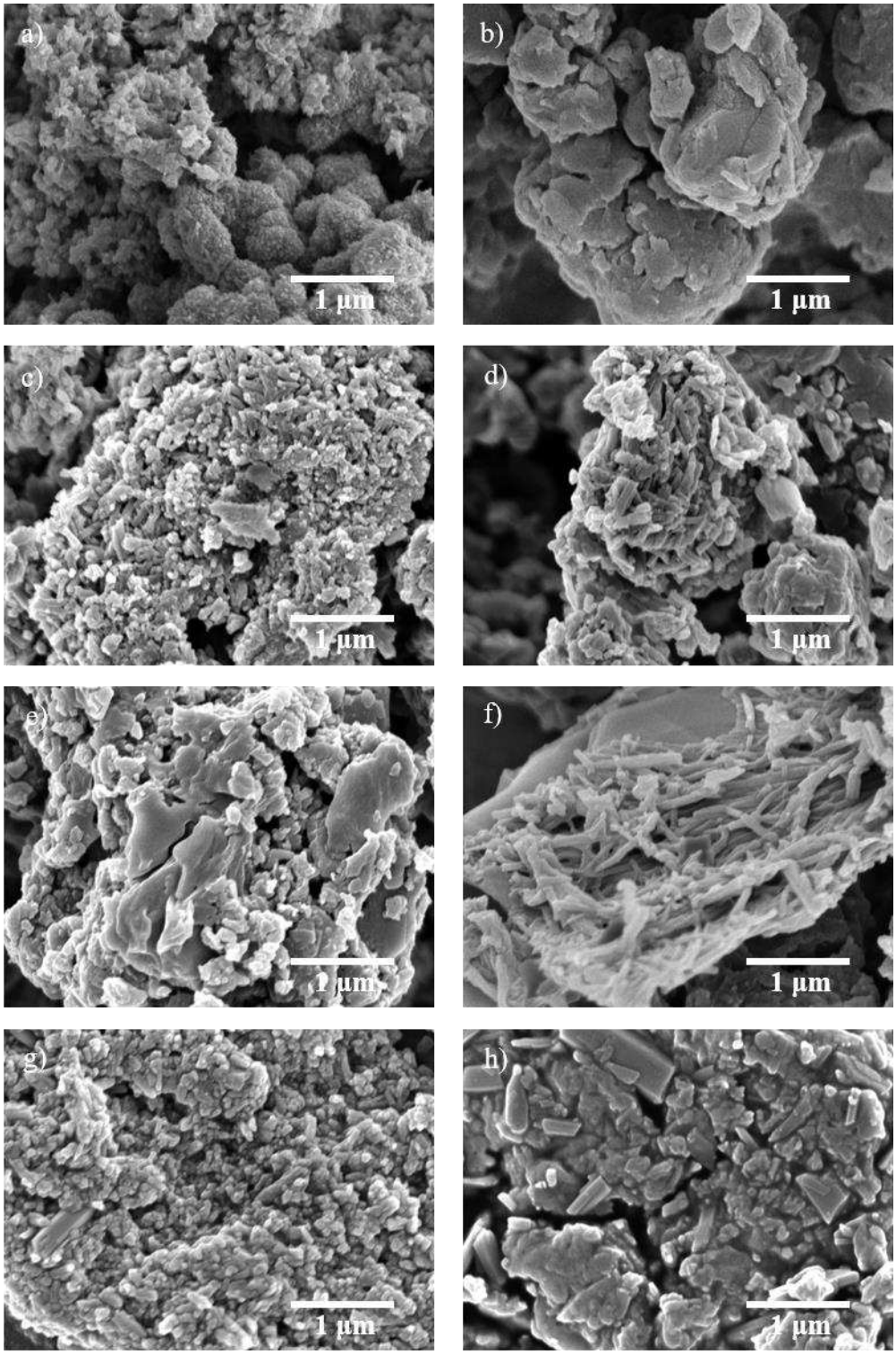

Figure 6-1. SEM images of polymer produced from aniline, PDA, and composites of PDA/ANI and PDA/ANI-SDS samples produced to change the dopant agent. Polyaniline polymer made with a) aniline (ANI) and b) PDA; and the copolymer samples c) PA, d) PAS, e) PAH, f) PAHS, g) PAC, and h) PACS.

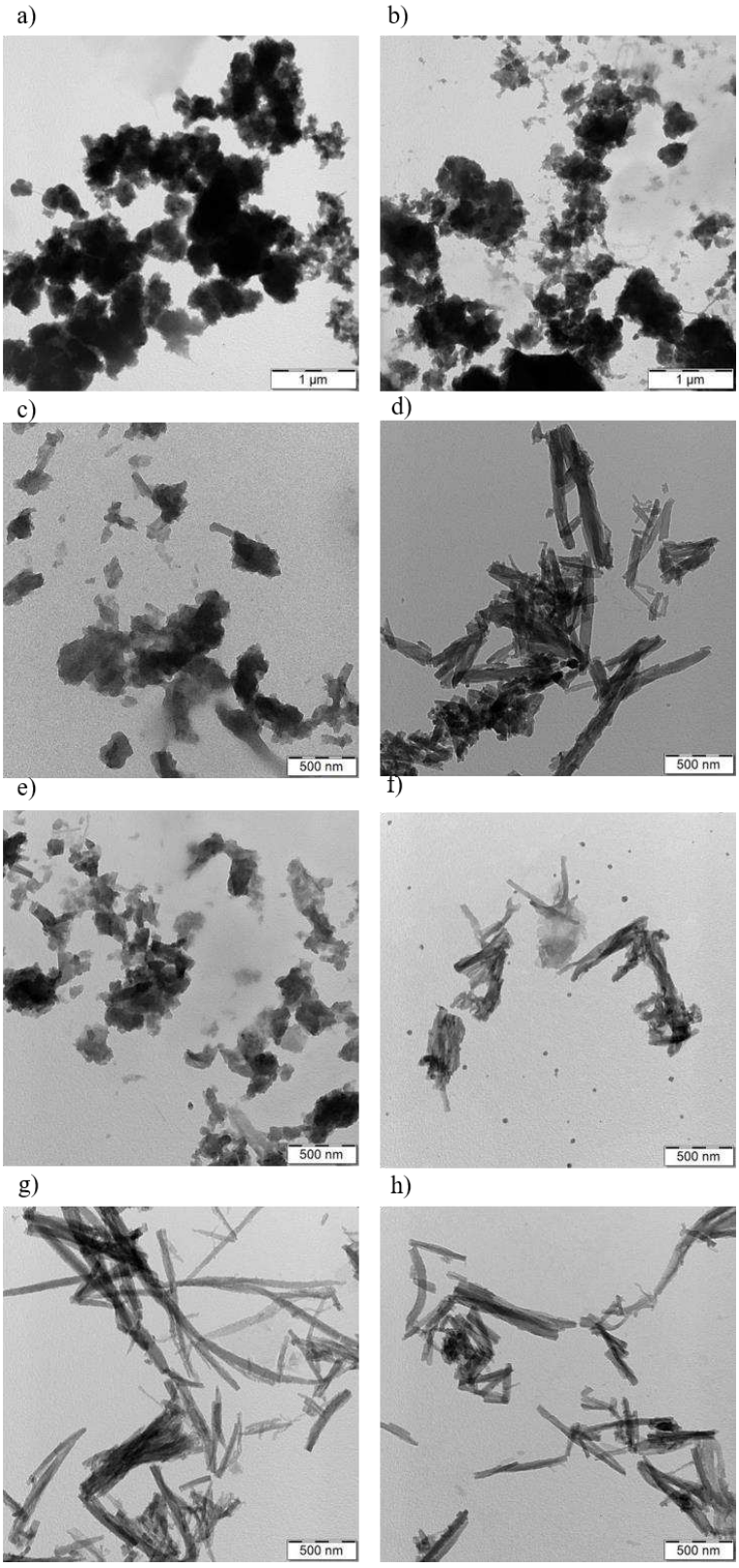

Figure 6-2. TEM images of polymer produced from aniline, PDA, and composites of PDA/ANI and PDA/ANI-SDS samples produced to change the dopant agent. Polyaniline polymer made with a) aniline (ANI) and b) PDA; and the copolymer samples c) PA, d) PAS, e) PAH, f) PAHS, g) PAC, and h) PACS.

Figure *6-2* shows that TEM images agree with the SEM analyses. The CSA acid, Figure *6-2* g) and h), produces more crystalline samples with rod-like morphology. It can be explained because the molecule of CSA acid, when released H^+ in solution, gains a negative part (SO_3^-) similar to the SDS. Therefore, CSA and PANI polymer can have an ionic interaction and form these supramolecular structures. The interaction may be identical to the PANI-SDS studied in the RESULTS AND DISCUSSIONS OF PANI-SDS SAMPLES.

6.2 Elemental Analysis

The elemental analysis results from ANI, PDA, PA, PAS, PAH, PAHS, PAC, and PACS samples are shown in Table *6-2*, where we obtained the percentage of the mass of each chemical element in the sample with precision.

Table 6-2. Results from Elemental Analysis of ANI, PDA, PA, PAS, PAH, PAHS, PAC, and PACS samples.

Sample	% C		% H		% N		% S		% Cl	
PA	55.1	55.2	4.8	4.8	11.7	11.5	5.3	5.2	2.4	
	55.3		4.8		11.3		5.2			
PAS	56.9	56.8	6.3	6.3	7.5	7.5	6.8	6.8	1.2	
	56.8		6.5		7.9		6.6			
	56.8		6.3		6.9		6.8			
PAH	48.2	48.2	4.3	4.2	7.1	7.0	9.9	9.8	0	
	48.2		4.1		7.0		9.7			
PAHS	52.4	52.5	6.2	6.1	6.7	6.9	9.5	9.5	0	
	52.6		6.0		7.1		9.5			
PAC	56.8	56.9	5.6	5.7	6.1	6.2	7.8	7.9	0	
	57.0		5.7		6.2		8.0			
PACS	57.0	57.0	6.7	6.9	6.1	6.0	8.2	8.2	0	
	57.4		6.9		6.0		8.2			
	57.0		6.9		5.4		8.1			
PDA	49.52	49.7	4.51	4.6	12.92	12.9	2.71	2.8	6.86	6.8
	49.8		4.59		12.84		2.87		6.74	
ANI	56.03	56.1	5.34	5.3	10.47	10.4	1.82	1.7	10.06	10.1
	56.12		5.34		10.44		1.74		10.1	
	56.34				10.24		1.66			

For analyses, the values were divided for the sulphur and nitrogen components to evaluate the composition of the samples, Table *6-3*. The *N/S* ratio is close to two for the copolymer samples with crystalline structures. The PAS sample indicates the presence of SDS between the layers of polymers. PAH and PAC are samples synthesized without SDS. Thus, the *N/S* ratio is low, representing the presence of ions from the acid solution between the layers of polymers. For the samples, PAHS and PACS between the layers of polymers can have the presence of SDS or the ions from the acid solution. Now, for the samples with only one monomer, PDA and ANI, the sulfur presence can be explained by the APS residues that remained after the cleaning process.

Table 6-3. Analysis from Elemental Analysis results of ANI, PDA, PA, PAS, PAH, PAHS, PAC, and PACS samples.

Samples	C/S	H/S	N/S	Cl/S	C/N	H/N	Cl/N
PA	28.2	29.3	5.0	0.4	5.6	5.8	0.1
PAS	22.5	29.9	2.6	0.2	8.8	11.7	0.1
PAH	13.1	13.6	1.6	0.0	8.0	8.3	0.0
PAHS	14.8	20.3	1.7	0.0	8.9	12.2	0.0
PAC	19.1	22.7	1.8	0.0	10.7	12.7	0.0
PACS	18.6	26.7	1.7	0.0	11.1	15.9	0.0
PDA	47.5	51.9	10.6	2.2	4.5	4.9	0.2
ANI	86.1	97.6	13.7	5.2	6.3	7.1	0.4

6.3 Maldi-TOF

To continue studying the chemical structures of the PDA/ANI and PDA/ANI-SDS samples, the Maldi-TOF analysis was made in the samples of ANI, PDA, PA, PAS, PAH, PAHS, PAC, and PACS. These results are shown in Figure *6-3*.

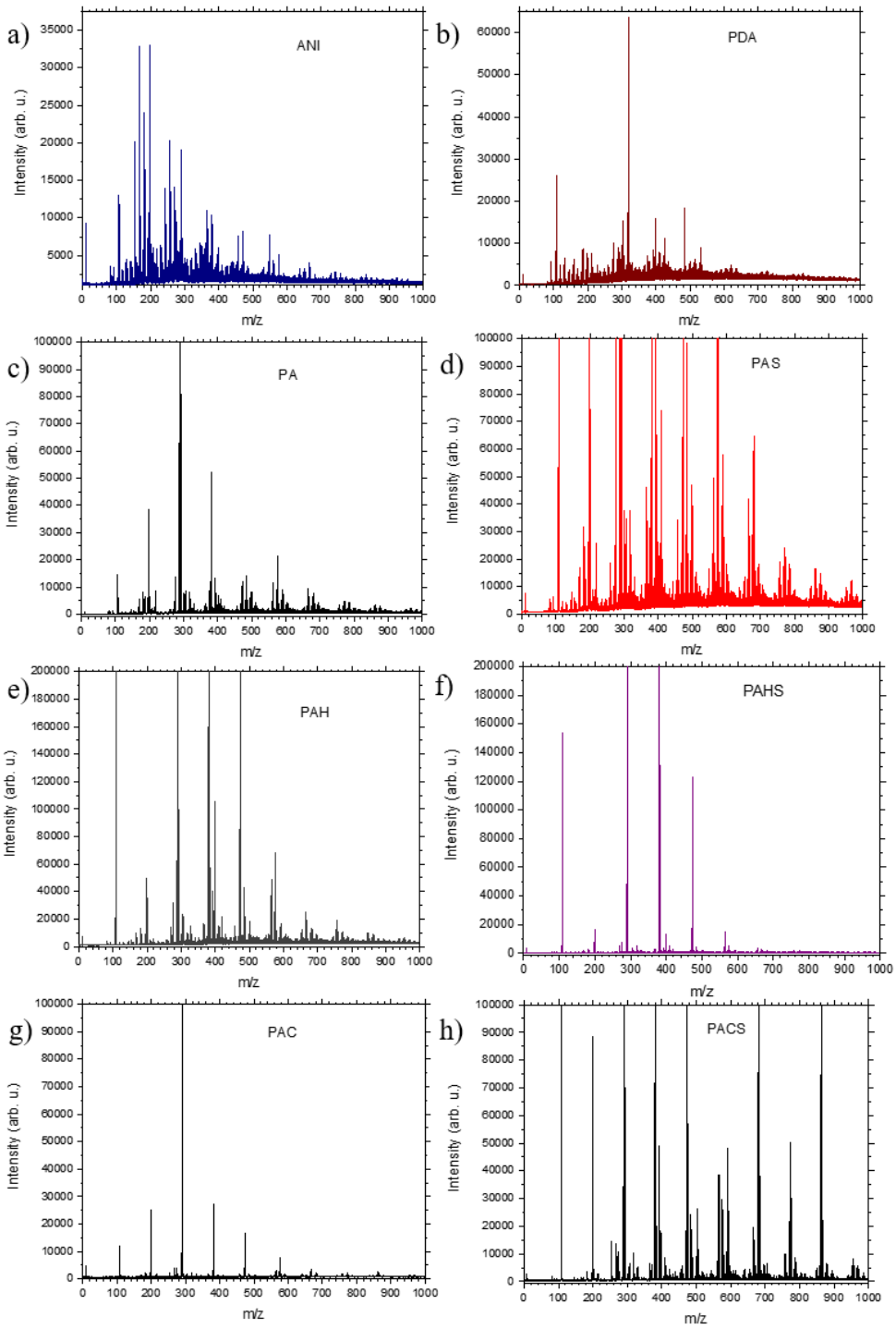

Figure 6-3. Maldi-TOF results for polyaniline polymer produced with a) aniline (ANI) and b) PDA; and the copolymer samples c) PA, d) PAS, e) PAH, f) PAHS, g) PAC, and h) PACS. The arrows represent the possible structures of the peaks.

Analyzing Figure *6-3*, it can be noted that the position of the peaks remains the same for all the samples, evidence that the addition of SDS and the change of dopant acid do not change the presence of the mass/charge structures in the material. However, the peaks become

more intense with the addition of SDS, demonstrating the SDS facility for forming oligomers in the composites. The highest peak around 300 *m/z* could be related to the presence of SDS-free molecules or the oligomer samples with 3 aniline, 2 aniline, and 1 PDA, or 1 aniline and 2 PDA molecules.

6.4 Thermogravimetric analysis (TGA)

The thermal stability of the samples was analyzed using thermogravimetric analysis (TGA) for the PDA/ANI and PDA/ANI-SDS samples; the TGA analysis was made in the samples of ANI, PDA, PA, PAS, PAH, PAHS, PAC, and PACS, where the results are shown in Figure *6-4*.

All the thermographs present in Figure *6-4* have three majors of weight loss. The first one was from 25 °C to around 120 °C, the second from 120 °C until around 350°C and the third after 400 °C. The first step can be associated with the evaporation of absorbed solutions in the samples, such as water, dopants acid (HCl, H_2SO_4, and CSA), and volatile solutions used in the clean process. The second step can be associated with the degradation of molecules with small molar masses, such as oligomers and SDS surfactants. The last one is related to the degradation of the PANI copolymers, molecules with higher molar mass in the samples (ALFANNAKH; ARAFAT; IBRAHIM, 2019; BEDNARCZYK *et al.*, 2021; SAADATTALAB; SHAKERI; GHOLAMI, 2016). Figure *6-4* a) and b) show that the first weight of loss is bigger in the ANI than in the PDA samples, which can be explained because the samples of ANI have a greater presence of polymers that absorb more concentration of dopant acid. The second weight loss confirms this statement because the weight loss of PDA is higher than ANI, showing the presence of more oligomers in this sample. For the PA and PAS samples, it can be noted that the samples without SDS have a higher concentration of solvents dopant because they do not have SDS interacting between the polymer chains. The second loss of weight can be explained by the presence of SDS and the oligomers formed by the presence of SDS. The samples using sulfuric acid and CSA have crystalline structures without SDS, Figure *6-1* and Figure *6-2*, probably because of the interaction between the acid ion and the SO_3^- group with the polymer chain.

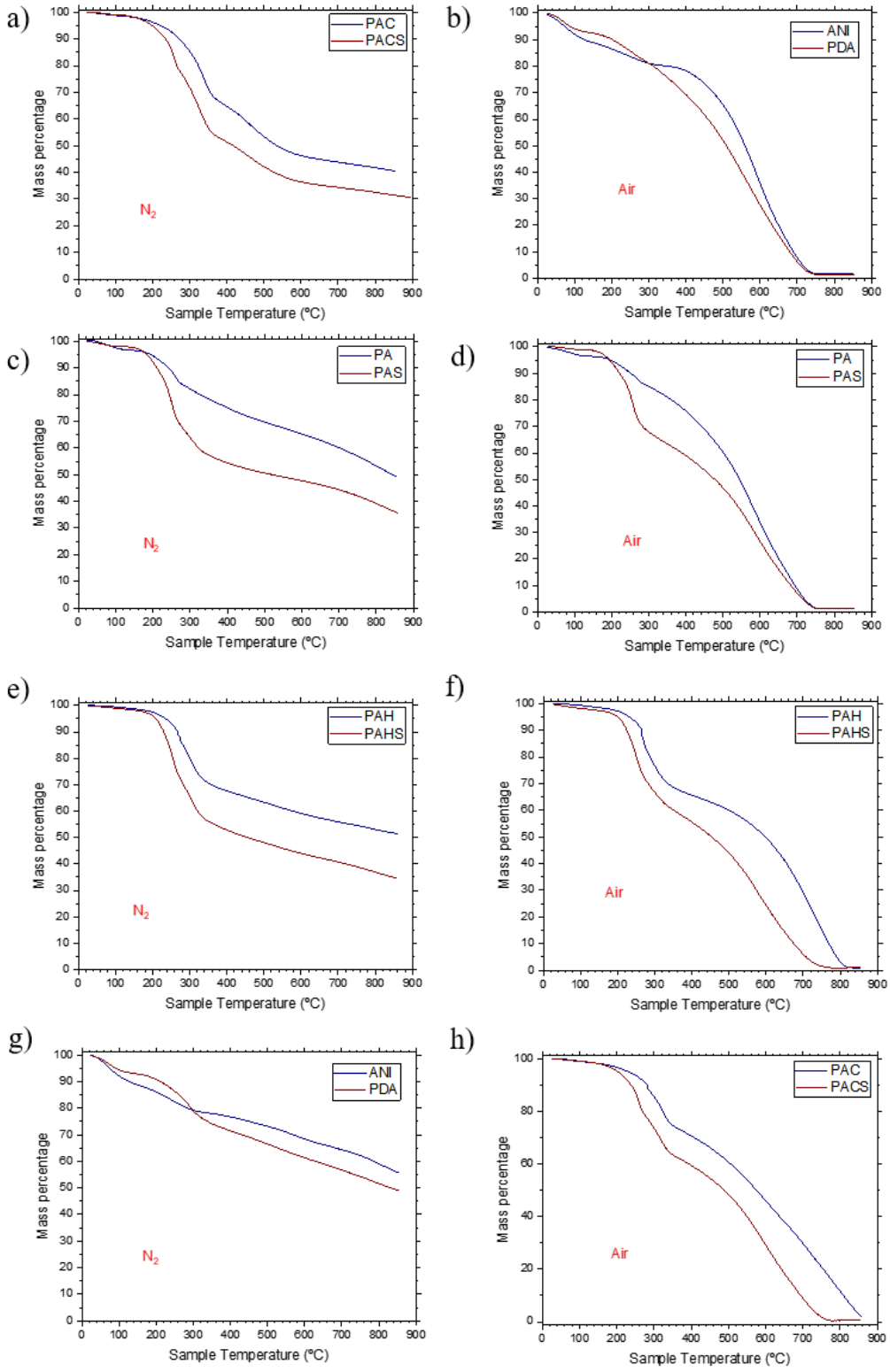

Figure 6-4. TGA thermographs obtained in inert atmosphere (N_2) and air comparing the polymer samples: a) ANI and PDA in N_2, and b) ANI and PDA in Air; and the copolymer samples c) PA and PAS in N_2, d) PA and PAS in Air, e) PAH and PAHS in N_2, f) PAH and PAHS in Air, g) PAC and PACS in N_2, and h) PAC and PACS in Air.

6.5 Fourier-Transform Infrared spectroscopy

The samples molecular structures were characterized using the FTIR technique to have more information about the intermolecular bounds. The PDA/ANI and PDA/ANI-SDS samples were prepared in KBr pellets for the transmission measurements. The initial measurements evaluated the PA, PAS, PAH, PAHS, PAC, and PACS samples and compared them with the SDS and CSA acid signal, Figure *6-5*. From the SDS, blue line Figure *6-5*, the FTIR spectrum consists of C-H stretching vibrations around 3000 cm^{-1}; C-H deformation at 1468 cm^{-1}; SO_4^- group stretching asymmetric (around 1250 cm^{-1}) and symmetric (1085 cm^{-1}); a group of SDS backbone bands around 1000 cm^{-1}; S-O-C stretching asymmetric (837 cm^{-1}) and symmetric (763 cm^{-1}); and an SO_4^- group deformation at 634 and 591 cm^{-1}. In the copolymer's samples with SDS, red line Figure *6-5*, the presence of the surfactant in the composites can be seen by peaks C-H stretching vibrations around 3000 cm^{-1} and SDS backbone bands around 1000 cm^{-1}; SO_4^- group stretching asymmetric (around 1250 cm^{-1}) and symmetric (1085 cm^{-1}) which are slightly shifted to different positions depending of the dopant acid solution.

The FTIR spectrum of CSA also consists of C-H stretching vibrations around 3000 cm^{-1}; carbonyl group-connected vibration bands (RCOR') at 1742, 491, and 427 cm^{-1}, sulfonic group vibrations (SO_3^-) around 1395, 1330, 1168, 1045 and 840 cm^{-1}. The samples of PAC and PACS were synthesized using CSA as a dopant acid; the carbonyl stretching band can note the presence of this acid at 1742 cm^{-1} and a small peak around 3000 cm^{-1} related to C-H stretching vibrations. The band at 3470 cm^{-1} is due to OH stretching in residual water in KBr pellets.

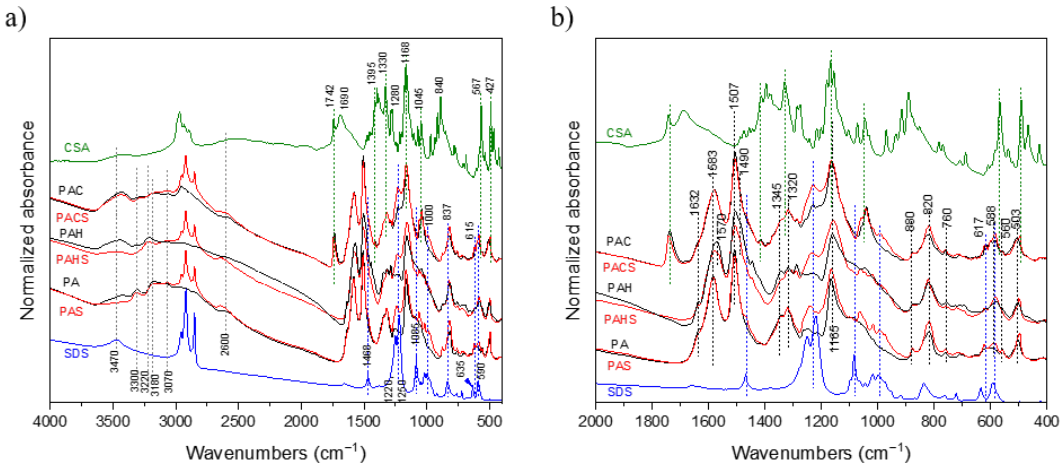

Figure 6-5. FTIR spectra of the copolymer's samples PA, PAS, PAH, PAHS, PAC, and PACS, and the molecules of SDS and CSA, obtained in transmission mode in KBr pellets. The peaks related to SDS (dashed blue line), CSA (dashed green line), and copolymer's samples (dashed black line). a) The complete spectra from 400 to 4000 cm^{-1} and b) the zoom spectra from 400 and 2000 cm^{-1}.

The copolymer's samples have a presence of unreacted amine groups because the peaks at 3300 cm^{-1}, 3180 cm^{-1}, 2580 cm^{-1}, 1632 cm^{-1}, and 1320 cm^{-1} stretching NH bonds, evidence the presence of molecules with low molecular weight (oligomer's). However, the presence of the polymer backbone manifested by bands at 3070 cm^{-1} (CH stretching of aromatic rings); 1583 cm^{-1} (C-C stretching in quinonoid units, this position of the vibration is typical of PANI base); 1507 cm^{-1} (C-C stretching in benzenoid units, this position of the vibration is typical of PANI base); 1345 cm^{-1} (C-N stretching); 1320 cm^{-1} (CN stretching); 1165 cm^{-1} (C=N stretching and CH deformation); 880 cm^{-1} (out of plane CH deformation of 1,2,4- and 1,2,4,5-substituted rings); 820 cm^{-1} (out of plane CH deformation of 1,4- and 1,2,3,4-substituted rings); 760 cm^{-1} (out of plane CH deformation of 1,2,4 trisubstituted rings); broad band around 600 cm^{-1} (ring deformation); 560 cm^{-1} (ring deformation of 1,2,3,4-substituted rings); and 503 cm^{-1} (ring deformation of 1,4-substituted rings) (BAIBARAC *et al.*, 2011; SEDLACIK *et al.*, 2013; SESTREM *et al.*, 2009; SOCRATES, 2004; TRCHOVÁ *et al.*, 2014). The spectrum reflects mainly a polyaniline-like structure. The change acid dopant (H_2SO_4 and CSA) and shoulders appear at 1570 and 1490 cm^{-1} (quinonoid and benzenoid ring-stretching, positions typical of protonated PANI). They are most pronounced in the sample doped with sulfuric acid.

6.6 Raman spectroscopy

Raman spectroscopy was used to characterize the the chemical structures in the samples complementing FTIR characterization. As resonance effects strongly influence the Raman spectroscopy, displaying selectively the spectral response of a species that is in resonance with the excitation wavelength; therefore, different laser beam frequency was used to evaluate the sample.

In Figure *6-6*, it can be see that the spectrum of the copolymer's samples is close to the protonated PANI for the wavelength beam of 633 nm (TRCHOVÁ *et al.*, 2014, 2012), with the bands: 1597 cm^{-1} (semiquinonoid ring stretching) with a shoulder at 1580 cm^{-1} (quinonoid ring stretching); 1504 cm^{-1} (NH deformation); 1420 cm^{-1} (phenazine-like structures); 1348 cm^{-1} (C~N stretching in delocalized polaronic structures); 1270 cm^{-1} (C-N stretching next to a quinonoid ring); 1230 cm^{-1} (C-N stretching in benzenoid or protonated structure); 1177 cm^{-1} (CH deformation); 850 cm^{-1} (breathing of rings undergoing π-π interaction – polaron π-dimer); 810 cm^{-1} (benzenoid ring deformation); 712 cm^{-1} (amine deformation); 603 cm^{-1} (ring deformation of benzenoid rings or rings in polaronic structure); 580 cm^{-1} (ring deformation of phenazine-like structure); 508 cm^{-1} (out of plane deformation of quinonoid rings or rings undergoing π-dimerization); and 417 cm^{-1} (out of plane ring deformation); with only very weak band of C=N stretching at 1452 cm^{-1} (BOYER *et al.*, 1998; DO NASCIMENTO; SILVA; TEMPERINI, 2006; MALINAUSKAS; BRON; HOLZE, 1998; MORÁVKOVÁ; DMITRIEVA, 2017; QUILLARD *et al.*, 1994; SESTREM *et al.*, 2009; TRCHOVÁ *et al.*, 2014, 2012).

When the dopant acid is changed from HCl to H_2SO_4 or CSA, a sharp band at 1625 cm^{-1} appears (ring stretching in benzenoid rings); the shoulder at 1580 cm^{-1} disappears (ring stretching in quinonoid rings); the band at 1504 cm^{-1} becomes sharper; the C=N stretching band at 1452 cm^{-1} decreases; the polaronic C~N stretching band now has two separate maxima at 1372 cm^{-1} (highly localized polarons) and 1330 cm^{-1} (highly delocalized polarons); the intensity of the C-N stretching band at 1230 cm^{-1} (semiquinonoid structures) increases in comparison to the band at 1270 cm^{-1} (deprotonated benzenoid structure); a weak band at 880 cm^{-1} (CNC wagging) becomes distinguishable; and the band at 508 cm^{-1} becomes dominant in the ring-deformation region.

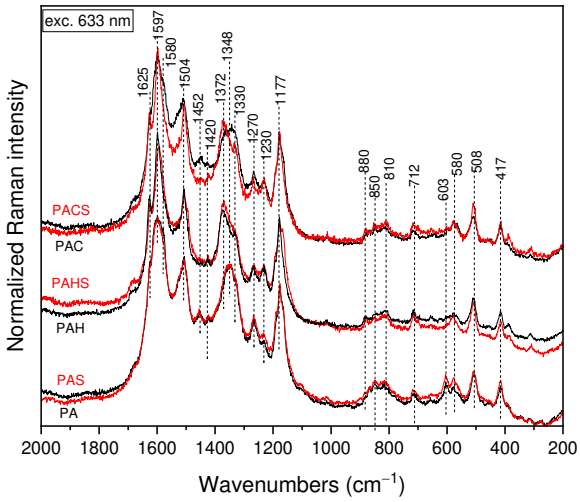

Figure 6-6. Raman spectra of the PA, PAS, PAH, PAHS, PAC, and PACS samples were excited with the 633 nm wavelength laser.

Using the laser with wavelength of 830 nm, Figure *6-7*, the spectrum of copolymer's samples display bands at 1616 cm^{-1} (benzenoid ring stretching); 1580 cm^{-1} (quinonoid ring stretching); 1500 cm^{-1} (NH deformation); 1452 cm^{-1} (C=N stretching); 1343 cm^{-1} (C~N stretching in delocalized polaron structures); 1267 cm^{-1} (C-N stretching in quinonoid structures); 1161 cm^{-1} (CH deformation in deprotonated structure) with shoulders at 1187 cm^{-1} (CH deformation in polaronic structures) and 1175 cm^{-1} (CH deformation in bipolaronic structures and π-dimers); 868 cm^{-1} (benzenoid ring deformation); 816 cm^{-1} (out of plane CH deformations of quinonoid rings); 777 cm^{-1} (quinonoid ring deformation); 718 cm^{-1} (amine deformation in bipolaronic structures); 657 cm^{-1} (out of plane ring deformations in localized polaron structures); 625 cm^{-1} (out of plane ring deformations in delocalized polaron structures); 598 cm^{-1} (out of plane quinonoid ring deformations); 500 cm^{-1} (out of plane CH deformations of neutral benzenoid rings) with a shoulder around 515 cm^{-1} (out of plane deformation of quinonoid rings); 395 cm^{-1} (in plane ring deformations) with shoulders at 433 cm^{-1} (out of plane deformation of quinonoid rings) and 414 cm^{-1} (out of plane CH deformation in bipolaronic structures); 342 and 307 cm^{-1} (skeletal vibration). The effect of the addition of the H_2SO_4 or CSA, replacing the HCl, and SDS could be seen in the separated ring stretching bands 1616 and 1580 cm^{-1} are connected to a single broadband with signal coming from various doped semiquinonoid rings; the C=N stretching band at 1452 cm^{-1} disappears; the C~N stretching band now has shoulders at 1372 cm^{-1} (localized polaron structures) and 1325 cm^{-1} (highly delocalized polaron structures); a band of C-N stretching in benzenoid structure appears at 1227

cm^{-1}; the band at 1161 cm^{-1} decreases compared with other C-H deformation bands at 1187 and 1175 cm^{-1}; the out of plane quinonoid ring deformation band at 598 cm^{-1} decreases; and the band at 414 cm^{-1} connected with bipolaronic structures increases significantly.

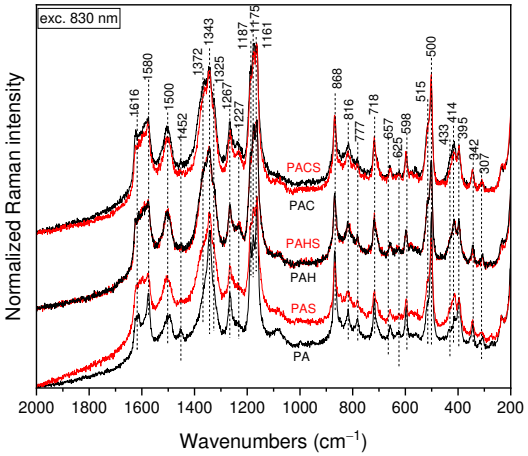

Figure 6-7. Raman spectra of the PA, PAS, PAH, PAHS, PAC, and PACS samples were excited with the 830 nm wavelength laser.

Therefore, the copolymer's samples contain a protonated PANI-like structure with NH_2 side groups and become even more protonated with SDS, sulfuric acid, and CSA. However, the signal is not the same as emeraldine salts, showing some crosslinked material halfway between PDA and ANI polymer.

6.7 X-ray diffraction

The images of SEM and TEM, Figure *6-1* and Figure *6-2*, respectively, permit us to observe the different morphology obtained in the samples. XRD diffraction was used to understand the influence of SDS and the dopant acid on the crystallinity of the samples. The samples of copolymers PA, PAS, PAH, PAHS, PAC, and PACS were compared with the neat components of ANI, PDA, and SDS, and the results are present in Figure *6-8*, and the degree of crystallinity (DOC) are shown in Table *6-4*.

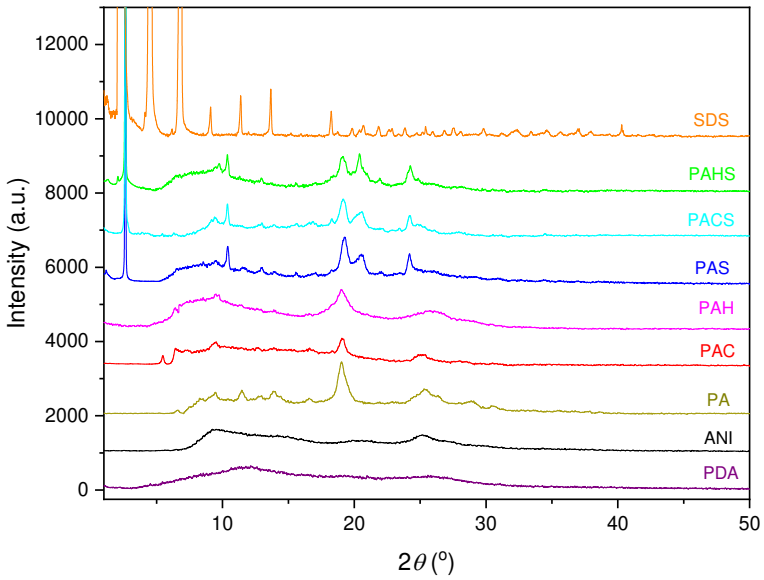

Figure 6-8. XRD patterns of the PDA, ANI, SDS, PA, PAS, PAH, PAHS, PAC, and PACS samples.

Table 6-4. Degree of crystallinity copolymer's samples.

Sample	DOC, %	Sample	DOC, %
PDA	18.2		
ANI	23.9		
PA	41.8	PAS	52.1
PAC	29.6	PACS	48.7
PAH	29.5	PAHS	46.6

Figure *6-8* shows that the pure polymer synthesized with only PDA and ANI shows mainly amorphous structures with three wide peaks for PDA around 2θ = 6.9°, 19.0°, and 26.4°, and for ANI around 2θ = 9.2°, 20.3°, and 25.2°. These peaks indicate the formation polymers with low crystallinity, causing a low degree of crystallinity (DOC) of the PDA (18.2%) and ANI (23.9%). The copolymer sample PA have amorphous peaks around 2θ = 14° and 25° and sharp peaks at 2θ = 6.57°, 9.40°, 12.74°, 13.87°, 16.58°, 19.01°, 25.34°, 28.85°, and 30.60°, exhibits a semi-crystalline structure with the DOC equal 41.8%. The strongest peak at 19.01° corresponds to an interplanar distance of 0.47 nm attributed to the interchain distance due to copolymer's π–π stacking interactions (BURON *et al.*, 2011), and the amorphous peak around 25.4° originates from the periodic arrangement in the direction perpendicular to the polymer chains (ZHANG *et al.*, 2022). The improvement of crystallinity in the PA samples compared to pure polymer samples, PDA and ANI, may suggest the presence of copolymer chains rather than a simple mixture of PDA and ANI polymers.

PAH and PAC samples have a degree of crystallinity around 29.5% lower than PA samples, showing that change in the dopant acid decreases the crystallinity of the samples; this disagrees with the SEM images. The PAH samples presents two amorphous peaks around 2θ = 10° and 18°, and others peaks at 2θ = 6.39°, 9.40°, 13.84°, 16.56°, 19.08°, 25.74°, and 28.19°. The PAC samples also presents two amorphous peaks around 2θ = 10° and 18°, and others peaks at 2θ = 6.51°, 9.36°, 12.68°, 13.71°, 16.60°, 19.09°, 25.16°, and 27.90°. The SDS improved the crystallinity of the samples (Table *6-3*) PAS (52.1%), PAHS (46.6%), and PACS (48.7%). For all the samples, the XRD spectra present peaks at 2θ = 2.62°, 10.37°, 19.25°, 20.40° and 24.20°, corresponding to interplanar distances of 3.37 nm, 0.85 nm, 0.46 nm, 0.43 nm, and 0.37 nm, respectively (LI *et al.*, 2013)he shift of the 25.4° peak to lower angles (24.20°) suggests bigger distances in the direction perpendicular to the polymer chains compared to samples without SDS. The appearance of a sharp peak at low angle values (2θ = 2.62°) implies the strong ordering of polymer chains at longer distances (3.37 nm); it can be caused by the addition of SDS and dopant acid molecules between the polymer chains.

6.8 Electrochemical Analysis

The results of the electrochemical analysis of PANI-SDS samples show that the composites have great potencial to be applied as electrochemical sensor of ascorbic acid and that is what this study aims. To prepare the samples for electrochemical analysis, the clean powder was ground using a mortar and pestle to produce a fine powder. 10 mg of the sample powder was added to an eppendorf with 400 μL isopropanol, 590 μL milli-Q water, and 10 μL Nafion solution, and the mixture was stirred for 15 minutes two times. The drop cast process deposited 1 μL of this solution in a carbon glass electrode (working electrode).

The cyclic voltammetry (CV) measurements were performed in HCl (0.2 M) solution for the samples ANI, PDA, PA, PAS, PAH, PAHS, PAC, and PACS to start the characterization. The measurements were performed using the sample deposited on a carbon glass electrode (CGE) (working electrode), platinum (counter-electrode), and silver (reference electrode). The CV results obtained for 4 cycles of measurements with the potential between (-0.1 V to 0.9 V) and for different scan rates of 2, 5, 10, 15, 20, 25, 50, 100, and 200 mV/s are shown in Figure *6-9* and Figure *6-10*.

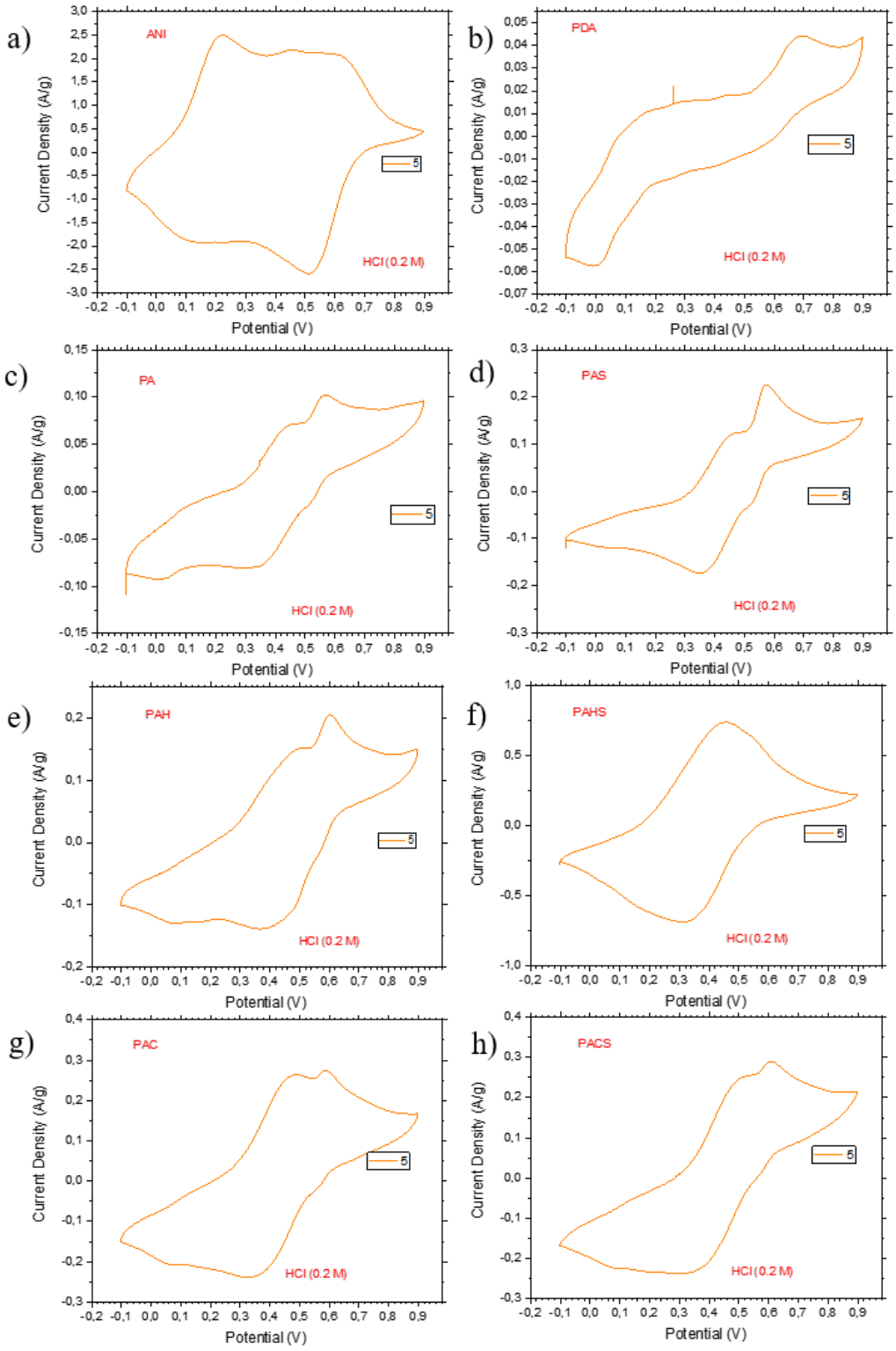

Figure 6-9. Cyclic voltammetry of ANI and PDA neat and copolymer samples in HCl (0.2 M) solution, with the scan rate of 5 mV/s. a) ANI, b) PDA, c) PA, d) PAS, e) PAH, f) PAHS, g) PAC, and h) PACS.

Figure *6-9* shows only the curve with a 5 mV/s scan rate for a facility to observe the oxidation and reduction peak. The polymer sample of ANI, Figure *6-9* a) has the peaks of oxidation (reduction) of the PANI. The peak around 0.2 V is related to the transition of the leucoemeraldine base (fully reduced) to the emeraldine salt (partially oxidized), and the peak around 0.6 V is associated with the transition from the emeraldine salt to the pernigraniline base (fully oxidized). The presence of a peak between the others (around 0.45 V) is related to the presence of oligomers in the composite. In the polymer sample of PDA, Figure *6-9* b), the CV curve shows that the process is reversible with an oxidation peak (0.7 V) and a reduction peak (0 V). Also, the gravimetric capacitance (Table *6-5*) of PDA is much smaller than ANI, indicating a higher concentration of oligomers in this sample than ANI. The copolymer's samples have two oxidative peaks around 0.45 and 0.6 V and reduction peaks around 0.4 and 0 V, showing that these composites have a reversible electrochemical process. The copolymer's samples have a higher gravimetric capacitance than the PDA samples, showing the addition of aniline monomers in the synthesis increases the conductivity of the samples. Also, we can note the addition of SDS and change in the dopant acid increase the capacitance of the copolymer's compounds.

To continue the cyclic voltammetry characterization, the electrolyte was changed to see the influence of the capacitance of the composites. The measurements using the H_2SO_4 (0.2 M) solution were performed in the potential range from -0.2 to 0.7 V and for different scan rates of 2, 5, 10, 15, 20, 25, 50, 100, and 200 mV/s are shown in Figure *6-11* and Figure *6-12*.

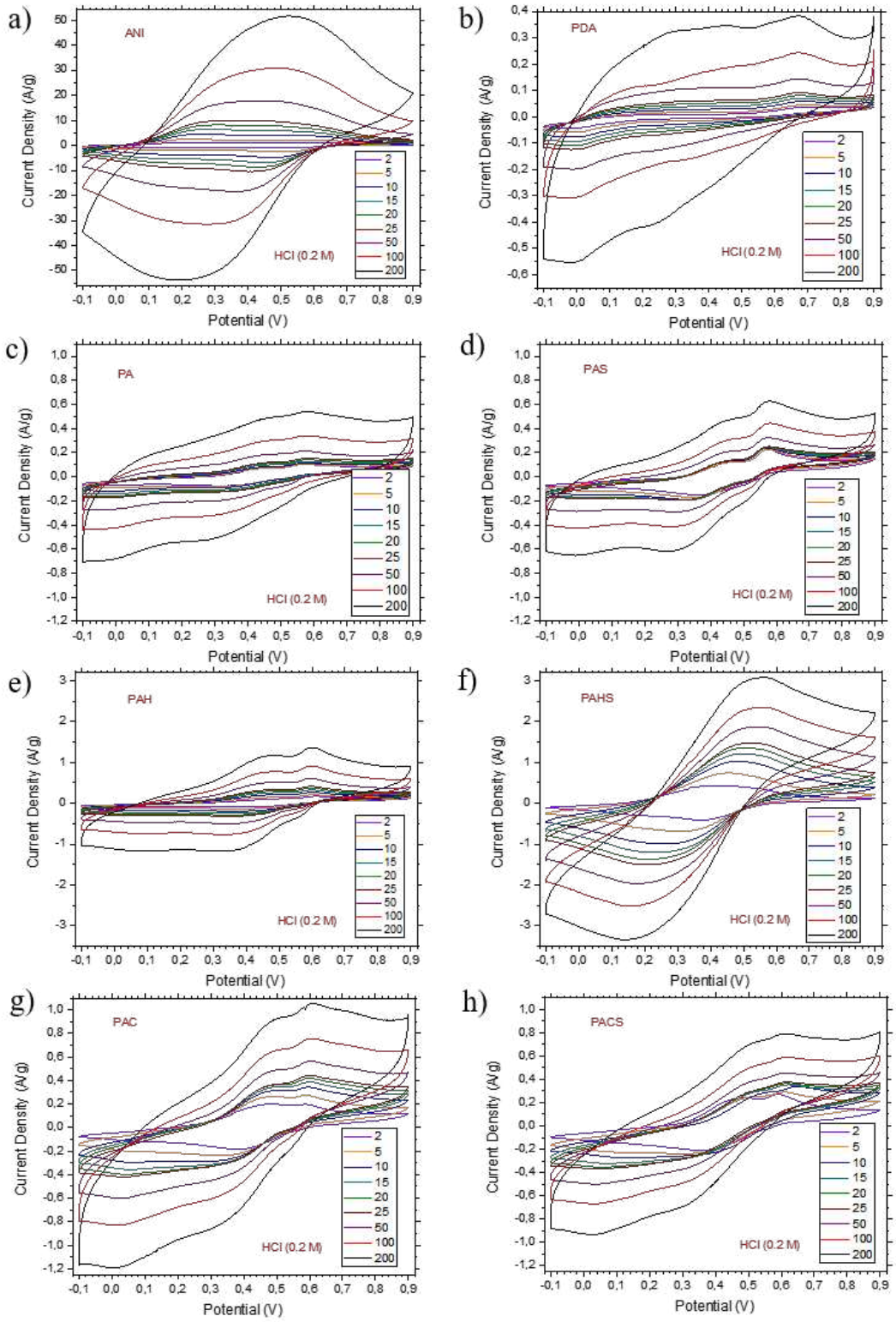

Figure 6-10. Cyclic voltammetry of ANI and PDA neat and copolymer samples in HCl (0.2 M) solution, varying the scan rate of 2, 5, 10, 15, 20, 25, 50, 100, and 200 mV/s. a) ANI, b) PDA, c) PA, d) PAS, e) PAH, f) PAHS, g) PAC, and h) PACS.

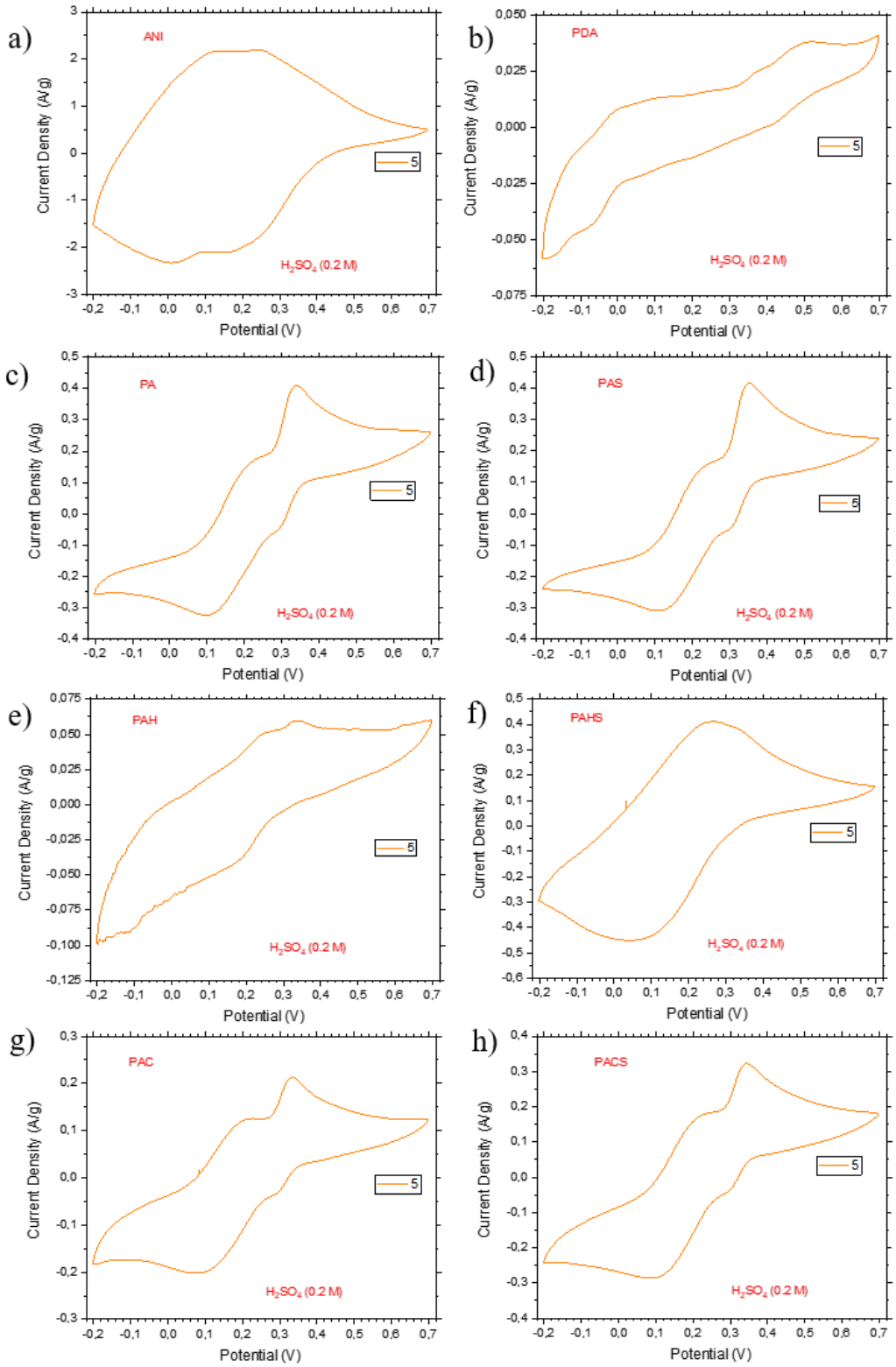

Figure 6-11. Cyclic voltammetry of ANI and PDA neat and copolymer samples in H_2SO_4 (0.2 M) solution, with the scan rate of 5 mV/s. a) ANI, b) PDA, c) PA, d) PAS, e) PAH, f) PAHS, g) PAC, and h) PACS.

It can be noted that the electrolyte influence in the peak positions of the samples shifted them to low potentials. The sample of ANI has the greatest capacitance. It is probably because of the formation of PANI polymers in this sample. The addition of SDS continues to improve the capacitance of the copolymer's samples.

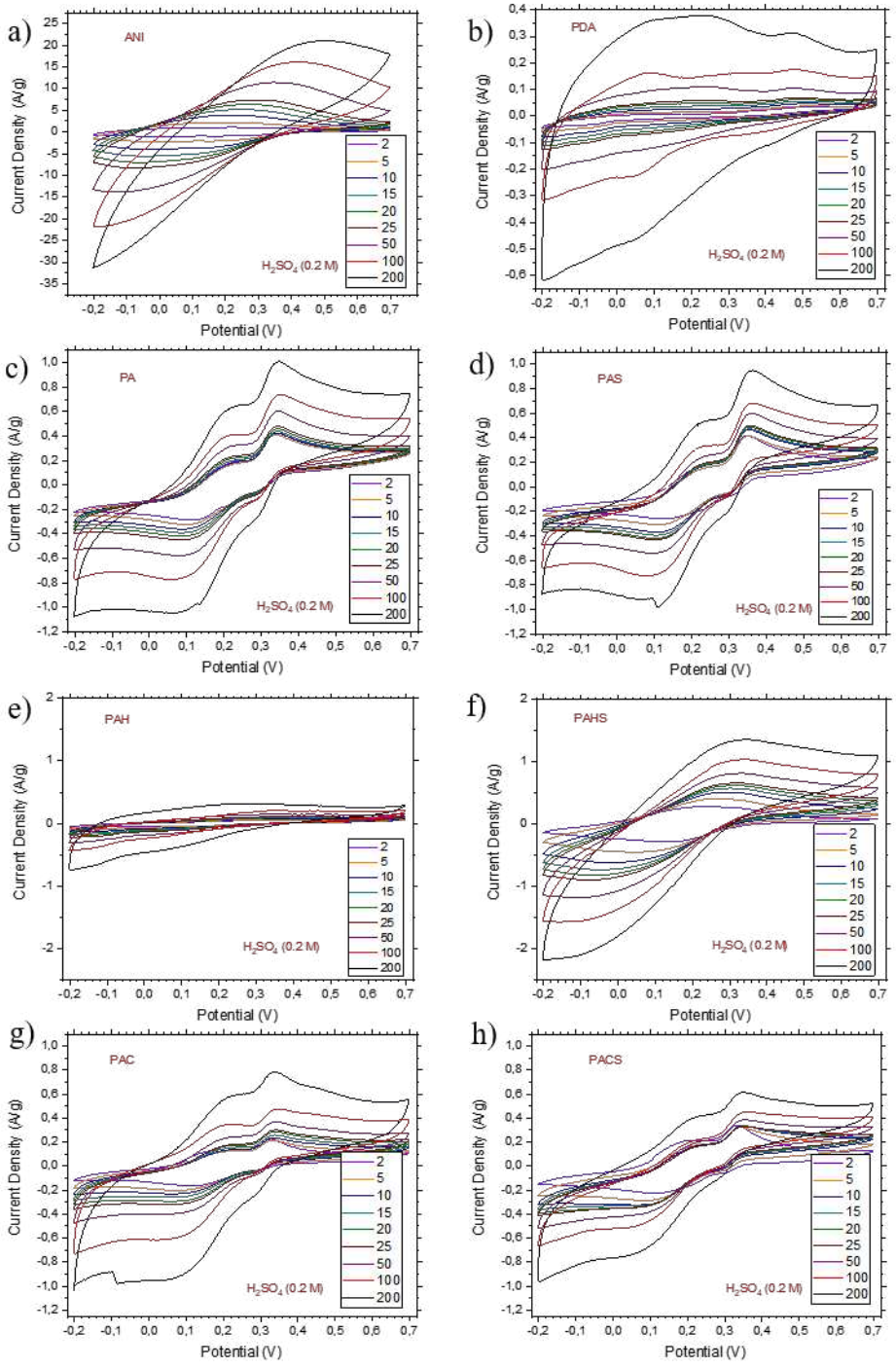

Figure 6-12. Cyclic voltammetry of ANI and PDA neat and copolymer's samples in H_2SO_4 (0.2 M) solution, varying the scan rate of 2, 5, 10, 15, 20, 25, 50, 100 and 200 mV/s. a) ANI, b) PDA, c) PA, d) PAS, e) PAH, f) PAHS, g) PAC, and h) PACS.

Comparing the gravimetric capacitance and the CV curves of the samples, we can conclude that samples of PDA, ANI, and SDS synthesized using H_2SO_4 as a dopant acid have bigger values. Therefore, to continue the study, we used the samples of PAH and PAHS for application in ascorbic acid sensors.

Table 6-5. The gravimetric capacitance of the copolymer's samples in HCl and H_2SO_4 solution.

Scan rate (mV/s)	**Gravimetric capacitance (F/g)**							
	PA	PAS	PAH	PAHS	PAC	PACS	ANI	PDA
HCl solution (0.2 M)								
2	15.80	26.39	21.71	79.79	37.02	42.44	295.96	4.36
5	6.82	10.81	12.66	52.75	20.11	18.39	270.67	2.96
10	4.20	5.98	9.12	37.43	12.29	9.87	247.47	2.40
15	3.47	4.33	7.68	29.75	9.23	7.05	233.12	2.15
20	3.04	3.32	6.84	24.84	7.42	5.52	221.53	2.01
25	2.66	2.61	6.12	21.48	5.97	4.37	213.86	1.91
50	2.17	2.22	4.81	13.46	4.31	3.07	186.89	1.69
100	1.93	1.82	3.89	8.32	3.17	2.29	157.61	1.34
200	1.62	1.50	3.07	5.63	2.42	1.77	128.22	1.22
H_2SO_4 solution (0.2 M)								
2	45.83	44.30	10.32	57.30	31.38	44.91	297.41	4.10
5	18.13	16.60	5.12	33.09	13.30	17.86	234.60	2.68
10	9.95	9.55	3.38	20.58	7.46	9.00	193.30	2.18
15	7.33	6.68	2.69	15.30	5.65	5.82	170.69	1.95
20	6.05	5.34	2.41	12.34	4.81	4.46	154.83	1.83
25	5.25	4.42	2.11	10.45	4.15	3.55	142.73	1.70
50	3.62	2.89	1.52	6.48	2.80	2.20	103.76	1.53
100	2.52	1.99	0.98	4.14	2.19	1.37	65.90	1.21
200	1.91	1.59	1.02	2.96	1.78	1.27	36.14	1.33

Before analyzing the effect of acid ascorbic on PAH and PAHS samples, we need to observe their behavior in a buffer solution of PBS with a pH of 7. This is important because we want to ensure that the current changes are due to the interaction between the acid and composites rather than a change in pH. Figure *6-13* has the CV curves from the measurements in the PBS solution. The copolymer's samples have oxidation (reduction) peaks, showing that the polymers remain electrochemical active in the buffer solution. The ANI and PDA samples do not have a well-distinguished peak, such as the copolymer's sample, showing improvement in these samples. Also, it can be noted that the capacitance of the copolymers is bigger than the PDA, and the presence of SDS also increases the capacitance.

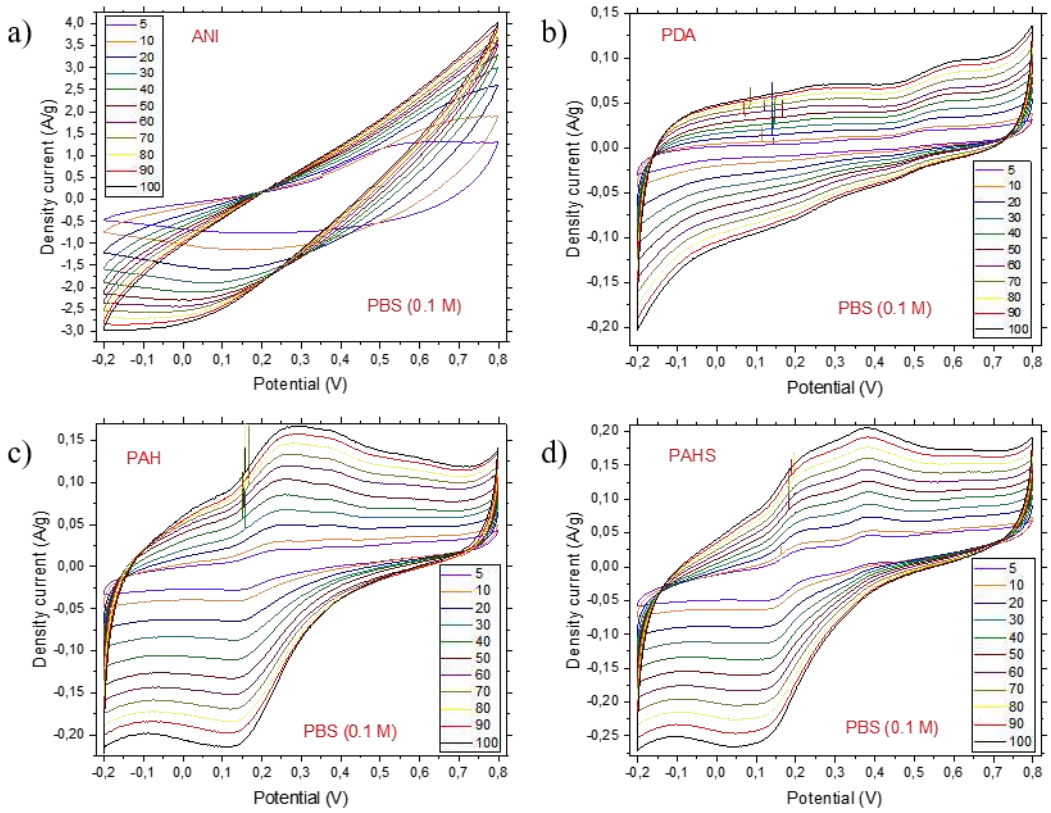

Figure 6-13. Cyclic voltammetry of ANI and PDA neat and copolymer's samples in PBS (0.1 M) solution, varying the scan rate of 5, 10, 20, 30, 40, 50, 60, 70, 80, 90, and 100 mV/s. a) ANI, b) PDA, c) PAH, and d) PAHS.

For evaluate the application of the samples as a electrochemical sensor of ascorbic acid, we compared the CV curves obtained in a scan rate equal to 10 mV/s, 50 mM of ascorbic acid, and 0.1 M of PBS solution, show in Figure *6-14*. It can be noted that for the copolymer samples without SDS (PAH) the curve is almost the same that the one obtained for only the carbon glass electrode (CGE) demonstrating that for this material the sensibility comes just from the CGE. However, the addition of the SDS (PAHS) increase the current response and shifted the peak showing an improvement compared to the CGE. To obtain information about the diffusion of ions in the layers of the sensors, cyclic voltammetry measurements of PAH and PAHS were performed for 50 mM ascorbic acid, 0.1 M of PBS solution, and varying the scan rate from 5 to 100 mV/s, Figure *6-15*.

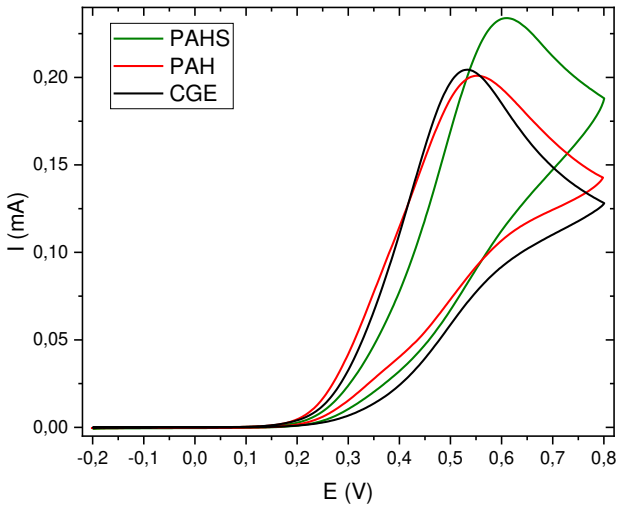

Figure 6-14. Cyclic voltammetry measurements of PAHS, PAH, and carbon glass electrode (CGE) for 50 mM Ascorbic Acid in 0.1 M PBS solution for the scan rate equal to 10 mV/s.

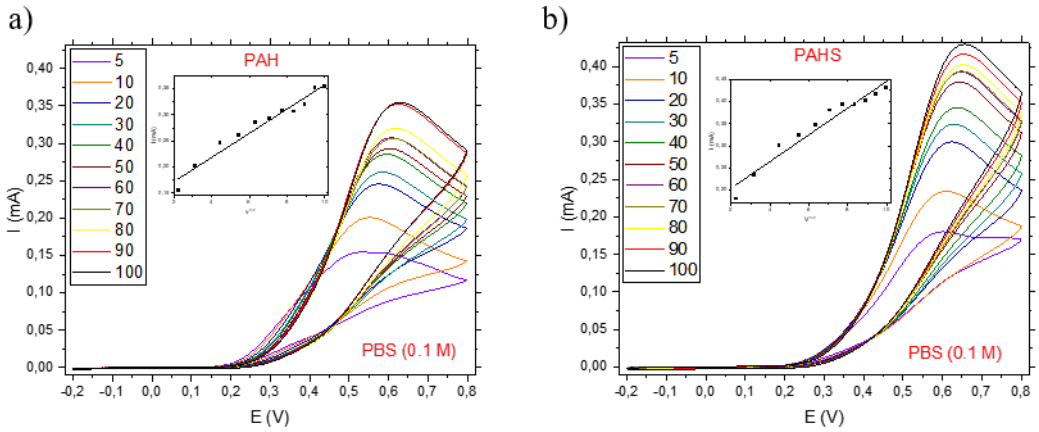

Figure 6-15. Cycling voltammetry of a) PAH and b) PAHS samples using 50 mM Ascorbic Acid ascorbic acid and 0.1 M PBS solution, varying the scan rate from 5 to 100 mV/s.

The inset graph plots the peak intensity versus the square root of the scan rate ($v^{1/2}$), giving us information about the diffusion of the ions. The linear behavior shows the process is an electrochemically reversible electron transfer process involving freely diffusing redox species for both the samples. The chronoamperometry was used obtain the calibration curve for the electrochemical sensor produced using the PAH and PAHS composites are show in Figure *6-16*. The linear fit was made for the curves to obtain the equation that related the current average (mA) to the ascorbic acid concentration (mA). The chronoamperometry measurements were performed injected 15 different concentrations of 0.02, 0.1, 0.2, 0.5, 1, 1.5, 2, 4.5, 7, 9.5, 12,

27, 50, 77, and 102 mM. After each injection, the solution is stirred during 1 minute and wait 5 minutes until take the current average values.

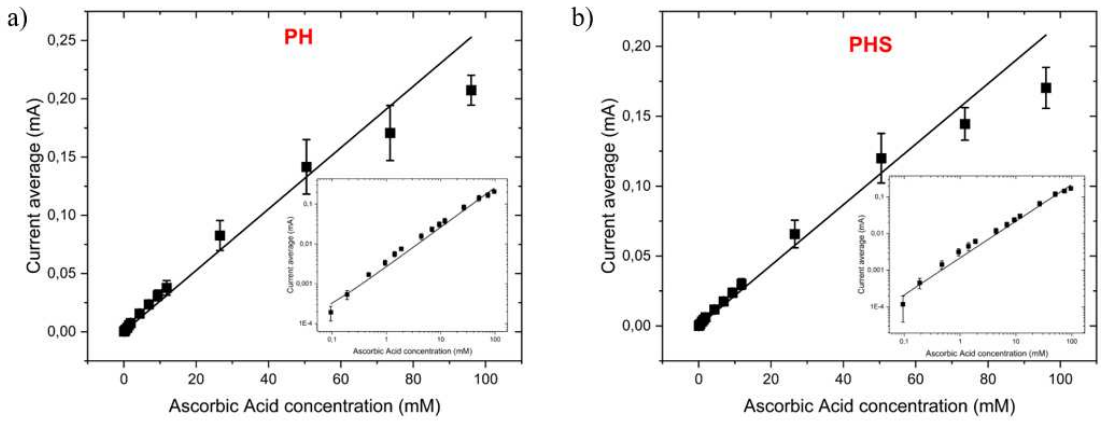

Figure 6-16. Calibration curve of the samples a) PAH and b) PAHS for ascorbic acid sensor.

The equation obtained for the copolymer's samples were I(mA) = 0.0003(2) + 0.0026(2)*[AA] (mM) for the PAH and I(mA) = 0.0009(3) + 0.0021(1)*[AA](mM) for the PHS, where *I* is the average current in mA and [AA] is the ascorbic acid concentration in mM. The equations are close, showing the samples have a behavior similar as electrochemical sensor of ascorbic acid. To test the sensor measurements were performed using a commercial orange juice to evaluate if the PAHS sensor can be selectively reutilized, and the results using a calibration curve are close to expected.

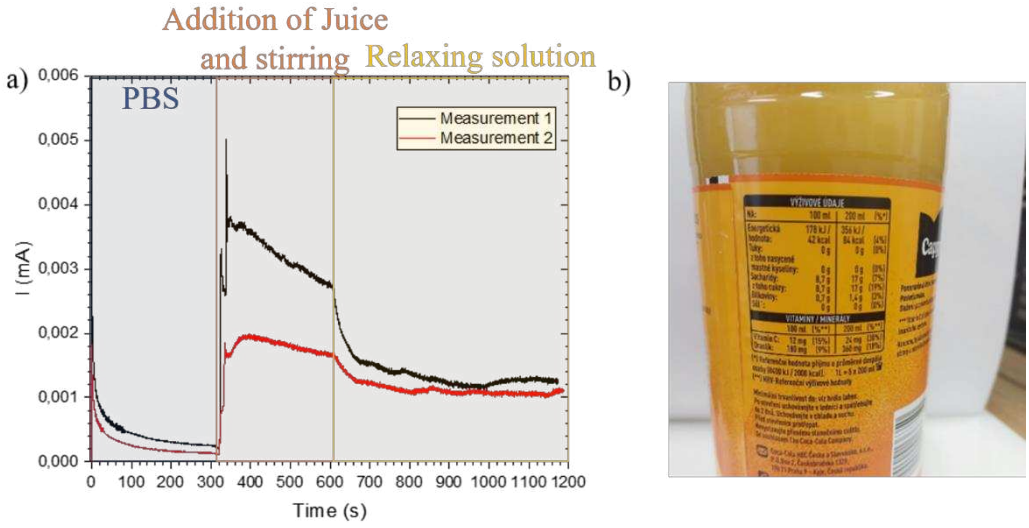

Figure 6-17. Sensor measurements testing copolymer PHS sample using a commercial orange juice to detect the ascorbic acid in a PBS (0.1 M) solution. a) The chronoamperometric curves for the two measurements and b) the specification of the commercial orange juice.

Figure *6-17*, the measurement 1 was performed adding an 8 mL of solution of juice in 4 mL of PBS solution. For the measurement 2 the sensor was cleaned with deionized water and using a new PBS solution. Comparing the curves, we can observe that the difference is in the time to samples are stirred (around 300 to 600 seconds). However, the current obtained in the measurement is calculated by the difference between the final stabilized current with the initial stabilized current. For the measurement 1 the I_1 = 0.00091 mA and I_2 = 0.00096 mA proving that the sensor can be reutilized. This measurement was made using a commercial orange juice that shows us the selectivity of our sensor for sensing just the ascorbic acid. The current plateau in Figure *6-17* can be utilized to find the concentration of the ascorbic acid in the juice; using this current to the calibration equation, the value measured of the ascorbic acid concentration was 0.38 mM, and the value expected (from the label) is 0.46 mM that represents a deviation of around 17%. The detection limit is 0.15 mM, and the quantification limit is 0.45 mM of Ascorbic acid for the PDA-ANI-SDS samples calculated following the rules of Agência Nacional de Vigilância Sanitária (ANVISA).

7 CONCLUSIONS

In this research, we synthesized supramolecular structures of PANI using different stabilizers to obtain the exact characteristics of the polymer in different morphology for diversified applications. Also, using various techniques to evaluate the structures, we proposed the chemical process behind the formation of these structures and the intramolecular interaction between the polymer and the stabilizers.

We successfully synthesized PANI particles obtained using the PVP with a spherical shape and non-amorphous morphology. Raman spectroscopy and EDS results showed that particles have the PANI and PVP in composition. Also, the DLS results show that the synthesis produces two populations of particles, one with hundreds of nanometers and the other with some micrometers of diameter. The hydrodynamic radius of the particles changed with the pH of the solution, obtaining the biggest particles with a pH equal to 14. This happens because the polymers do not have charges in the chain, facilitating the aggregation inside the particles. The optical tweezer analysis shows that the particles can be trapped using a Gaussian laser beam. The study demonstrated that the PANI particles behave the same as the inorganic particles, with the absorption coefficient increasing with the laser power. Because organic semiconductor polymers form the particles, the adsorption coefficient and refraction index characteristics can be modulated to possibly an oscillatory behavior in the trapped process. Also, the polymer can be easily functionalized with other polymers and/or molecules to use this particle in microrheology or biological analysis.

The PANI-SDS tube/rods and plates were successfully obtained by changing the concentration of APS in the synthesis. The temperature did not have much influence on the shape and chemical structures of the particles. The samples produced using low concentrations of APS only have the formation of oligomers, and the proportion of the SDS and aniline molecules in the rods is 1:1. For high concentrations of APS could be noted the formation of doped polyaniline in emeraldine salt and some oligomers. The plate structures formed in high concentration have more molecules of aniline than SDS, in the proportion of 4:1. From the structural analysis, the formation of the unit cell in the rods could be studied. The polarized Raman spectroscopy shows that the polymer chains are oriented at 30° from the principal axes of the rods, and the surfactants are bound with these polymers by ionic interaction, forming an angle around 65°. From XRD, we could conclude that SDS increases the crystallinity of the

samples and the formation of a double layer of surfactant between the molecules of polymers. Electrochemical characterization was performed to study the sample and its application in ascorbic acid sensors. It could be noted that the addition of SDS decreases the capacitance of the PANI samples; however, the SDS increases the stability of the polymer in medium or basic solutions, making the polymer electrochemical active in this medium. The application as a sensor of ascorbic acid was successfully achieved, showing that the sensor is accurate (10% deviation), selective, and reutilized.

The copolymer molecules were studied to analyze the influence of the PDA in the PANI and SDS sample morphology. Also, we investigated the impact of different dopant solutions. The copolymer sample produces crystalline structures with the addition of SDS or by changing the dopant acid from HCl to CSA. The elemental analysis shows that the dopant acid is absorbed between the polymer chain, making them the ratio of N/S does not change with the addition of SDS. The Raman and FTIR analysis shows the formation of hybrid polymers with the aniline and PDA in the composition. It could be noted that adding PDA increases the samples' crystallinity, and the samples with SDS are more crystalline. The electrochemical analysis shows the copolymer samples produced using sulfuric acid as a dopant have a higher capacitance. This sample was chosen for the application in ascorbic acid sensors. The application as a sensor of ascorbic acid was successfully achieved, showing that the sensor is accurate (17% deviation), selective, and reutilized.

References

ALFANNAKH, H.; ARAFAT, S. S.; IBRAHIM, S. S. Synthesis, electrical properties, and kinetic thermal analysis of polyaniline/polyvinyl alcohol-magnetite nanocomposites film. **Science and Engineering of Composite Materials**, vol. 26, no. 1, p. 347–359, 2019.

ANDRADE, U. M. S.; GARCIA, A. M.; ROCHA, M. S. Bessel beam optical tweezers for manipulating superparamagnetic beads. **Applied Optics**, vol. 60, no. 12, p. 3422–3429, 2021.

ASHKIN, A. Forces of a single-beam gradient laser trap on a dielectric sphere in the ray optics regime. **Biophysical journal**, vol. 61, no. 2, p. 569–582, 1992.

BAIBARAC, M.; BALTOG, I.; SCOCIOREANU, M.; BALLESTEROS, B.; MEVELLEC, J. Y.; LEFRANT, S. One-dimensional composites based on single walled carbon nanotubes and poly (o-phenylenediamine). **Synthetic metals**, vol. 161, no. 21–22, p. 2344–2354, 2011.

BEDNARCZYK, K.; MATYSIAK, W.; TAŃSKI, T.; JANECZEK, H.; SCHAB-BALCERZAK, E.; LIBERA, M. Effect of polyaniline content and protonating dopants on electroconductive composites. **Scientific Reports**, vol. 11, no. 1, p. 7487, 2021.

BEYGISANGCHIN, M.; ABDUL RASHID, S.; SHAFIE, S.; SADROLHOSSEINI, A. R.; LIM, H. N. Preparations, properties, and applications of polyaniline and polyaniline thin films—A review. **Polymers**, vol. 13, no. 12, p. 2003, 2021.

BOEVA, Z. A.; SERGEYEV, V. G. Polyaniline: Synthesis, properties, and application. **Polymer Science Series C**, vol. 56, no. 1, p. 144–153, 2014.

BOYER, M.-I.; QUILLARD, S.; REBOURT, E.; LOUARN, G.; BUISSON, J. P.; MONKMAN, A.; LEFRANT, S. Vibrational analysis of polyaniline: a model compound approach. **The Journal of Physical Chemistry B**, vol. 102, no. 38, p. 7382–7392, 1998.

BRINSON, H. F.; BRINSON, L. C.; BRINSON, H. F.; BRINSON, L. C. Characteristics, applications and properties of polymers. **Polymer engineering science and viscoelasticity: An introduction**, , p. 57–100, 2015.

BURON, C. C.; LAKARD, B.; MONNIN, A. F.; MOUTARLIER, V.; LAKARD, S. Elaboration and characterization of polyaniline films electrodeposited on tin oxides. **Synthetic Metals**, vol. 161, no. 19–20, p. 2162–2169, 2011.

CAZZOLLI, G.; CAPONI, S.; DEFANT, A.; GAMBI, C. M. C.; MARCHETTI, S.; MATTARELLI, M.; MONTAGNA, M.; ROSSI, B.; ROSSI, F.; VILIANI, G. Aggregation processes in micellar solutions: a Raman study. **Journal of Raman spectroscopy**, vol. 43, no. 12, p. 1877–1883, 2012.

CEREGATTI, T. **Preparação e caracterização de eletrodos de polianilina sobre fibra de carbono tratada por plasma de N2/H2**. 2018. 86 f. Universidade do Estado de Santa Catarina - UDESC, 2018. Available at: https://www.udesc.br/arquivos/cct/id_cpmenu/4183/PPGQ_UDESC_Dissertacao_Thayara_Ceregatti_15701442246774_4183.pdf.

COCHET, M.; LOUARN, G.; QUILLARD, S.; BOYER, M. I.; BUISSON, J. P.; LEFRANT, S. Theoretical and experimental vibrational study of polyaniline in base forms: non-planar

analysis. Part I. **Journal of Raman Spectroscopy**, vol. 31, no. 11, p. 1029–1039, 2000.

DAVE, N.; JOSHI, T. A concise review on surfactants and its significance. **Int. J. Appl. Chem**, vol. 13, no. 3, p. 663–672, 2017.

DE CARVALHO TEIXEIRA, A. V. N. Estudo da Dinâmica de Cadeias e Redes Polímericas por Simulação e Espalhamento de Luz. 1998.

DE PAIVA, A. B.; CORRER, G. I.; UGUCIONI, J. C.; CARVALHO, G. R.; JASINEVICIUS, R. G.; DE GODOY, M. P. F. On the photoconductivity behavior of emeraldine-salt polyaniline films. **Synthetic Metals**, vol. 281, p. 116915, 2021.

DE SANTANA, H.; QUILLARD, S.; FAYAD, E.; LOUARN, G. In situ UV–vis and Raman spectroscopic studies of the electrochemical behavior of N, N′-diphenyl-1, 4-phenylenediamine. **Synthetic metals**, vol. 156, no. 1, p. 81–85, 2006.

DEB, K.; BERA, A.; SAHA, B. Tuning of electrical and optical properties of polyaniline incorporated functional paper for flexible circuits through oxidative chemical polymerization. **RSC advances**, vol. 6, no. 97, p. 94795–94802, 2016.

DING, K.; CHEN, J.; ZHANG, D.; SHI, F.; LI, B.; TIAN, W.; HE, X.; WANG, L.; WANG, H. Electrochemical deposition of leaf stalk-shaped polyaniline doped with sodium dodecyl sulfate on aluminum and its use as a novel type of current collector in lithium ion batteries. **Synthetic Metals**, vol. 278, p. 116837, 2021.

DO NASCIMENTO, G. M.; SILVA, C. H. B.; TEMPERINI, M. L. A. Electronic structure and doping behavior of PANI-NSA nanofibers investigated by resonance Raman spectroscopy. **Macromolecular Rapid Communications**, vol. 27, no. 4, p. 255–259, 2006.

DONOSO, J. P. Espectroscopia Infravermelha: Moléculas. **IFSC, São Paulo. Disponível em:< http://www. ifsc. usp. br/~ donoso/espectroscopia/>. Acesso em**, vol. 13, 2012.

DOS SANTOS, I. F. S.; TEMPERINI, M. L. A. Investigation of the correlation between chemical structure and morphology in oligoaniline microspheres produced in buffered conditions. **European Polymer Journal**, vol. 122, p. 109345, 2020.

ELGRISHI, N.; ROUNTREE, K. J.; MCCARTHY, B. D.; ROUNTREE, E. S.; EISENHART, T. T.; DEMPSEY, J. L. A practical beginner's guide to cyclic voltammetry. **Journal of chemical education**, vol. 95, no. 2, p. 197–206, 2018.

FARAG, A. A. M.; ASHERY, A.; RAFEA, M. A. Optical dispersion and electronic transition characterizations of spin coated polyaniline thin films. **Synthetic metals**, vol. 160, no. 1–2, p. 156–161, 2010.

FELDMAN, D. Polymer history. **Designed monomers and polymers**, vol. 11, no. 1, p. 1–15, 2008.

FERREIRA, D. C.; PIRES, J. R.; TEMPERINI, M. L. A. Spectroscopic Characterization of Oligoaniline Microspheres Obtained by an Aniline− Persulfate Approach. **The Journal of Physical Chemistry B**, vol. 115, no. 6, p. 1368–1375, 2011.

FOX, M. Optical properties of solids. 2002.

HAZELTON, P.; YE, M.; CHEN, X. Introduction to Conducting Polymers. **Electrically Conducting Polymers and Their Composites for Tissue Engineering**. [*S. l.*]: ACS Publications, 2023. p. 1–7.

HEEGER, A. J. Semiconducting and metallic polymers: the fourth generation of polymeric materials (Nobel lecture). **Angewandte Chemie International Edition**, vol. 40, no. 14, p. 2591–2611, 2001.

INZELT, G. **Conducting polymers: a new era in electrochemistry**. [*S. l.*]: Springer Science & Business Media, 2012.

KABABYA, S.; APPEL, M.; HABA, Y.; TITELMAN, G. I.; SCHMIDT, A. Polyaniline− Dodecylbenzene Sulfonic Acid Polymerized from Aqueous Medium: A Solid State NMR Characterization. **Macromolecules**, vol. 32, no. 16, p. 5357–5364, 1999.

KHALID, M.; HONORATO, A. M. B.; VARELA, H. Polyaniline: synthesis methods, doping and conduction mechanism. **Polyaniline—From Synthesis to Practical Applications; IntechOpen: London, UK**, 2018.

KIM, B.-J.; OH, S.-G.; HAN, M.-G.; IM, S.-S. Synthesis and characterization of polyaniline nanoparticles in SDS micellar solutions. **Synthetic Metals**, vol. 122, no. 2, p. 297–304, 2001.

LI, T.; YUAN, C.; ZHAO, Y.; CHEN, Q.; WEI, M.; WANG, Y. Synthesis, characterization, and properties of aniline-p-phenylenediamine copolymers. **High Performance Polymers**, vol. 25, no. 3, p. 348–353, 2013.

LIU, N.; SLECK, M. D.; JONES, W. D. Direct Aniline Formation with Benzene and Hydroxylamine. **Chemistry**, vol. 5, no. 4, p. 2056–2067, 2023.

LOUARN, G.; LAPKOWSKI, M.; QUILLARD, S.; PRON, A.; BUISSON, J. P.; LEFRANT, S. Vibrational properties of polyaniline isotope effects. **The Journal of Physical Chemistry**, vol. 100, no. 17, p. 6998–7006, 1996.

LOWER, S. Chem1 virtual textbook. **Burnaby, Vancouver: Retrieved from http://www. chem1. com/acad/webtext**, 1999.

LUO, Y.-L.; FAN, L.-H.; GAO, G.-L.; CHEN, Y.-S.; SHAO, X.-H. Fe3O4/PANI/P (MAA-co-NVP) multilayer composite microspheres with electric and magnetic features: assembly and characterization. **Journal of nanoscience and nanotechnology**, vol. 9, no. 11, p. 6439–6452, 2009.

MALINAUSKAS, A.; BRON, M.; HOLZE, R. Electrochemical and Raman spectroscopic studies of electrosynthesized copolymers and bilayer structures of polyaniline and poly (o-phenylenediamine). **Synthetic metals**, vol. 92, no. 2, p. 127–137, 1998.

MEYER, J. R.; BARTOLI, F. J.; KRUER, M. R. Optical heating in semiconductors. **Physical Review B**, vol. 21, no. 4, p. 1559, 1980.

MEYER, J. R.; KRUER, M. R.; BARTOLI, F. J. Optical heating in semiconductors: Laser damage in Ge, Si, InSb, and GaAs. **Journal of Applied Physics**, vol. 51, no. 10, p. 5513–5522, 1980.

MIRSAKIYEVA, A. Electronic and optical properties of conducting polymers from quantum mechanical computations. 2017.

MORÁVKOVÁ, Z.; DMITRIEVA, E. Structural changes in polyaniline near the middle oxidation peak studied by in situ Raman spectroelectrochemistry. **Journal of Raman Spectroscopy**, vol. 48, no. 9, p. 1229–1234, 2017.

MORÁVKOVÁ, Z.; ŠEDĚNKOVÁ, I.; BOBER, P. The first stages of chemical and electrochemical aniline oxidation—spectroscopic comparative study. **Applied Sciences**, vol.

10, no. 6, p. 2091, 2020.

MORÁVKOVÁ, Z.; TRCHOVÁ, M.; TOMSIK, E.; ZHIGUNOV, A.; STEJSKAL, J. Transformation of oligoaniline microspheres to platelike nitrogen-containing carbon. **The Journal of Physical Chemistry C**, vol. 117, no. 5, p. 2289–2299, 2013.

MURUGESAN, R.; SUBRAMANIAN, E. Effect of organic dopants on electrodeposition and characteristics of polyaniline under the varying influence of H2SO4 and HClO4 electrolyte media. **Materials chemistry and physics**, vol. 80, no. 3, p. 731–739, 2003.

NARAYANANKUTTY, S. K. Polyaniline coated short nylon fiber/elastomer composites: electrical and microwave characteristics. [*s. d.*].

NASAJPOUR-ESFAHANI, N.; DASTAN, D.; ALIZADEH, A. ad; SHIRVANISAMANI, P.; ROZATI, M.; RICCIARDI, E.; LEWIS, B.; APHALE, A.; TOGHRAIE, D. A critical review on intrinsic conducting polymersand their applications. **Journal of Industrial and Engineering Chemistry**, 2023.

OLIVEIRA, K. M.; MOURA, T. A.; LUCAS, J. L. C.; TEIXEIRA, A. V. N. C.; ROCHA, M. S.; MENDES, J. B. S. Use of Organic Semiconductors as Handles for Optical Tweezers Experiments: Trapping and Manipulating Polyaniline (PANI) Microparticles. **ACS Applied Polymer Materials**, 2023.

POUGET, J. P.; OBLAKOWSKI, Z.; NOGAMI, Y.; ALBOUY, P. A.; LARIDJANI, M.; OH, E. J.; MIN, Y.; MACDIARMID, A. G.; TSUKAMOTO, J.; ISHIGURO, T. Recent structural investigations of metallic polymers. **Synthetic Metals**, vol. 65, no. 2–3, p. 131–140, 1994.

PRASANNAN, A.; TRUONG, T. L. B.; HONG, P.-D.; SOMANATHAN, N.; SHOWN, I.; IMAE, T. Synthesis and characterization of “hairy urchin”-like polyaniline by using β-cyclodextrin as a template. **Langmuir**, vol. 27, no. 2, p. 766–773, 2011.

QUILLARD, S.; LOUARN, G.; LEFRANT, S.; MACDIARMID, A. G. Vibrational analysis of polyaniline: A comparative study of leucoemeraldine, emeraldine, and pernigraniline bases. **Physical Review B**, vol. 50, no. 17, p. 12496, 1994.

RIEDE, A.; HELMSTEDT, M.; RIEDE, V.; STEJSKAL, J. Polyaniline dispersions. 9. Dynamic light scattering study of particle formation using different stabilizers. **Langmuir**, vol. 14, no. 23, p. 6767–6771, 1998.

ROCHA, M. S. Optical tweezers for undergraduates: theoretical analysis and experiments. **American Journal of Physics**, vol. 77, no. 8, p. 704–712, 2009.

SAADATTALAB, V.; SHAKERI, A.; GHOLAMI, H. Effect of CNTs and nano ZnO on physical and mechanical properties of polyaniline composites applicable in energy devices. **Progress in Natural Science: Materials International**, vol. 26, no. 6, p. 517–522, 2016.

SEDLACIK, M.; PAVLÍNEK, V.; MRLIK, M.; MORÁVKOVÁ, Z.; HAJNÁ, M.; TRCHOVÁ, M.; STEJSKAL, J. Electrorheology of polyaniline, carbonized polyaniline, and their core–shell composites. **Materials Letters**, vol. 101, p. 90–92, 2013.

SESTREM, R. H.; FERREIRA, D. C.; LANDERS, R.; TEMPERINI, M. L. A.; DO NASCIMENTO, G. M. Structure of chemically prepared poly-(para-phenylenediamine) investigated by spectroscopic techniques. **Polymer**, vol. 50, no. 25, p. 6043–6048, 2009.

SHI, M.; BAI, M.; LI, B. Synthesis of mesoporous crosslinked polyaniline using SDS as a soft template for high-performance supercapacitors. **Journal of Materials Science**, vol. 53,

no. 13, p. 9731–9741, 2018.

SINGH, N.; RIAZ, U. Recent trends on synthetic approaches and application studies of conducting polymers and copolymers: a review. **Polymer Bulletin**, p. 1–32, 2022.

SOCRATES, G. **Infrared and Raman characteristic group frequencies: tables and charts**. [*S. l.*]: John Wiley & Sons, 2004.

SOLEIMANI ZOHR SHIRI, M.; HENDERSON, W.; MUCALO, M. R. A review of the lesser-studied microemulsion-based synthesis methodologies used for preparing nanoparticle systems of the noble metals, Os, Re, Ir and Rh. **Materials**, vol. 12, no. 12, p. 1896, 2019.

SONG, T.; GAO, F.; GUO, S.; ZHANG, Y.; LI, S.; YOU, H.; DU, Y. A review of the role and mechanism of surfactants in the morphology control of metal nanoparticles. **Nanoscale**, vol. 13, no. 7, p. 3895–3910, 2021.

SPERLING, L. H. **Introduction to physical polymer science**. [*S. l.*]: John Wiley & Sons, 2005.

STEJSKAL, J.; KRATOCHVÍL, P.; ARMES, S. P.; LASCELLES, S. F.; RIEDE, A.; HELMSTEDT, M.; PROKEŠ, J.; KŘIVKA, I. Polyaniline dispersions. 6. Stabilization by colloidal silica particles. **Macromolecules**, vol. 29, no. 21, p. 6814–6819, 1996.

STEJSKAL, J.; KRATOCHVÍL, P.; HELMSTEDT, M. Polyaniline dispersions. 5. Poly (vinyl alcohol) and poly (N-vinylpyrrolidone) as steric stabilizers. **Langmuir**, vol. 12, no. 14, p. 3389–3392, 1996.

STEJSKAL, J.; PEKÁREK, M.; TRCHOVÁ, M.; KOLSKÁ, Z. Adsorption of organic dyes on macroporous melamine sponge incorporating conducting polypyrrole nanotubes. **Journal of Applied Polymer Science**, vol. 139, no. 20, p. 52156, 2022.

STEJSKAL, J.; SAPURINA, I.; TRCHOVÁ, M. Polyaniline nanostructures and the role of aniline oligomers in their formation. **Progress in Polymer Science**, vol. 35, no. 12, p. 1420–1481, 2010.

STEJSKAL, J.; SAPURINA, I.; TRCHOVÁ, M.; KONYUSHENKO, E. N.; HOLLER, P. The genesis of polyaniline nanotubes. **Polymer**, vol. 47, no. 25, p. 8253–8262, 2006.

STEJSKAL, J.; SPIRKOVA, M.; RIEDE, A.; HELMSTEDT, M.; MOKREVA, P.; PROKES, J. Polyaniline dispersions 8. The control of particle morphology. **Polymer**, vol. 40, no. 10, p. 2487–2492, 1999.

TRCHOVÁ, M.; MORÁVKOVÁ, Z.; BLÁHA, M.; STEJSKAL, J. Raman spectroscopy of polyaniline and oligoaniline thin films. **Electrochimica Acta**, vol. 122, p. 28–38, 2014.

TRCHOVÁ, M.; MORÁVKOVÁ, Z.; ŠEDĚNKOVÁ, I.; STEJSKAL, J. Spectroscopy of thin polyaniline films deposited during chemical oxidation of aniline. **Chemical Papers**, vol. 66, no. 5, p. 415–445, 2012.

VALMALETTE, J.-C.; TAN, Z.; ABE, H.; OHARA, S. Raman scattering of linear chains of strongly coupled Ag nanoparticles on SWCNTs. **Scientific Reports**, vol. 4, no. 1, p. 5238, 2014.

WU, K.; HUANG, J.; TU, J.; XU, X.; HUANG, H.; LIU, Y.; LI, L.; YAO, J. Reinforced polyaniline-dodecyl benzene sulfonate hydrogel with well-aligned fibrous morphology as durable electrode materials for Zn-ion battery. **Synthetic Metals**, vol. 274, p. 116721, 2021.

YAASHIKAA, P. R.; KUMAR, P. S.; KARISHMA, S. J. E. R. Review on biopolymers and composites–Evolving material as adsorbents in removal of environmental pollutants. **Environmental Research**, vol. 212, p. 113114, 2022.

YOO, W. S.; HARIMA, H.; YOSHIMOTO, M. Polarized Raman signals from Si wafers: dependence of in-plane incident orientation of probing light. **ECS Journal of Solid State Science and Technology**, vol. 4, no. 9, p. P356, 2015.

ZHANG, X.; GAO, C.; ZHANG, Y.; WANG, X.; DUAN, Y.; PENG, J.; LUO, P.; PENG, Y.; WANG, X.; WANG, S. Copolymerization of Aniline, Melamine and p-Phenylenediamine for Enhanced Pseudocapacitance Hydrogel Supercapacitor Electrodes. **Macromolecular Materials and Engineering**, vol. 307, no. 9, p. 2200180, 2022.

ZHENG, X.; KHAOULANI, S.; KTARI, N.; LO, M.; KHALIL, A. M.; ZERROUKI, C.; FOURATI, N.; CHEHIMI, M. M. Towards clean and safe water: A review on the emerging role of imprinted polymer-based electrochemical sensors. **Sensors**, vol. 21, no. 13, p. 4300, 2021.

ZHOU, C.; HAN, J.; GUO, R. Dilute anionic surfactant solution route to polyaniline rectangular sub-microtubes as a novel nanostructure. **The Journal of Physical Chemistry B**, vol. 112, no. 16, p. 5014–5019, 2008.

ZHOU, C.; HAN, J.; GUO, R. Synthesis of polyaniline hierarchical structures in a dilute SDS/HCl solution: nanostructure-covered rectangular tubes. **Macromolecules**, vol. 42, no. 4, p. 1252–1257, 2009.

ZHOU, C.; HAN, J.; SONG, G.; GUO, R. Fabrication of polyaniline with hierarchical structures in alkaline solution. **European polymer journal**, vol. 44, no. 9, p. 2850–2858, 2008.

HAYNES, A.; GOUMA, P. I. Perspective—Conducting Polymer Hybrids as Diagnostic Chemosensors. **Journal of The Electrochemical Society**, v. 169, n. 3, p. 037513, 2022.

HEEGER, Alan J.; MACDIARMID, ALAN G.; SHIRAKAWA, Hideki. The Nobel Prize in chemistry, 2000: conductive polymers. **Stockholm, Sweden: Royal Swedish Academy of Sciences**, p. 1-16, 2000.

ALONSO, Pedro Emanuel de Gouveia. Alternative synthesis methods of electrically conductive bacterial cellulose-polyaniline composites for potential drug delivery application. 2017. **Tese de Doutorado**.

HUANG, W. S.; MACDIARMID, A. G. Optical properties of polyaniline. Polymer, v. 34, n. 9, p. 1833-1845, 1993.

STEJSKAL, Jaroslav et al. Conducting polymers: polyaniline. **Encyclopedia of polymer science and technology**, p. 1-44, 2002.

SILVA JR, Ademário Íris da; ARAÚJO FILHO, Hiram da Costa; SILVA, Reinaldo Carvalho. Testes de desempenho de eletrodos: eletrodos de referência. **Química Nova**, v. 23, p. 512-517, 2000.

ALEIXO, Luiz Manoel. Voltametria: conceitos e técnicas. **Revista Chemkeys**, n. 3, p. 1-21, 2003.

APPENDIX A – Papers published

ACS APPLIED POLYMER MATERIALS

pubs.acs.org/acsapm

Use of Organic Semiconductors as Handles for Optical Tweezers Experiments: Trapping and Manipulating Polyaniline (PANI) Microparticles

Kairon M. Oliveira,* Tiago A. Moura, Janaísa L. C. Lucas, Alvaro V. N. C. Teixeira, Márcio S. Rocha, and Joaquim B. S. Mendes*

Cite This: *ACS Appl. Polym. Mater.* 2023, 5, 3912−3918 Read Online

ACCESS | Metrics & More | Article Recommendations | Supporting Information

ABSTRACT: Here we propose the use of the organic semiconductor polyaniline (PANI) for the preparation of spherical-shaped microparticles to serve as handles in optical tweezers (OT) experiments. The stable trapping and manipulation of PANI beads was demonstrated for the first time, using a Gaussian (TEM_{00}) beam optical tweezers. The trap stiffness was characterized for various different parameters such as the bead radius, the laser power, and the distance between the bead and the coverslip of the sample chamber, attesting the viability of using such material for optical manipulation. Since the effective optical properties of PANI can be modulated by the synthesis process, some related applications are also proposed. The results of the present work therefore open the door for using semiconductor polymeric materials in OT applications.

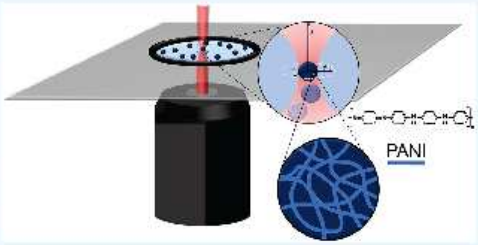

KEYWORDS: *organic semiconductors, optical tweezers, polyaniline microparticles, optical traps*

INTRODUCTION

The use of optical trapping approaches to manipulate micrometer-sized and nanometer-sized objects promoted a revolution in several areas of knowledge since the seminal work of Arthur Ashkin in the late 1960s.[1] Among some of the main applications we highlight here the trapping of single viruses and bacteria,[2] single cell manipulation,[3] single molecule force spectroscopy for studying intermolecular interactions,[4−6] and microrheology.[7] Furthermore, in the past decade optical tweezers (OT) have also become the basis of emerging technologies such as tractor beams,[8] volumetric displays,[9] biosensors,[10] micromotors,[11,12] and others.[13] This recent change of paradigm in using optical tweezers is based on two pillars: the generation of more complex trapping configurations employing spatial light modulators that allow the creation of structured beams, such as frozen waves,[14] and the emergence of applications involving materials that allow exploring other types of interactions between radiation and matter that are beyond the classical and well studied optical forces (scattering and gradient forces).

Recently, our group showed that micrometer-sized particles made of topological insulators exhibit a very interesting oscillatory dynamics when manipulated by a traditional Gaussian (TEM_{00}) beam optical tweezers. Such dynamics can be modulated by changing simple setup parameters such as the laser power or the distance between the particle and the coverslip used to construct the sample chamber.[11] After that work, a similar behavior was also observed for semiconductor particles (germanium[12] and silicon[15]) with an additional feature: the oscillations in this case depend on the polarization direction of the laser beam. This oscillatory dynamics observed for semiconductor and topological insulator beads opened the door for promising applications of optical tweezers, *e.g.*, in microrheological studies and in the development of single molecule heat engines[16] and micromotors.[17]

Within this perspective, developing other types of particles, whose optical properties can be modulated in their synthesis processes, becomes fundamental for the construction of innovative technologies based on optical manipulation. In particular, among the various available materials, the polymer polyaniline (PANI) presents a great alternative by the fact that many of its optical and conductive parameters (charge carrier density, absorption coefficient, refractive index, reflectance, etc.) can be modulated through changes in the pH of the surrounding solution. By changing the pH, in fact, one can

Received: January 3, 2023
Accepted: March 15, 2023
Published: March 29, 2023

https://doi.org/10.1021/acsapm.3c00015
ACS Appl. Polym. Mater. 2023, 5, 3912−3918